ALEX(01)-TR-76-08

12 NW

A TIME-VARIANT WIENER FILTER FOR DISPERSED WAVEFORMS

TECHNICAL REPORT NO. 8
VELA NETWORK EVALUATION AND AUTOMATIC PROCESSING RESEARCH

Prepared by
Rudolf Unger

TEXAS INSTRUMENTS INCORPORATED
Equipment Group
Post Office Box 6015
Dallas, Texas 75222

Prepared for

AIR FORCE TECHNICAL APPLICATIONS CENTER
Alexandria, Virginia 22314

Sponsored by

ADVANCED RESEARCH PROJECTS AGENCY
Nuclear Monitoring Research Office
ARPA Program Code No. 6F10
ARPA Order No. 2551

29 October 1976

Acknowledgment: This research was supported by the Advanced Research Projects Agency, Nuclear Monitoring Research Office, under Project VELA-UNIFORM, and accomplished under the technical direction of the Air Force Technical Applications Center under Contract Number F08606-76-C-0011.

ALEX(01)-TR-76-08

A TIME-VARIANT WIENER FILTER FOR DISPERSED WAVEFORMS

TECHNICAL REPORT NO. 8
VELA NETWORK EVALUATION AND AUTOMATIC PROCESSING RESEARCH

Prepared by
Rudolf Unger

TEXAS INSTRUMENTS INCORPORATED
Equipment Group
Post Office Box 6015
Dallas, Texas 75222

Prepared for

AIR FORCE TECHNICAL APPLICATIONS CENTER
Alexandria, Virginia 22314

Sponsored by

ADVANCED RESEARCH PROJECTS AGENCY
Nuclear Monitoring Research Office
ARPA Program Code No. 6F10
ARPA Order No. 2551

29 October 1976

Acknowledgment: This research was supported by the Advanced Research Projects Agency, Nuclear Monitoring Research Office, under Project VELA-UNIFORM, and accomplished under the technical direction of the Air Force Technical Applications Center under Contract Number F08606-76-C-0011.

UNCLASSIFIED

SECURITY CLASSIFICATION OF THIS PAGE (When Data Entered)

REPORT DOCUMENTATION PAGE		READ INSTRUCTIONS BEFORE COMPLETING FORM
1. REPORT NUMBER	2. GOVT ACCESSION NO.	3. RECIPIENT'S CATALOG NUMBER
4. TITLE (and Subtitle) A TIME-VARIANT WIENER FILTER FOR DISPERSED WAVEFORMS		5. TYPE OF REPORT & PERIOD COVERED Technical
		6. PERFORMING ORG. REPORT NUMBER ALEX(01)-TR-76-08
7. AUTHOR(s) Rudolf Unger		8. CONTRACT OR GRANT NUMBER(s) F08606-76-C-0011 ARPA Order 2551
9. PERFORMING ORGANIZATION NAME AND ADDRESS Texas Instruments Incorporated Equipment Group Dallas, Texas 75222		10. PROGRAM ELEMENT, PROJECT, TASK AREA & WORK UNIT NUMBERS VELA T/6705/B/ETR
11. CONTROLLING OFFICE NAME AND ADDRESS Advanced Research Projects Agency Nuclear Monitoring Research Office Arlington, Virginia 22209		12. REPORT DATE 29 October 1976 13. NUMBER OF PAGES 113
14. MONITORING AGENCY NAME & ADDRESS (if different from Controlling Office) Air Force Technical Applications Center VELA Seismological Center Alexandria, Virginia 22314		15. SECURITY CLASS. (of this report) UNCLASSIFIED 15a. DECLASSIFICATION/DOWNGRADING SCHEDULE

16. DISTRIBUTION STATEMENT (of this Report)

APPROVED FOR PUBLIC RELEASE, DISTRIBUTION UNLIMITED

17. DISTRIBUTION STATEMENT (of the abstract entered in Block 20, if different from Report)

18. SUPPLEMENTARY NOTES

ARPA Order No. 2551

19. KEY WORDS (Continue on reverse side if necessary and identify by block number)

Time-variant	Maximum entropy spectrum
Wiener filter	Long-period surface waves
Dispersion	Narrowband filter
Dispersion-related filter	Signal estimation

20. ABSTRACT (Continue on reverse side if necessary and identify by block number)

A time-variant Wiener filter based on the regionally dispersive characteristics of long-period surface waves is presented. The dispersion curves are determined with maximum entropy spectral analysis. The filter performance is tested with synthetic chirp waveforms and with real seismic data. The filter enhances the estimation of signals and, in particular, the surface wave magnitude measurability, for waveforms with signal-to-noise → next page

DD FORM 1 JAN 73 1473 EDITION OF 1 NOV 65 IS OBSOLETE

UNCLASSIFIED

SECURITY CLASSIFICATION OF THIS PAGE (When Data Entered)

19. continued

Sinkiang region
Group velocity curves .

20. continued

cont. → ratios down to 0 dB RMS. For lower signal-to-noise ratios the signal estimates are less reliable, and magnitude estimates may be biased. Compared with bandpass filtering, noise rejection improvement ranges from 3 to 9 dB. The filter's ability to separate multiple signals is limited by filter impulse response side lobe interference. The filter performance is furthermore limited by dispersion of noise, by non-stationary noise, by the filter's inherent ability to generate false signals from broadband noise components, by the signal bandwidth, by the regional dispersion curve variation, by narrowband filter response characteristics, and by the reliability and resolution of state-of-the-art spectral analysis methods. The filter appears to be more effective as a signal estimator than as a detector.

LIST OF ABBREVIATIONS

AFTAC . . . Air Force Technical Applications Center

ALPA . . . . Alaskan Long-Period Array

BPF . . . . . Bandpass Filter

DRF . . . . . Dispersion-Related Filter

LP . . . . . Long-Period

MES . . . . . Maximum-Entropy Spectrum

MF. . . . . Matched Filter

NBF . . . . . Narrowband Filter

RMS . . . . . Root-Mean-Square

SNR . . . . . Signal-To-Noise Ratio

TVWF . . . . Time-Variant Wiener Filtering

WF. . . . . Wiener Filter

ABSTRACT

A time-variant Wiener filter based on the regionally dispersive characteristics of long-period surface waves is presented. The dispersion curves are determined with maximum entropy spectral analysis. The filter performance is tested with synthetic chirp waveforms and with real seismic data. The filter enhances the estimation of signals and, in particular, the surface wave magnitude measurability, for waveforms with signal-to-noise ratios down to 0 dB RMS. For lower signal-to-noise ratios the signal estimates are less reliable, and magnitude estimates may be biased. Compared with bandpass filtering, noise rejection improvement ranges from 3 to 9 dB. The filter's ability to separate multiple signals is limited by filter impulse response side lobe interference. The filter performance is furthermore limited by dispersion of noise, by non-stationary noise, by the filter's inherent ability to generate false signals from broadband noise components, by the signal bandwidth, by the regional dispersion curve variation, by narrowband filter response characteristics, and by the reliability and resolution of state-of-the-art spectral analysis methods. The filter appears to be more effective as a signal estimator than as a detector.

ACKNOWLEDGMENTS

Dispersion-related filtering was originally suggested by Dr. R. W. Alewine of the Air Force Technical Applications Center (AFTAC). The idea was developed into the present concept by T. E. Barnard of Texas Instruments Incorporated. Further discussions with T. E. Barnard, T. W. Harley, Dr. S. S. Lane, Dr. R. L. Sax, Dr. D. Sun, and Dr. L. S. Turnbull were greatly contributive. Most of the software was written by S. D. Fobes and R. L. Whitelaw. Mrs. M. E. Palmer and Mrs. C. B. Saunders prepared the print of text and figures.

TABLE OF CONTENTS

TABLE OF CONTENTS
(continued)

LIST OF FIGURES

LIST OF FIGURES
(continued)

LIST OF FIGURES
(continued)

LIST OF TABLES

SECTION I
INTRODUCTION

Dispersion of surface waves has been used in signal processing and analysis of long-period (LP) seismic waveforms. For instance, correlation processes, such as reference waveform and chirp waveform matched filtering (MF), compress the available signal energy while averaging the supposedly random noise, to yield correlation peaks of high signal-to-noise ratio (SNR). Because of signal energy compression in time, these techniques do not improve the estimate of the original signal and are therefore more useful for detection purposes.

This report presents a method to enhance the estimate of an LP signal, by utilizing prior knowledge of its dispersive characteristics. We call this technique dispersion-related filtering (DRF).

The most elementary form of DRF consists of time-variant narrowband filtering along the signal's presumed dispersion curve. In this manner considerably more noise energy can be rejected than in stationary bandpass filtering of the waveform over the entire expected signal frequency band. This method has the inherent ability, however, to generate dispersed waveforms, easily mistaken as signals, from any broadband input, including pure noise. For this reason, DRF is not well suited for signal detection; its main function is signal estimation.

For a given region-station combination the expected dispersion curve may be obtained by overlaying time-variant signal spectra measured from strong events occurring in a given region. The spread or variance of

the dispersion curve ensemble and the signal bandwidth at each point in time then determine the bandwidth which should be applied at each point along the dispersion curve.

The signal estimate can be further improved by performing time-variant Wiener filtering (TVWF); i.e., for each point along the dispersion curve the expected signal power and the expected noise power are balanced to yield a signal estimate of minimum mean square error. In particular, TVWF tends to reduce signal over-estimation at frequencies of relatively high noise power, e.g., at 0.06 Hz (17-second micro-seismic noise), and at frequencies around 0.02 Hz (50 seconds).

Besides ambient noise rejection, DRF is theoretically capable of separating multiple dispersed signals, provided that the individual dispersion curves can be resolved by spectral analysis.

It is clear that in all cases the DRF and TVWF performance depends largely on the effectiveness and reliability of the spectral analysis method applied. Therefore, part of this study's effort was dedicated to the use of a high-resolution spectral analysis method, the maximum entropy spectrum (MES) technique (Burg, 1967).

In this study the DRF and TVWF methods were developed and tested on synthetic chirp waveforms and on beamed waveforms from Sinkiang Province seismic events, recorded at the Alaskan Long-Period Array (ALPA). The use of this data base permits comparison with the results of a previous matched filtering performance study (Unger, 1973). The emphasis was placed on the feasibility of dispersion-related filtering and on its potential and limitations to improve the estimation of long-period seismic signals from noisy waveforms.

Discussion of the above topics is presented in the following sections. The spectral analysis technique and its results are discussed in

Section II. Section III presents the DRF and TVWF development and discusses various design aspects and performance expectations. The DRF and TVWF performance are evaluated in Section IV, and the study and its conclusions are summarized in Section V. Related literature is listed in Section VI. Some related details are contained in the appendices.

SECTION II
SPECTRAL ANALYSIS

A. INTRODUCTION

A prerequisite for the success of dispersion-related and Wiener filtering is a reliable, high-resolution spectral analysis. The maximum entropy spectrum (MES), first presented by J. P. Burg (Burg, 1967) and comprehensively discussed by T. E. Barnard (Barnard, 1975) is a high-resolution spectrum obtained from a relatively small number of lags of a waveform's auto-correlation function. However, the reliability and the resolution of the spectrum depend strongly on the selected input parameters: the waveform gate or window length and the number of correlation lags used.

For time-variant spectra such as those of dispersed waveforms, the choice of this parameter combination is even more delicate than for stationary spectra. On the one hand, a shortest possible gate must be selected to best describe the spectral variation with time. On the other hand, the spectral reliability increases with the ratio of gate length to the number of lags used, while the resolution improves with the number of lags used.

Yet another aspect is the sampling rate of the waveform, or equivalently, its Nyquist frequency. For an oversampled waveform the MES algorithm might find peaks beyond the actual signal frequency band. This would result in a loss of resolution in the frequency band of interest. Thus, it seems appropriate to use the lowest possible sampling rate that, according to the sampling theorem, still adequately describes the signal, i.e.,

$$T_s = 1 / (2W) , \qquad \text{(II-1)}$$

where T_s is the sampling period and W is the signal cut-off frequency. ALPA LP signals, for instance, usually do not extend (partly due to the instrument response) beyond 0.06 Hz, so that we could low-pass the waveform at 0.06 Hz and sample every 8 seconds (0.125 Hz sampling rate). On the other hand, over-sampling provides us with a greater number of points per time unit, which might permit us to take shorter gates. However, the fact that these points are no longer independent may nullify this assumed advantage.

Since it appears to be difficult to analytically establish an optimum MES parameter combination (Barnard, 1975), an attempt was made in this study to empirically arrive at some best set of parameters, based on spectral analysis of synthetic linear chirp waveform combinations and real data. The "best" parameter combination found in this manner was then applied in the dispersion curve analysis of Sinkiang Province events. The noise spectral analysis, required by the Wiener filter, demands a different set of parameters.

The MES parameter analysis, the Sinkiang region dispersion curve analysis, and the noise spectral analysis, respectively, are presented in the following subsections. The maximum entropy spectra used in the analysis were computed using a variation of the MES algorithm, the Burg technique (Burg, 1968), which is especially efficient for the computation of spectra from short waveform windows. It bypasses the computation of the actual auto-correlation function and derives the spectrum directly from the coefficients of a waveform prediction error filter (Burg, 1968; Barnard, 1975). The number of filter coefficients used (the filter length) equals the number of auto-correlation lags in the original MES computation.

B. MAXIMUM ENTROPY SPECTRUM PARAMETERS

Combinations of linear chirp waveforms were synthesized to test the reliability and the resolution of the maximum entropy spectra (MES) and to obtain a best combination of window length, number of lags, and sample rate as parameters for the MES algorithm.

Figures II-1 through II-4 present the moving-window maximum entropy spectra of a 0.015-0.055 Hz single linear chirp waveform and of a combination of two waveforms, for various parameter combinations. Each waveform has a 24-second cosine taper at both ends. For each point in time specified (here, every 8 seconds) the spectrum is computed from a waveform window taken symmetrically about that point. At every 80 seconds the spectrum is fully plotted, with its power density in the direction of the time axis; the power density reference (origin) is at the corresponding time point indicated, where not obscured by plotted data, by a tickmark on the upper side of the time axis. The spectra are held constant where they fall below their reference power level and where they exceed the length of the time axis to the far right. The reference (origin) power level (relative to 1 computer count) annotated below the figure depends on the average power of the waveform; the logarithmic power scale (dB) drawn above the figure depends on the space between the plotted spectra. For each computed spectrum the frequencies with highest, second highest, and third highest power density are indicated by a circle, triangle, and plus sign, respectively. The pattern of these symbols establishes the basic dispersion curves; the individual spectra give additional information about the signal bandwidth along the dispersion curves. The actual dispersion curves are given in solid lines.

We observe from Figure II-1 that the dispersion of a single linear chirp waveform is described adequately by the spectra of Figure II-1b; the peaks are well defined and narrow and accurately follow the actual dispersion curve. Increasing the number of lags leads to spurious peaks as shown by the spectra in Figures II-1c, II-1d, and II-1e. In Figure II-1c this causes

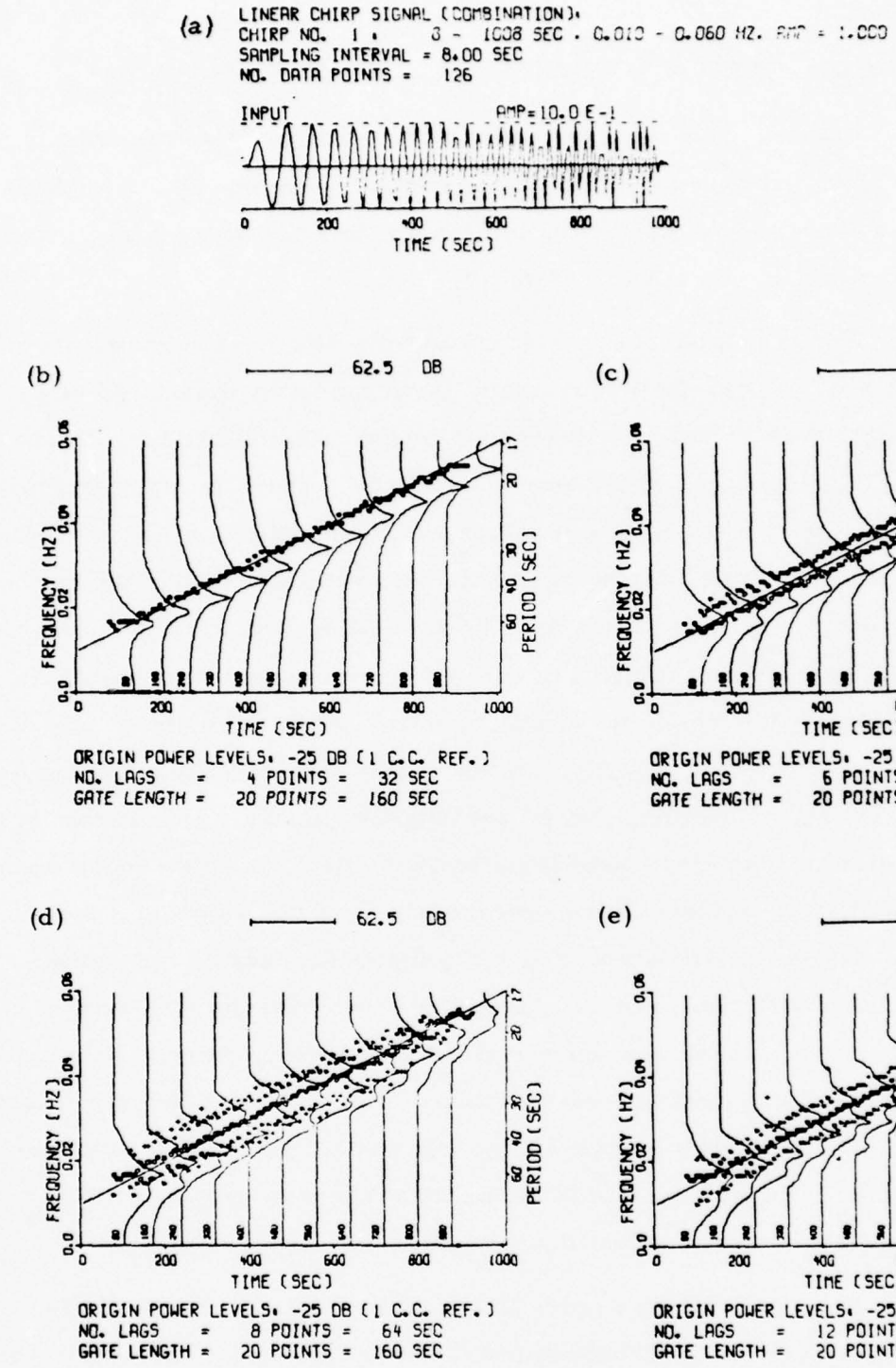

FIGURE II-1

MES PARAMETER ANALYSIS: SPECTRAL VARIATION AS A FUNCTION OF THE NUMBER OF LAGS FOR A SINGLE LINEAR CHIRP WAVEFORM

(a) LINEAR CHIRP SIGNAL (COMBINATION).
CHIRP NO. 1 . 8 - 1008 SEC . 0.010 - 0.060 HZ. AMP = 1.000
CHIRP NO. 2 . 208 - 1008 SEC . 0.040 - 0.040 HZ. AMP = 1.000
SAMPLING INTERVAL = 8.00 SEC
NO. DATA POINTS = 126

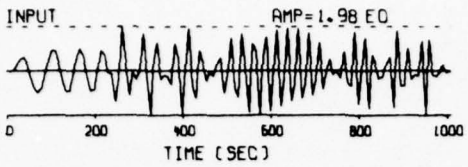

(b) 62.5 DB

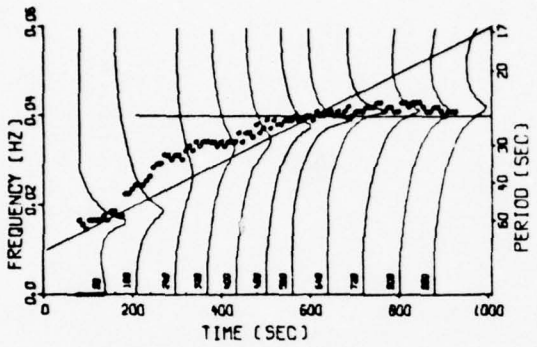

ORIGIN POWER LEVELS. -25 DB (1 C.C. REF.)
NO. LAGS = 4 POINTS = 32 SEC
GATE LENGTH = 20 POINTS = 160 SEC

(c) 62.5 DB

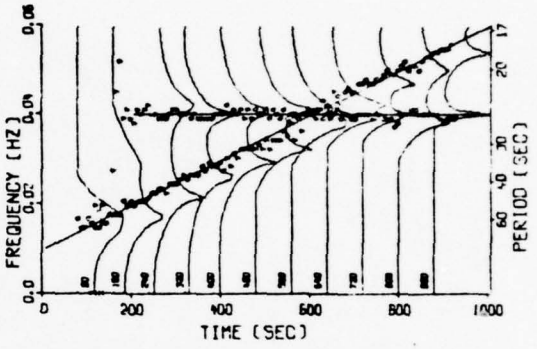

ORIGIN POWER LEVELS. -25 DB (1 C.C. REF.)
NO. LAGS = 6 POINTS = 48 SEC
GATE LENGTH = 20 POINTS = 160 SEC

(d) 62.5 DB

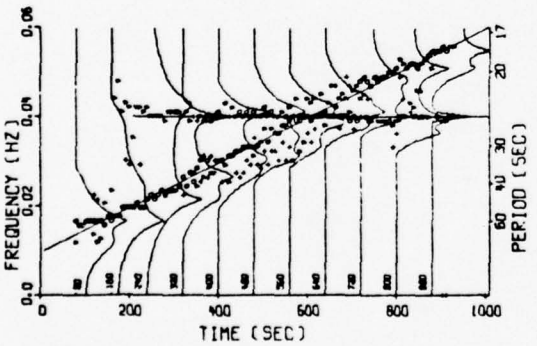

ORIGIN POWER LEVELS. -25 DB (1 C.C. REF.)
NO. LAGS = 8 POINTS = 64 SEC
GATE LENGTH = 20 POINTS = 160 SEC

(e) 62.5 DB

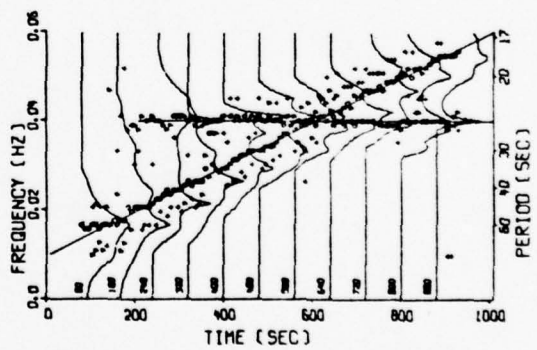

ORIGIN POWER LEVELS. -25 DB (1 C.C. REF.)
NO. LAGS = 12 POINTS = 96 SEC
GATE LENGTH = 20 POINTS = 160 SEC

FIGURE II-2

MES PARAMETER ANALYSIS: SPECTRAL VARIATION AS A FUNCTION OF THE NUMBER OF LAGS FOR TWO SIMULTANEOUS WAVEFORMS

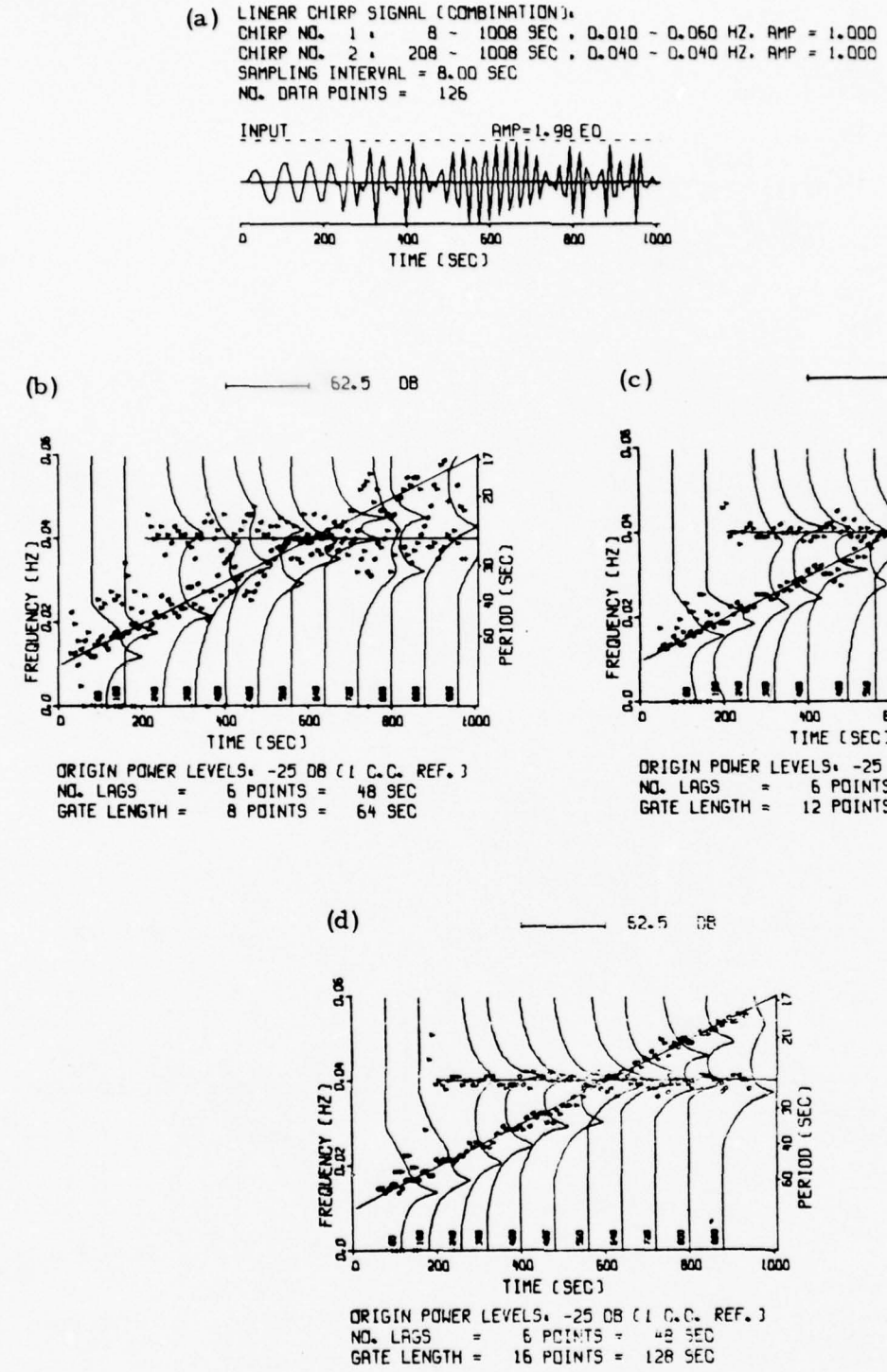

FIGURE II-3

MES PARAMETER ANALYSIS: SPECTRAL VARIATION AS A FUNCTION OF GATE LENGTH

(a) LINEAR CHIRP SIGNAL (COMBINATION):
CHIRP NO. 1 : 2 - 1002 SEC . 0.010 - 0.060 HZ. AMP = 1.000
CHIRP NO. 2 : 202 - 1002 SEC . 0.040 - 0.040 HZ. AMP = 1.000
SAMPLING INTERVAL = 2.00 SEC
NO. DATA POINTS = 501

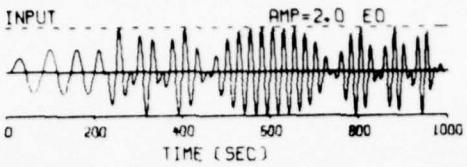

(b) 62.5 DB

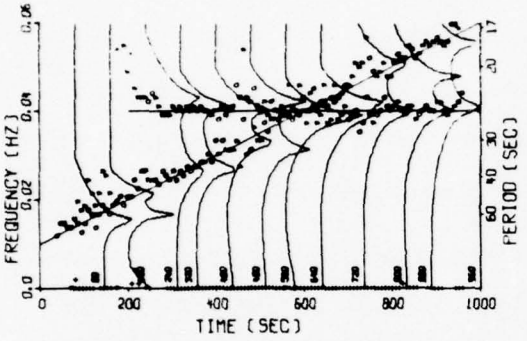

ORIGIN POWER LEVELS: -25 DB (1 C.C. REF.)
NO. LAGS = 6 POINTS = 12 SEC
GATE LENGTH = 40 POINTS = 80 SEC

(c) 62.5 DB

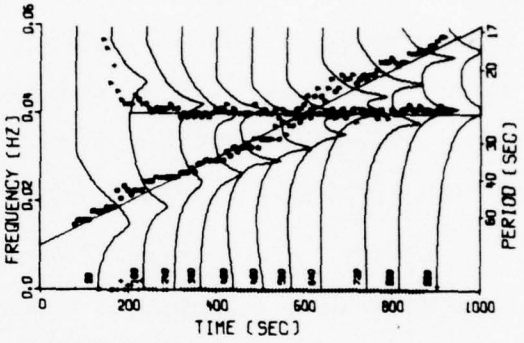

ORIGIN POWER LEVELS: -25 DB (1 C.C. REF.)
NO. LAGS = 6 POINTS = 12 SEC
GATE LENGTH = 80 POINTS = 160 SEC

(d) 62.5 DB

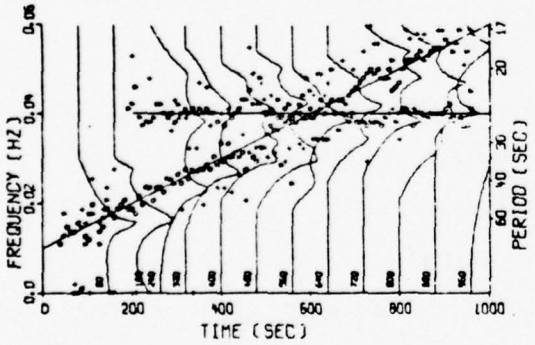

ORIGIN POWER LEVELS: -25 DB (1 C.C. REF.)
NO. LAGS = 12 POINTS = 24 SEC
GATE LENGTH = 40 POINTS = 80 SEC

(e) 62.5 DB

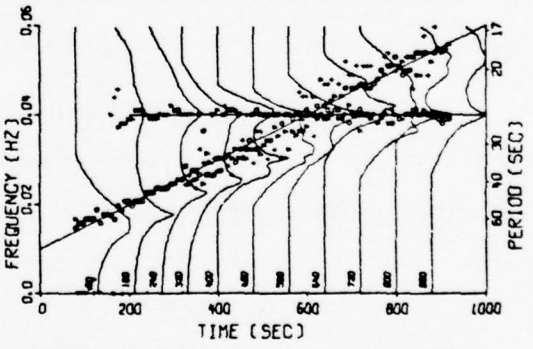

ORIGIN POWER LEVELS: -25 DB (1 C.C. REF.)
NO. LAGS = 12 POINTS = 24 SEC
GATE LENGTH = 80 POINTS = 160 SEC

FIGURE II-4

MES PARAMETER ANALYSIS: EFFECTS OF A HIGHER SAMPLING RATE

ambiguity and inaccuracy in the description of the dispersion curve; in Figures II-1d and II-1e it suggests the presence of multiple signals with parallel dispersions in addition to the waveform actually present.

Figure II-2 shows the spectra for a combination of two waveforms: the same linear chirp waveform as used in Figure II-1, plus a monochromatic waveform starting 200 seconds later. We notice that four lags are not sufficient to describe the dual dispersion. The spectra obtained with six lags, however, adequately describes and delineates the two curves and especially at the intersection show sufficient resolution power. Again, increasing the number of lags leads to spurious spectral peaks beyond those that correctly follow the dispersion curves, with Figure II-2e possibly suggesting the presence of a third, weaker waveform dispersed in parallel to the first one.

The spectra of Figure II-3 were obtained using shorter waveform windows in combination with the six lags found to be adequate in the previous figure. We observe that shortening the gates causes more scatter in the description of the dispersion curves.

Next, in Figure II-4, we investigate the effect of using a higher sampling rate. Probably because of the fact that the data points are not independent, this does not allow us to use shorter time gates, despite the fact that a greater number of waveform points is used.

Thus, summarizing the effects of various parameter combinations on the spectra of known waveform combinations, it appears that applying the Nyquist sampling rate (8-second period or 0.125-Hz sampling rate for a 0.06-Hz signal cut-off frequency) and using a 160-second time gate, in combination with six auto-correlation lags in the MES computations, adequately describe and separate the dispersion curves of two simultaneously occurring signals. For a single signal only four lags should be used. It is also possible that the dispersion rate (i.e., frequency change/signal length) affects the MES. This was not investigated in this study.

Now the problem arises that with real signals we do not know how many spectral peaks are authentically present at a given time, so that we do not know how many lags to use to adequately describe the various, and variant number of, spectral peaks. For instance, LP waveforms, in general, consist of multipath signals, may contain higher modes, and are affected by noise which in itself may possess several (possibly non-stationary) spectral peaks. There does not seem to be a ready solution to this problem, and the best that one can do, therefore, is to experiment with the parameters and to accept the most plausible outcome. This means that the specification of regional dispersion curves is highly subject to an analyst's spectral interpretation.

As an example, we will investigate the Love wave beam spectra of one of the Sinkiang region's strong events for various numbers of lags, as given in Figure II-5. To a large extent, it is difficult to decide which spectral peaks are spurious and which ones are not. But there is sufficient consistency in the patterns of Figures II-5c, II-5d, and II-5e to suggest that at least two main dispersion branches are present. Since the SNR is high, about 30 dB RMS*, the noise is probably of minor influence. For the purpose of this study,this analyst settled for the spectra of Figure II-5c, thus assuming that basically two dispersion curves are simultaneously present for at least part of the time.

Accordingly, the 8-second sampling time, a 160-second gate, and six auto-correlation lags will be used in the further spectral analysis of signals. The use of this parameter combination, however, may cause spurious peaks to appear where, in reality, only a single spectral peak is present; and it may cause spectral inaccuracies where, in fact, there are more than two peaks.

---

* RMS SNR (in dB) $= 20 \log \frac{\text{RMSS}}{\text{RMSN}} = 10 \log \frac{\text{mean signal power}}{\text{mean noise power}}$; see Sec. IV.

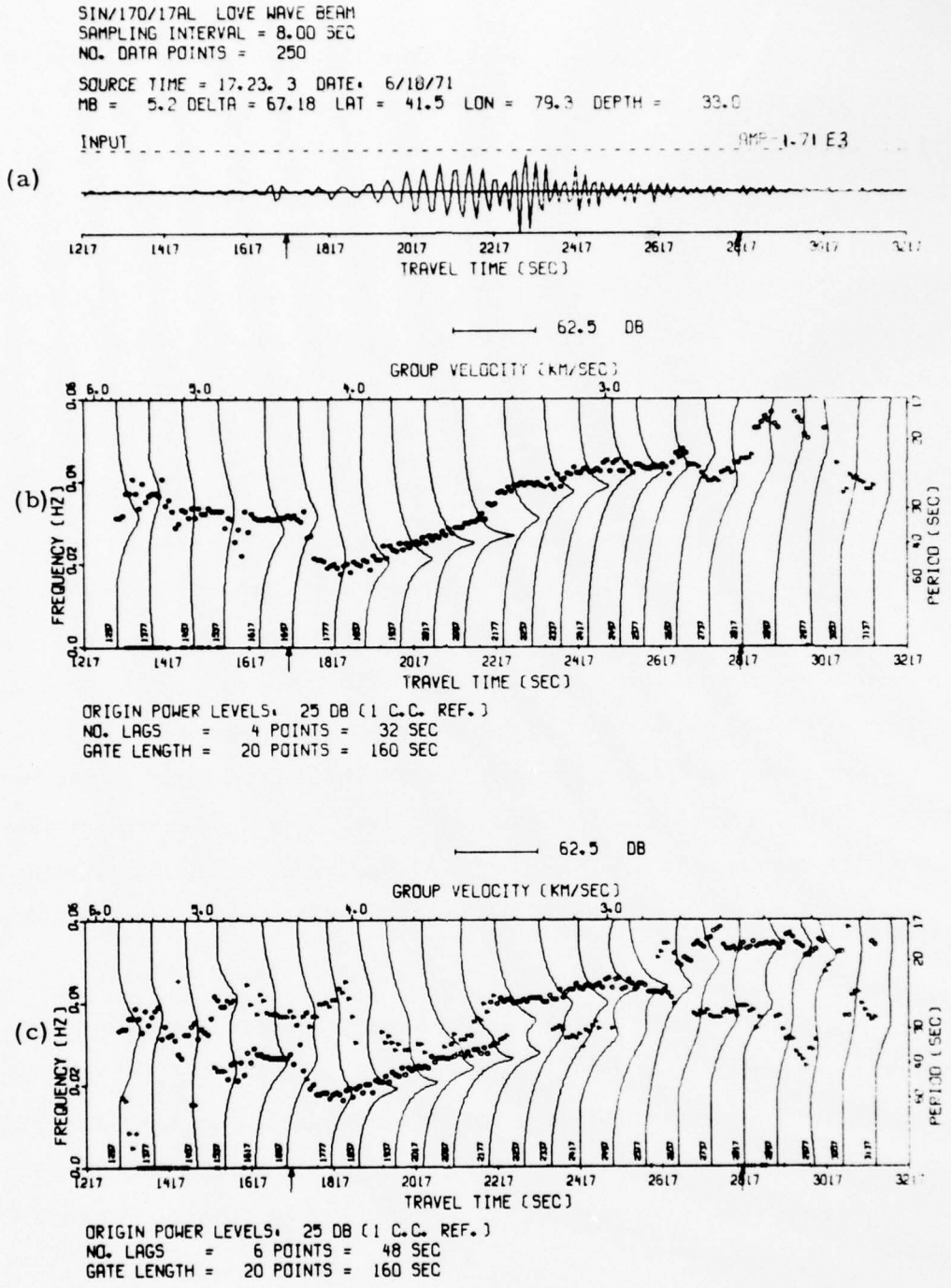

FIGURE II-5

MES PARAMETER ANALYSIS: REAL DATA
(PAGE 1 OF 2)

(d)

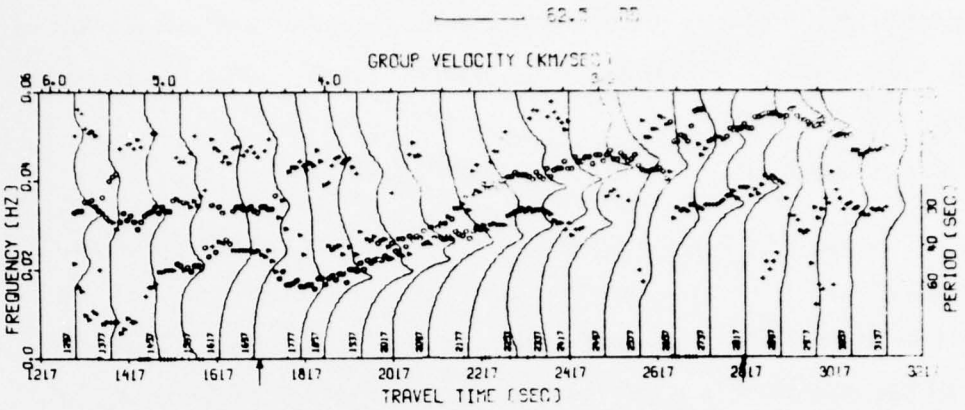

ORIGIN POWER LEVELS: 25 DB (1 C.C. REF.)
NO. LAGS = 8 POINTS = 64 SEC
GATE LENGTH = 20 POINTS = 160 SEC

(e)

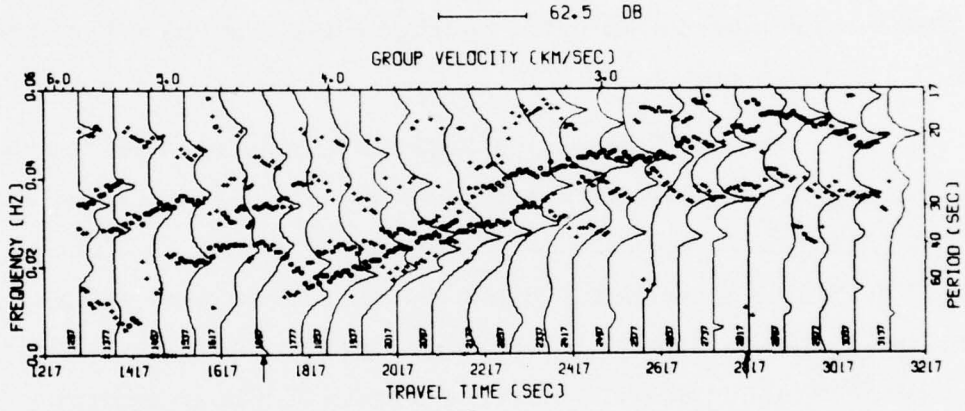

ORIGIN POWER LEVELS: 25 DB (1 C.C. REF.)
NO. LAGS = 12 POINTS = 96 SEC
GATE LENGTH = 20 POINTS = 160 SEC

FIGURE II-5

MES PARAMETER ANALYSIS: REAL DATA
(PAGE 2 OF 2)

Since the noise spectra may authentically contain more than two peaks, the noise spectral analysis may require a different set of parameters. This is investigated in the noise spectral analysis subsection.

C. SINKIANG REGION DISPERSION ANALYSIS

MES analysis using the parameters established in the previous subsection was performed on the Love wave beams of some of the stronger events of the Sinkiang data base presented in Table II-1. This data base is part of the one used in a previous matched filter study (Unger, 1973). The results of that study indicate a good correlation between the signals of these events. The distance between event epicenters is less than 300 km (Figure II-6); their great circle epicentral azimuths toward ALPA differ by less than 2°. The event numbers used in the matched filter study have been adopted in Table II-1 and in Figure II-6.

Figure II-7 shows the dispersion, both as moving-window spectra plots and as group velocity curves derived from these spectra, for the event SIN/170/17AL, which was used as a reference event in the matched filter study. Figure II-8 presents the signal spectra of four other relatively strong events; their reference power levels are indicated. The figures are aligned with respect to their dispersion curves. Figure II-9 is an overlay of the dispersion curves of these five events. Since for each event the group velocity scale and the travel time are slightly different, the group velocity and travel time scales of event SIN/170/17AL were taken as references in this picture and in the discussion to follow.

We observe that for each event individually the dispersion is rather complex. However, over most of the signal duration - i.e., between roughly 4.1 and 2.9 km/sec group velocity - the five events show considerable consistency. In the lower frequency part, from 0.016 Hz to 0.032 Hz (between 4.1 and 3.3 km/sec group velocity) the regional dispersion seems

TABLE II-1

COLLECTION OF SINKIANG PROVINCE EVENTS

Event Number	Event Name	Location		Δ^o	Az^o	Depth (km)	m_b and Data**) Source	No. Good Sites	Distance to Reference Event (km)
		Lat N	Lon E						
1	SIN/167/13AL	41.3	79.3	67.4	-36.6	33	5.1 P	4	22
2	SIN/168/15AL	41.3	79.4	67.3	-36.6	33	4.9 P	9	24
3 *)	SIN/170/17AL	41.5	79.3	67.2	-36.5	33	5.2 P	10	0
5	SIN*184*04AL	41.3	79.3	67.4	-36.6	17	4.9 P	14	22
12	SIN*181*13AL	39.0	79.0	69.6	-37.1	--	4.6	12	279
13	SIN-042-05QD	39.9	77.4	69.2	-35.6	23	4.9 P	8	234
14	SIN-047-23QC	41.7	80.7	66.6	-37.5	29	4.8 P	12	118
15	SIN-064-04AL	40.2	79.0	68.5	-36.9	--	4.5 I	15	147

*) Reference Event

**) Data Source: P = P.D.E. listing; I = International Seismic Bulletin; blank = unknown

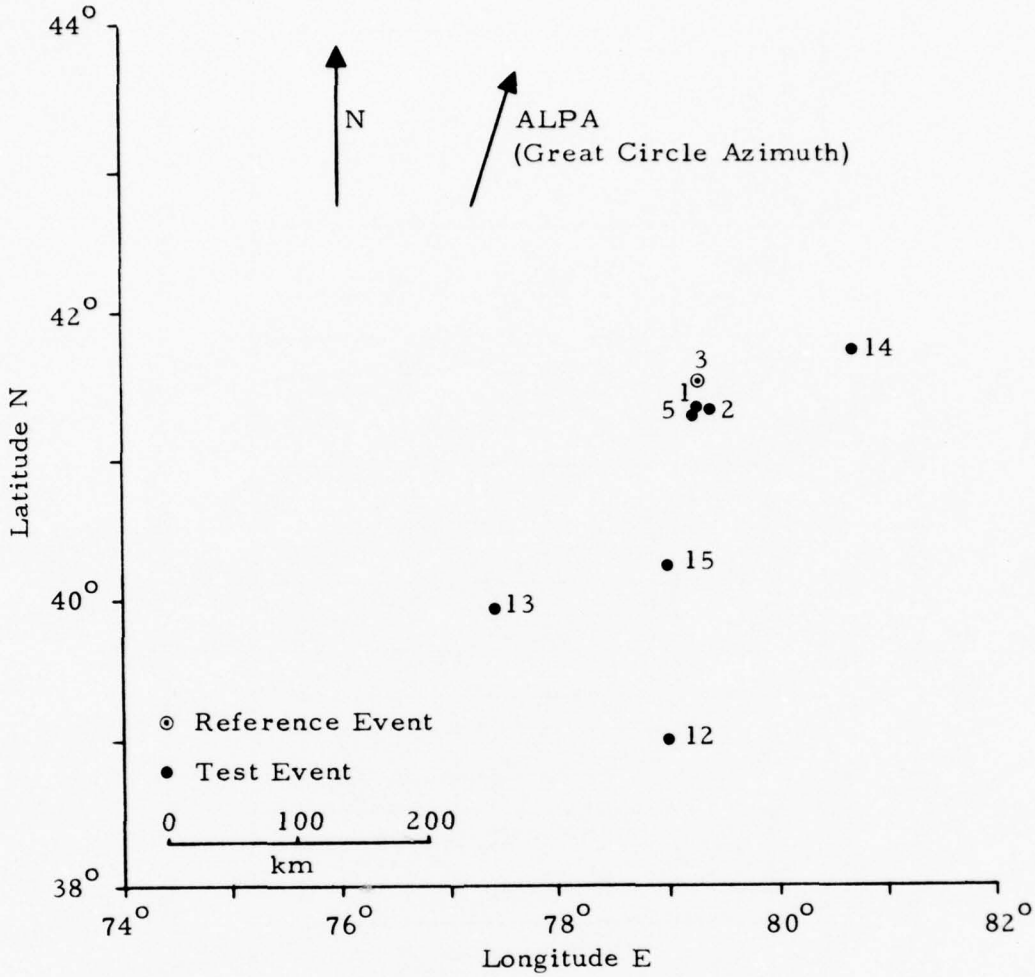

FIGURE II-6

LOCATION OF EVENTS, SINKIANG PROVINCE

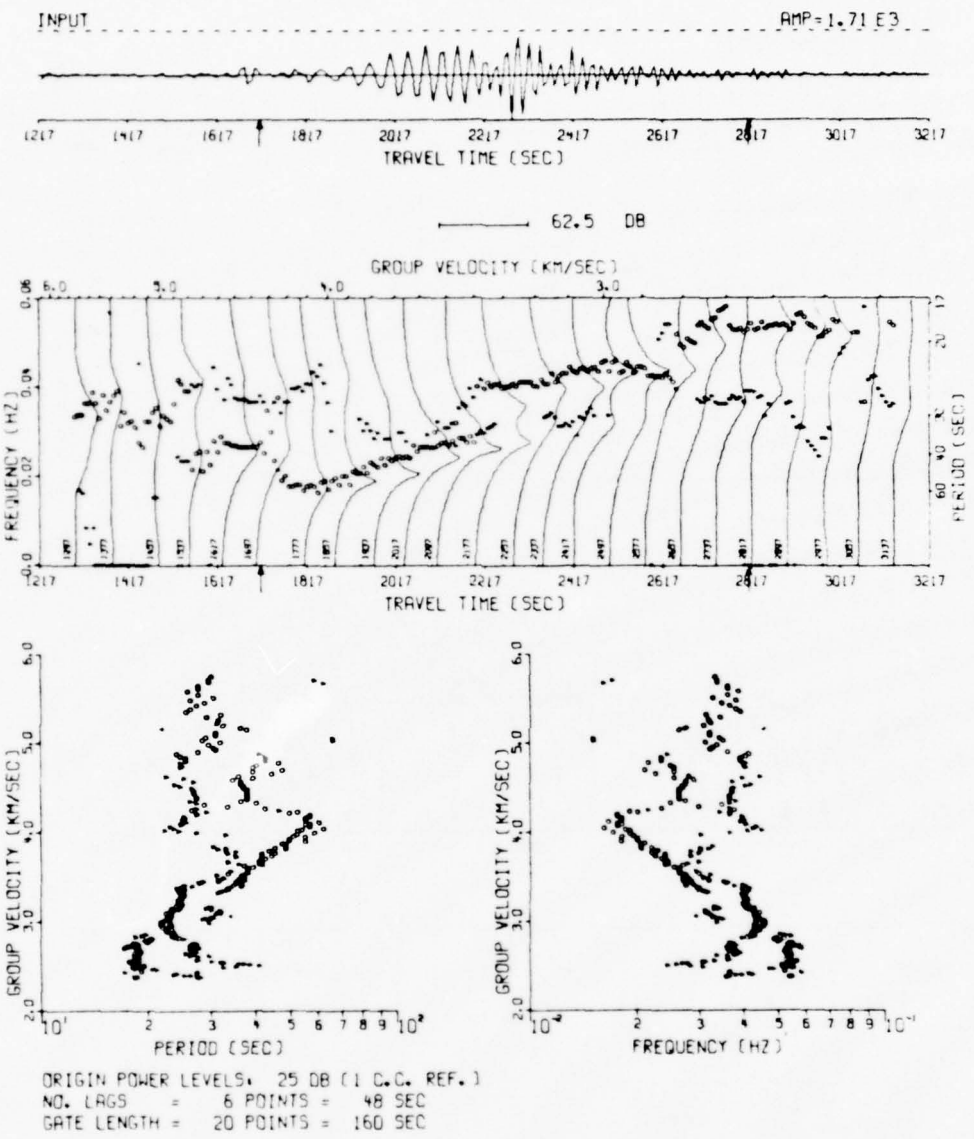

FIGURE II-7

SINKIANG REGION DISPERSION

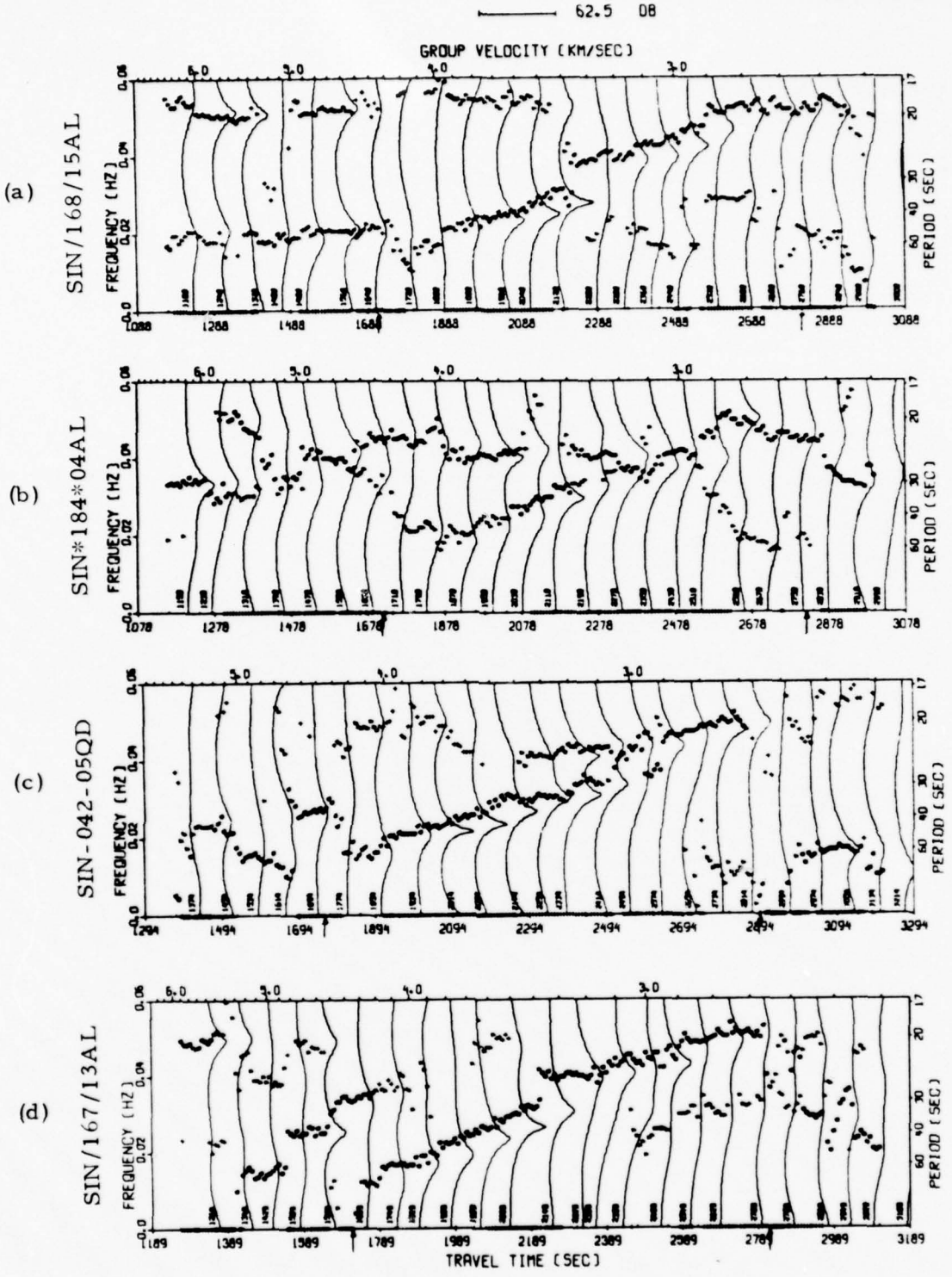

FIGURE II-8

SINKIANG REGION DISPERSION

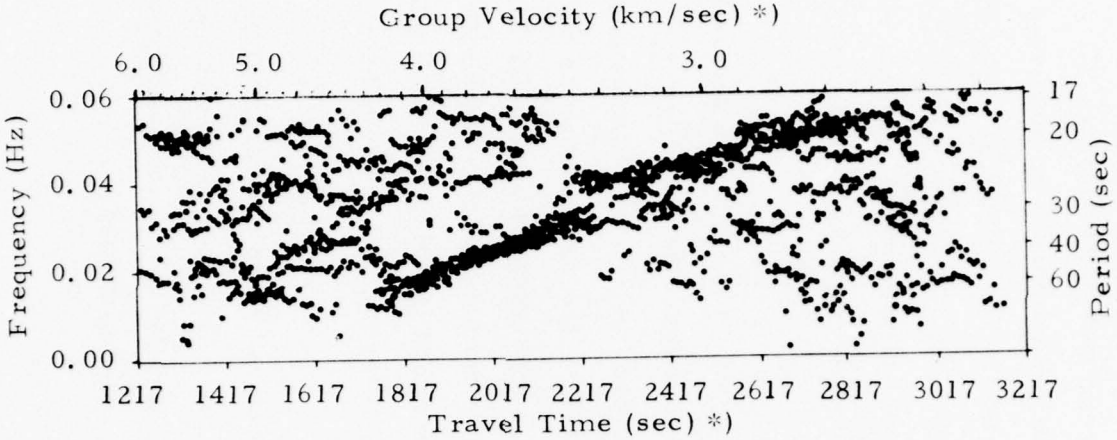

*) scales taken from spectra of SIN/170/17AL (Figure II-7)

FIGURE II-9

OVERLAY OF SINKIANG REGION DISPERSION CURVES

well defined and relatively narrow (less than 0.005 Hz variation). This part is followed by a discontinuity near 3.4 km/sec where a branch with almost zero dispersion about 0.040 Hz occurs. This branch terminates approximately where a third branch (perhaps a continuation of the first one) of higher frequencies seems to start up (near 3.1 km/sec). At the 3.4 km/sec discontinuity, both the signal bandwidth and the spectral uncertainty (reflected by the amount of scatter in Figure II-9) appear to have increased. For each individual event there seems to be additional structure beyond the dispersion curves or branches described here, but the overlay picture does not show this structure to be very consistent. The spectral analysis method as applied here apparently is not capable of resolving possible multiple signals in the coda.

An extensive discussion on the possible seismological causes and the plausibility of the measured dispersion structure is beyond the scope of this report. For this study's objective - i.e., to demonstrate the feasibility of dispersion-related filtering - the main feature is the establishment of a dispersion pattern which to a large extent is regionally consistent. This same feature, of course, is used in the concept of matched filtering. In this respect, linear chirp waveform matched filtering is probably less successful than reference waveform matched filtering, due to the presence of more than one dispersion branch.

Since the "no-dispersion" branch about 0.040 Hz resembles part of an oceanic group velocity curve (although shifted in frequency, Figure II-10), we should mention the fact that the 67° great circle propagation path includes a 10° to 15° span over the Arctic Ocean.

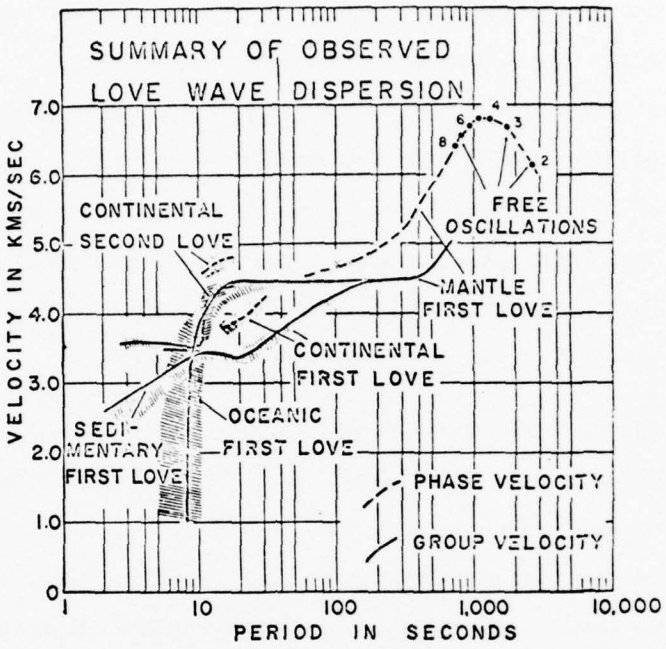

FIGURE II-10

LOVE WAVE DISPERSION (OLIVER, 1962)

D. NOISE SPECTRAL ANALYSIS

The Wiener filter requires the expected values of the noise power densities present at each point during signal reception (Section III). One way of obtaining these expected values is to assume the noise to be stationary over an interval of about four times the signal duration, and to measure the power density spectrum of a relatively large noise gate preceding the signal. Another method would be to assume the noise to be long term (at least seasonally) stationary, and to average the spectra over an ensemble of typical (seasonal) noise samples. Because of time limitations, we will not be able to verify which method would give the best results, and we will proceed with investigating the less time consuming first method.

Thus, we will examine the relatively short term stationarity of a typical noise sample. Later, in Section IV, we will use this same noise sample in the actual testing of the dispersion-relation filter. First, however, we must evaluate which parameters to use in the MES noise analysis, since we do not know a priori how many distinct spectral peaks will authentically be present at a given time in the noise sample.

Figure II-11 shows the spectral analysis for various MES parameter combinations, of the first 2000 seconds of a typical 3800-second ALPA horizontal component, north-looking beam noise sample, low-pass filtered (with a fourth-order Butterworth filter) at 0.06 Hz, and sampled every 8 seconds. A plausible result seems to be obtained with a 160-second gate and a number of either 8, 10, or 12 auto-correlation lags. These patterns show a good consistency; yet they give some idea of the degree of non-stationarity, under the (somewhat ambiguous) assumption that three to five peaks describe the moving-window spectra more or less adequately. We will choose ten lags for this analysis.

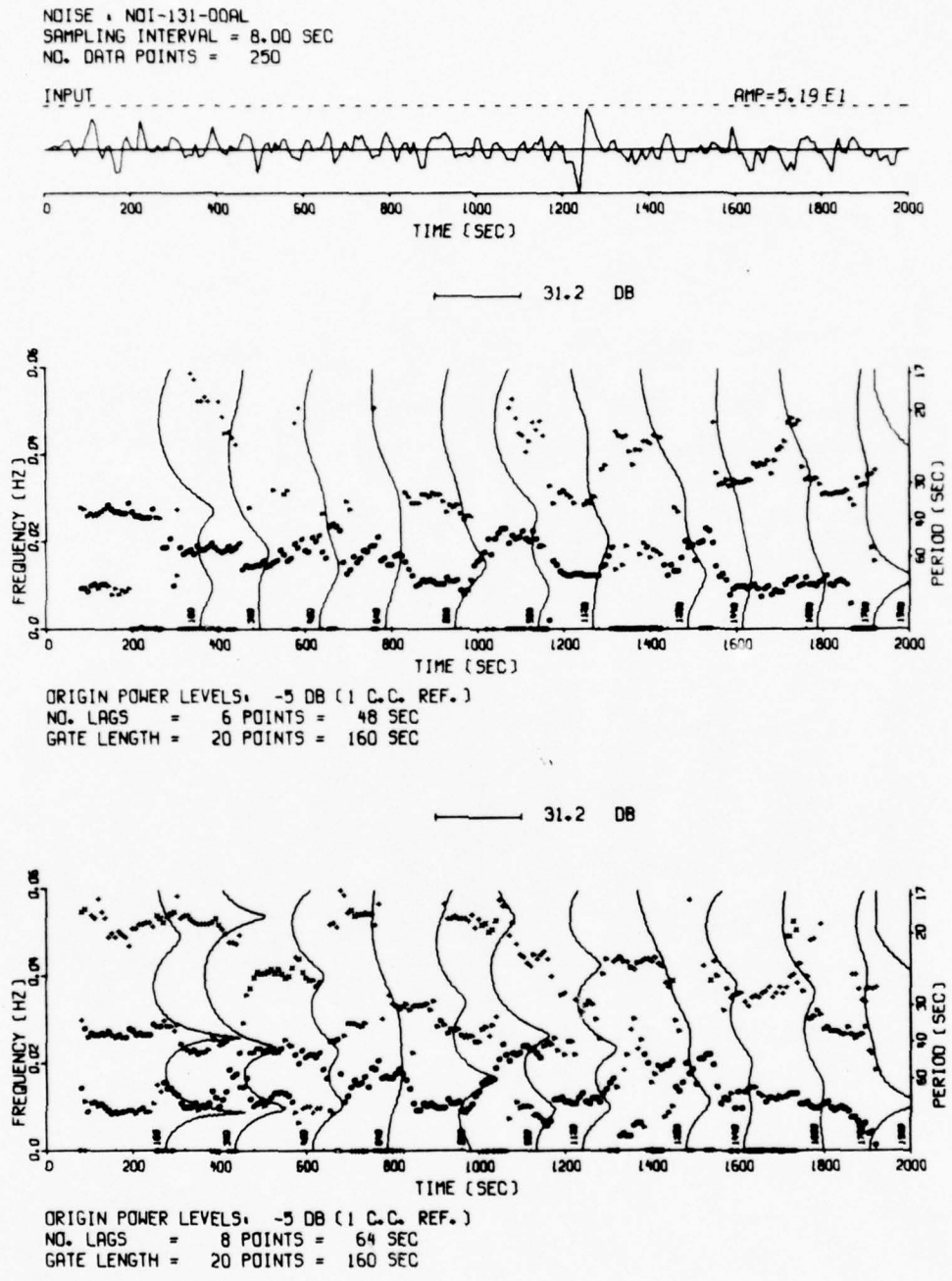

FIGURE II-11

NOISE SPECTRA FOR VARIOUS MES PARAMETER COMBINATIONS
(PAGE 1 OF 2)

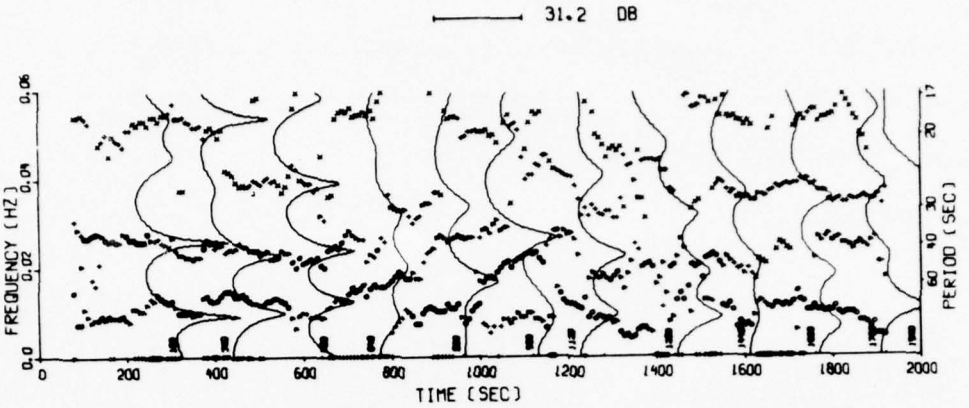

ORIGIN POWER LEVELS: -5 DB (1 C.C. REF.)
NO. LAGS = 10 POINTS = 80 SEC
GATE LENGTH = 20 POINTS = 160 SEC

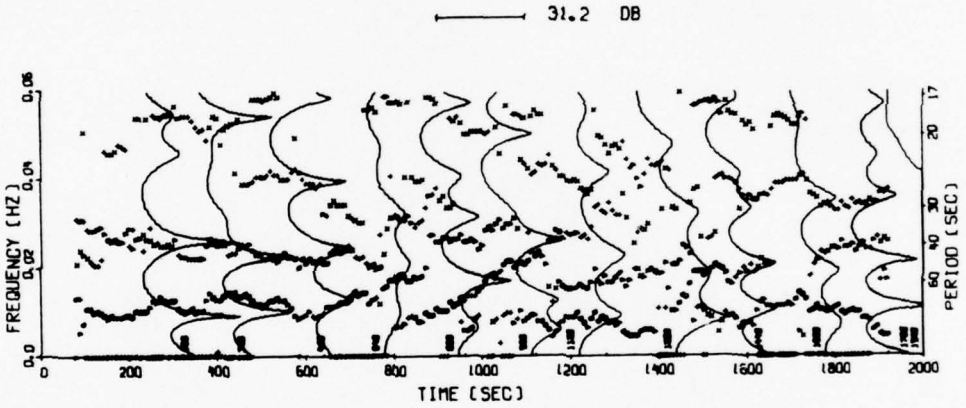

ORIGIN POWER LEVELS: -5 DB (1 C.C. REF.)
NO. LAGS = 12 POINTS = 96 SEC
GATE LENGTH = 20 POINTS = 160 SEC

FIGURE II-11

NOISE SPECTRA FOR VARIOUS MES PARAMETER COMBINATIONS
(PAGE 2 OF 2)

The spectra clearly show that there is significant variation, both in the distribution of the peaks over frequency, as well as in the peak magnitude and gate average power levels. Note that the plotted spectra are independent; i.e., they were computed from non-overlapping time gates.

Figure II-12 is the MES measured from the first 1400 seconds (a time interval corresponding to the noise gate in general available before the first P-wave arrival on ALPA records) of this noise sample. This spectrum is the expected power density spectrum for each point of the noise occurring in the last 1800 seconds, assuming a signal would be present in the latter interval. We will now investigate how well this estimate qualifies.

Figure II-13 shows the 160-second moving-window noise spectra of the second part of the noise sample. For comparison, the expected spectrum has been drawn in as a dotted curve. We observe power density deviations typically on the order of 6 dB (occasionally as much as 15 dB). In the Wiener filter design discussion in Section III, we will see how these deviations affect the filter performance.

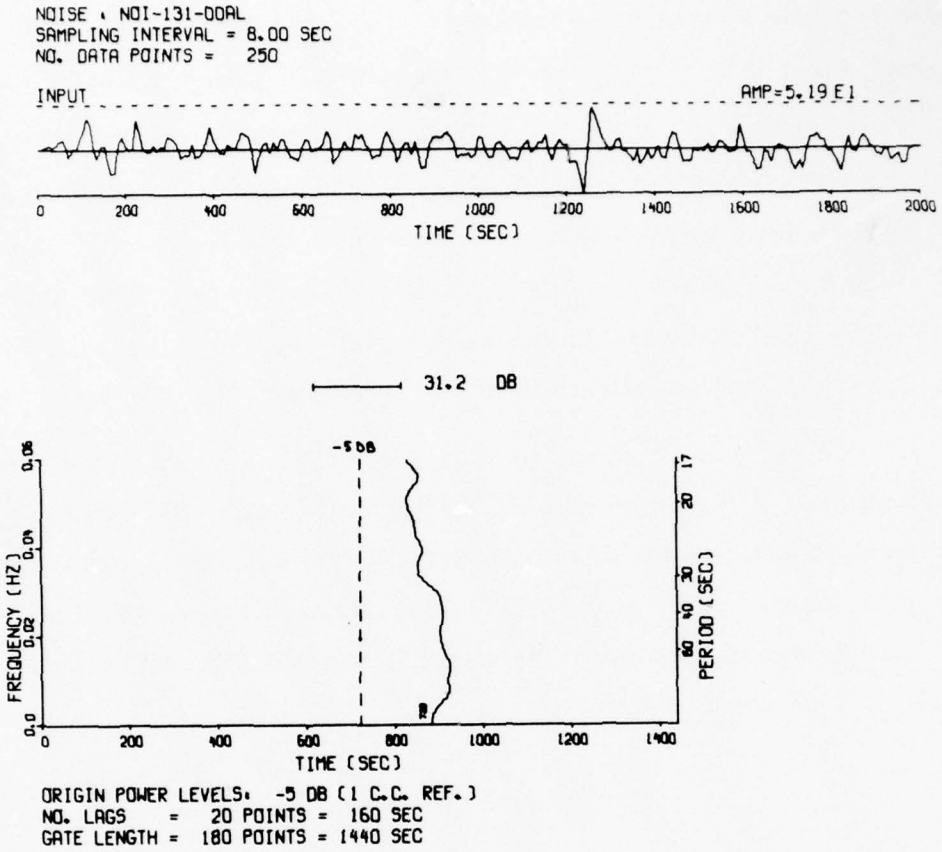

FIGURE II-12

EXPECTED NOISE SPECTRUM

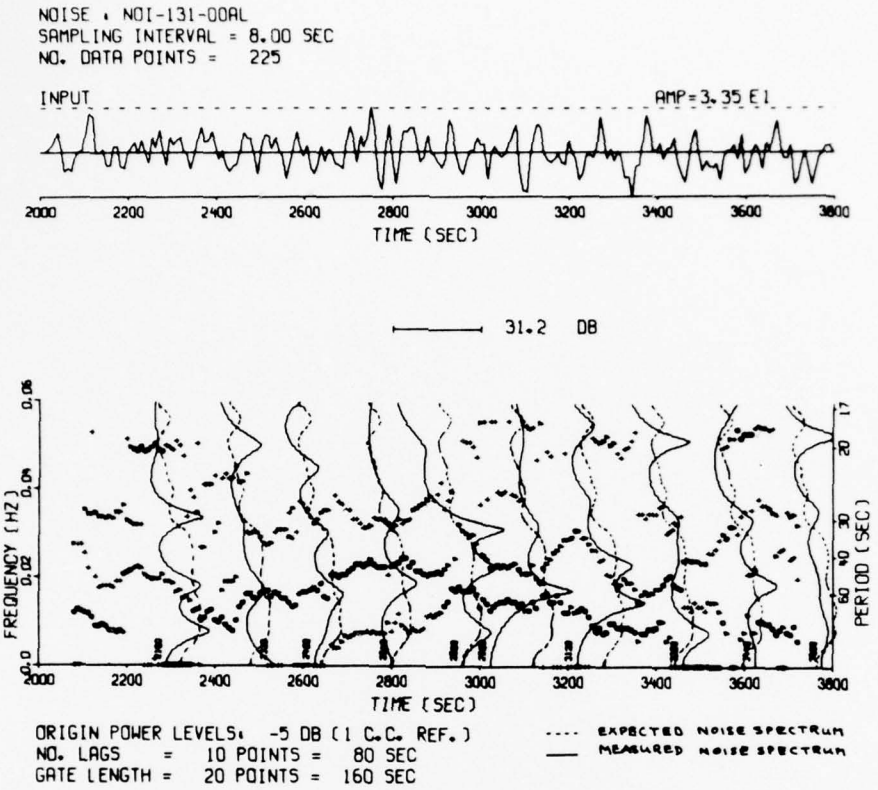

FIGURE II-13

DEVIATION OF MOVING-WINDOW SPECTRA FROM EXPECTED NOISE SPECTRUM

SECTION III
FILTER DESIGN

A. INTRODUCTION

This section presents the dispersion-related filtering (DRF) and time-variant Wiener filtering (TVWF) developments. Included are various design aspects, and the filter performance anticipation based on the results of the spectral analysis obtained in the previous section. Subsection B discusses the basic DRF design; Subsection C presents the TVWF process.

B. DISPERSION-RELATED FILTERING

Dispersion-related filtering can be performed as a sampled, time-variant convolution along the signal's presumed dispersion curve:

$$y(t) = \sum_{n=1}^{N} \left[x(t) * h(n, t) \right] \cdot \delta(t - n \cdot \Delta t) \qquad \text{(III-1)}$$

where

- $y(t)$ is the DRF output,
- $x(t)$ is the DRF input,
- $h(n,t)$ is the DRF impulse response at time $n \cdot \Delta t$,
- $\delta(t)$ is the Dirac function,
- N is the number of dispersion curve time points,
- Δt is the sampling interval.

In our DRF implementation the convolution is performed via the frequency domain:

$$y(t) = \sum_{n=1}^{N} \left\{ F^{-1}\left[X(j\omega) \cdot (H(n,\omega)) \right] \right\} \cdot \delta(t - n \cdot \Delta t) \qquad \text{(III-2)}$$

where

F^{-1} denotes the inverse Fourier transformation,

$X(j\omega)$ is the Fourier transform of $X(t)$,

$H(n,\omega)$ is the (phaseless) transfer function of the narrowband filter applied at the nth dispersion point.

Thus, the DRF consists of a bank of narrowband filters (NBFs), in principle one NBF for each dispersion point, and the DRF output is synthesized from adjacent samples, each one taken from the output of its corresponding NBF. This process involves one forward Fourier transform and in principle N inverse transforms. However, at points where the NBF specification remains unchanged (for instance, if part of the dispersion curve is flat), the same NBF output can be re-used to establish the next DRF output sample.

The shape of the NBF transfer function applied is basically rectangular; its gain equals one for the frequencies within the filter band specified, except for a 0.002 Hz cosine taper near the cut-off frequencies. The impulse response of a rectangular transfer function with bandwidth W Hz has a sin x/x envelope (where $x = \pi W t$) with zeros occurring every $1/W$ seconds from the maximum. The cosine taper serves to reduce the amplitude of the impulse response sidelobe; however, it also changes an originally specified bandwidth of W_0 Hz into an effective bandwidth of approximately $W = W_0 - 0.002$ Hz, and may change slightly the shape of the impulse response also in other aspects.

To specify the desired dispersion band, the user inputs several dispersion band points as x-y coordinates in inches, based on his measurement and interpretation of the moving-window signal spectra. These points are

then interpolated, either in a linear or in a quadratic fashion as specified, to establish the total dispersion band to be used by the DRF. In the case of a linear chirp waveform, a constant bandwidth of linearly increasing center frequencies can be applied. However, real data, at least as shown by the Sinkiang region dispersion, dictate the need for a dispersion band which varies in width along the dispersion curve.

The DRF process is illustrated with the filtering of a linear chirp waveform in Figure III-1. Figure III-1a presents the dispersion band applied in the DRF; Figure III-1b shows the original waveform; Figures III-1c, III-1d, and III-1e are the respective NBF outputs for three equally spaced points along the dispersion curve; Figure III-1f is the DRF output; Figure III-1g is the error trace obtained by subtracting the signal from the DRF output. All traces are plotted on the same scale. Note the character of the NBF outputs; they consist of a main lobe and reduced sidelobes; the node interval (approximately 350 seconds) corresponds to a 0.003 Hz effective (0.005 Hz specified) filter bandwidth. The NBF output data samples which synthesize the DRF output are indicated with arrows and dots. A correction factor, required in the narrowband filtering of time-variant waveforms (explained later in the text and in Appendix A), was used in generating the NBF outputs.

We observe that the original waveform is reproduced fairly accurately; there is some distortion due to NBF end effects. The first and last sample of the DRF output waveform, at 500 and 1500 seconds, respectively, should equal zero, but the NBF is not infinitessimally narrow, thus permitting the signal energy at neighboring frequencies to pass through and to establish non-zero values at those points. On the other hand, the fact that, for the NBFs applied over approximately the first and last 100 seconds of the waveform, the signal energy of the neighboring frequencies on one side is missing results in signal underestimation over those intervals. We furthermore notice some overshoot (approximately 15%) around 670 seconds and 1360 seconds, and a very small amount of ripple over the rest of the waveform.

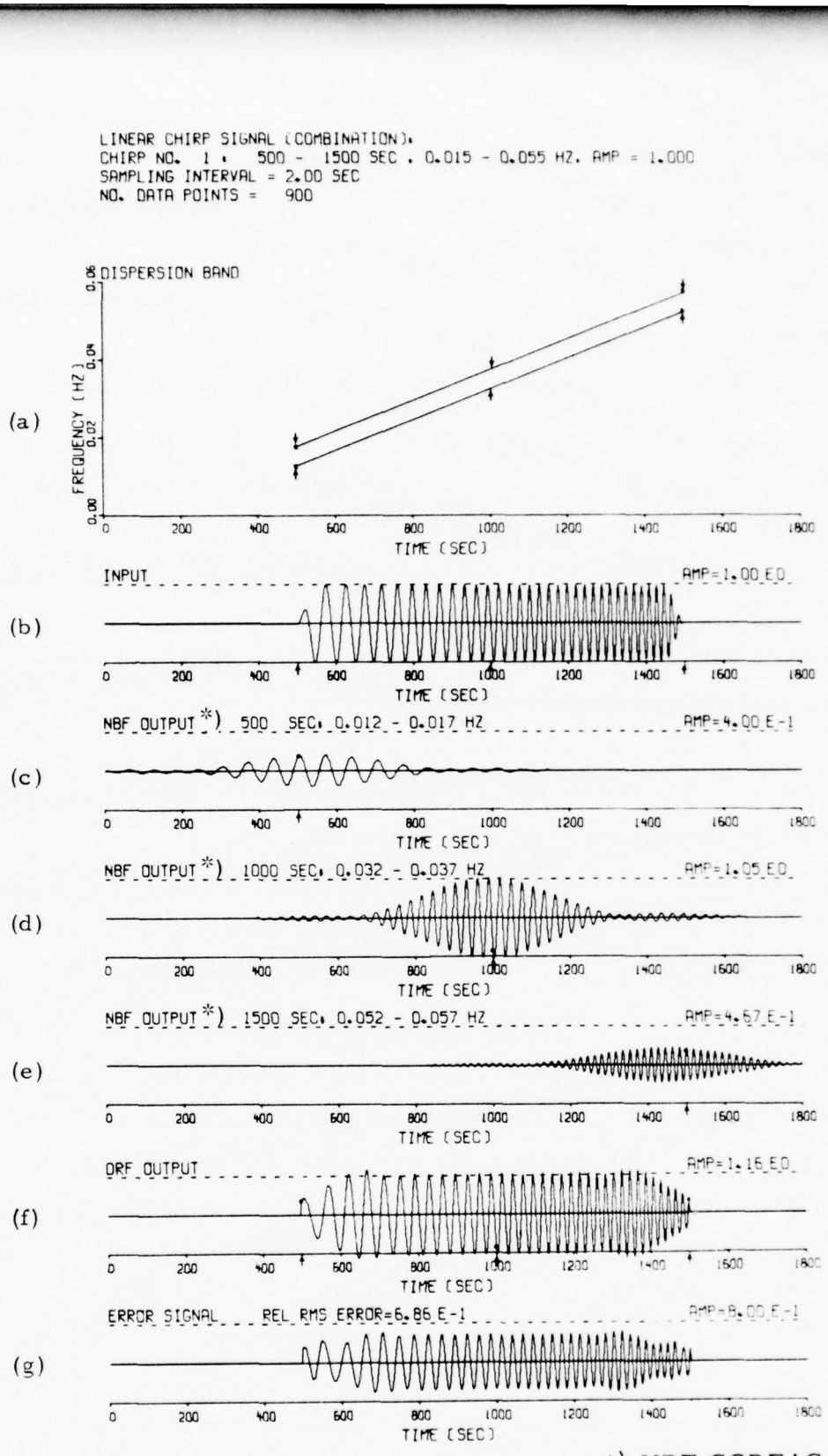

*) NBF CORFAC applied

FIGURE III-1

DRF PROCESS

The NBF process inherently produces amplitude and phase errors; these are treated in more detail in Appendix A. According to this treatment, the main cause of the NBF amplitude error is the fact that the narrowband frequency energy is distributed in the output over a relatively wide NBF response interval. This error can be corrected by applying a bandwidth and dispersion rate dependent correction factor (CORFAC). Other effects, which could not be compensated for at this point in the development, cause additional amplitude errors as well as phase errors. The magnitude of these errors seems to depend on the nature and amplitude of the input signal and on the bandwidth of the NBF applied. In Figure III-1 the amplitude error (after NBF amplitude correction) is less than 5%, excluding the overshoot at the beginning and at the end of the DRF output. The relatively large error signal displayed in Figure III-1g results mainly from the phase error, leading to an unrealistic 68.6% RMS error relative to the RMS signal. Appendix A shows that in some cases the uncorrectable part of the amplitude error can amount to 30%, i.e., 2.3 dB or 0.115 surface wave magnitude units. This potential signal distortion must be weighed against the signal estimate improvement obtained from the filter's noise rejection capability, which ranges approximately from 3 to 9 dB as will be shown next.

At each point along the dispersion curve the amount of noise rejection is determined by the width of the dispersion band specified, and by the actual distribution of noise energy over the total signal frequency band. For instance, the Sinkiang region dispersion, according to Figure II-9, requires a bandwidth of at least 0.005 Hz for the lower frequency part, and a bandwidth of possibly as much as 0.020 Hz starting at the dispersion discontinuity at 3.4 km/sec group velocity. With respect to stationary bandpass filtering over a 0.015 to 0.055 Hz signal band (0.040 Hz bandwidth), and assuming the noise to be white over that frequency band, the DRF would be capable of 10 log (0.040/0.005) = 9 dB noise rejection over the first part of

10 log (0.040/0.020) = 3 dB over the second part. However, some signal energy, contributed by frequencies outside the dispersion band applied, is possibly sacrificed in the filtering process.

These amounts of DRF noise rejection are on the same order as that of a 9-element beamsteer filter, and as the matched filter SNR gains over bandpass filtering (Capon et al., 1969; Strauss, 1973). However, it would be dangerous to use the DRF as a signal detector since it is inherently capable of generating false alarms, in the form of partial chirp waveforms, from noise, as will be shown in the filter performance analysis (Section IV). Also, the Sinkiang signals appear to have their highest amplitudes occur during the second part of the dispersion curve, where the DRF noise rejection is less.

To apply the DRF correctly we must know in advance the signal start time. The DRF design allows for "searching" the signal by sliding the dispersion band through the received waveform data, and comparing the output peak amplitudes and RMS values for each shift. Supposedly, the shift yielding the highest output values then would indicate the best time alignment between the signal and the DRF dispersion band. This, however, is either a computer time, or a computer core consuming process. Moreover, the signal spectrum uncertainty may further obscure the actual signal positions in time. The procedure works well for noise-free linear chirp waveforms, but loses its effect under marginal noise conditions (about 0 dB RMS SNR). The starting problem is further analyzed in Appendix B where alternative attempts to find a signal's start time also are described. Among these alternatives are the time-domain signal phase detection method and the MES detection method. All these methods seem to have their limit around 0 dB RMS SNR.

C. TIME-VARIANT WIENER FILTERING

The DRF reduces the error in the estimation of signals from LP waveforms by eliminating the noise energy from frequencies outside the signal dispersion band. The presence of noise from frequencies inside the dispersion band, however, still causes some interference, in general leading to signal overestimation.

A well-known technique of reducing the estimation error is Wiener filtering (WF). This filtering process minimizes the mean-square estimation error by balancing, at each frequency, the signal and noise power densities (e.g., Papoulis, 1967). If the noise is uncorrelated with the signal, the time-variant WF transfer function is:

$$H(t, \omega) = \frac{E\phi_S(t, \omega)}{E\phi_S(t, \omega) + E\phi_N(t, \omega)} \qquad \text{(III-3)}$$

where

$H(t, \omega)$ is the time variant, phaseless WF transfer function,

$E\phi_S(t, \omega)$ is the expected value of the time-variant signal power density spectrum, and

$E\phi_N(t, \omega)$ is the expected value of the time-variant noise power density spectrum.

We can also write the WF transfer function as:

$$H(t, \omega) = \frac{1}{1 + \dfrac{E\phi_N(t, \omega)}{E\phi_S(t, \omega)}} \quad . \qquad \text{(III-4)}$$

To show the effect of Wiener filtering, we will consider some hypothetical cases. For a noise-free input the WF transfer function equals one, thus passing the input waveform unchanged. If, at a given time, the

expected values of the noise and signal power densities are equal for all frequencies, the transfer function equals 0.5 for all frequencies; i.e., it is expected that in the mean, for equal noise and signal amplitudes, the best estimate is half the value of signal plus noise. If at a given time and for a given frequency, the signal power density equals twice the noise power density, then the frequency component concerned of the input waveform is attenuated with a factor 0.67. In general, for high SNRs the filter effect is little; for low SNRs the WF performs a frequency and time-dependent attenuation.

In the case of DRF we are concerned with the power density ratios within a relatively narrow band at each point in time along the signal dispersion curve. For a given region the expected values of the time-varying power densities can be obtained by taking the moving-window spectra from a strong (reference) event signal, or by averaging the spectra of strong, regional event signals. The expected value of the noise power densities can be obtained by assuming the noise to be stationary and by measuring the noise spectrum of a large input waveform gate just prior to the arrival of any signal phase, as discussed in Section II.

Since we will apply this filter to signals of different strengths and under variant noise conditions, we must adapt the spectral ratio term $E\phi_N / E\phi_S$ according to the expected SNR. This can be achieved by first normalizing the measured noise and signal spectra to unit power, i.e., dividing the power densities by the average signal and noise power, respectively, or by the squares of the signal and noise RMS values. We then multiply this term by the WF design parameter, the inverse of the square of the expected RMS SNR:

$$H(t,\omega) = \frac{1}{1 + \frac{1}{ESNR^2} \cdot \frac{P_N(\omega)}{P_S(t,\omega)}} \quad , \qquad \text{(III-5)}$$

where

$P_N(\omega)$ is the normalized, supposedly stationary noise power density spectrum,

$P_S(t,\omega)$ is the normalized, time-variant signal power density spectrum,

ESNR is the expected RMS SNR of the input waveform.

We will now investigate the WF effect when the actual power density ratios deviate from the expected ratios. These effects, calculated from Equation III-5, are shown in Figure III-2 for various true SNR situations. The values at 0 dB error are the correct WF attenuations applied to the input waveform in order to minimize the signal estimation mean-square (m.s.) error. The WF gain factor becomes more erroneous as the amount of power density ratio error increases. In the case of SNR overestimation, the WF still reduces further the DRF signal estimation error. For SNR underestimation, a point may be reached where the WF attenuation is greater than twice the correct WF attenuation, indicated by the vertical dash-dot line at 0 dB SNR error. Beyond that point, the signal estimation error caused by excessive WF attenuation is greater than the DRF signal overestimation error. The excessive WF attenuation is represented by the dotted parts of the WF gain curves. Considering this, and also the non-linearity of the curves, it is concluded that less error is made when overestimating than when underestimating the SNR.

The power density SNR deviations from the expected SNR at each frequency are caused by two factors:

- The moving-window noise spectrum fluctuations about the expected value of the noise spectrum (typically 6 dB, occasionally 10 to 15 dB).
- The misestimation of the ESNR, since it is difficult to estimate the SNR from low SNR waveforms (probably as much as 6 dB SNR error at 0 dB true SNR; larger errors for lower true SNRs).

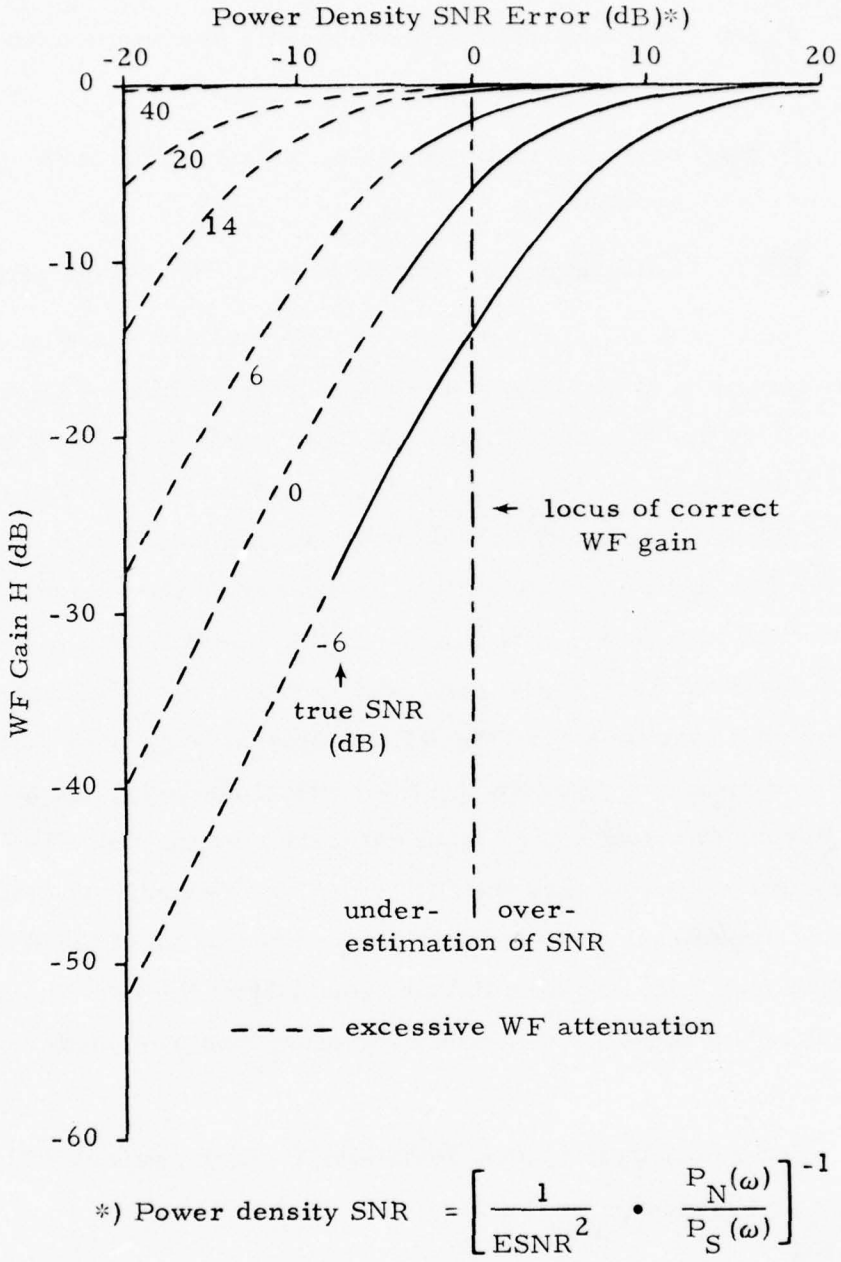

FIGURE III-2

EFFECT OF POWER DENSITY SNR ESTIMATION ERROR ON WF GAIN

Thus, the two effects combined can amount to deviations spanning the range given in the figure. In the case of a 0 dB true SNR at a given frequency, this means that the WF gain can be as much as 15 dB (a factor 5.6) too low or 6 dB (a factor 2) too high when underestimating and overestimating, respectively, the power density SNR. For lower true SNR situations, these errors are larger. For a true SNR of 14 dB or higher the WF has little effect, and is also little affected by SNR estimation errors.

This rapidly puts a limit to the general WF performance; at the lower SNRs, where improved signal estimation is desired most, the ESNR is difficult to estimate, resulting in large errors in the WF gain factor which in turn cause larger signal estimation errors. From the curves in Figure III-2 we anticipate unreliable signal estimation for waveforms with less than 0 dB RMS SNR.

For a given waveform the SNR is probably best estimated by visual comparison with waveforms obtained through simulation of various SNR situations, for instance, by burying the regional reference signal in various levels of true seismic noise. An alternative method is to deduce the SNR from the bodywave magnitude and measure the noise level just prior to signal arrivals. Because of m_b and m_b-to-M_s conversion uncertainties, the uncertainty in the ESNR value would be on the order of 10 dB, slightly less accurate than SNR estimation directly from a waveform of 0 dB true SNR, but probably equally or more accurate for lower true SNR waveforms.

A third method is to compute the RMS ratio for the expected signal and noise gates; if signal and noise are uncorrelated, the ESNR can be obtained from:

$$ESNR^2 \approx \frac{RMSSN^2}{RMSN^2} - 1 \quad , \qquad \text{(III-6)}$$

where

RMSSN = signal-plus-noise RMS value, and

RMSN = noise RMS value.

Experiments will have to be conducted to evaluate this method.

SECTION IV
FILTER PERFORMANCE EVALUATION

A. INTRODUCTION

In this section we will evaluate the performance of both the basic DRF concept and the TVWF process. First, the DRF and TVWF are applied to a linear chirp signal with added seismic noise for various SNR levels. Second, we will apply the TVWF to a Sinkiang region reference Love wave beam signal under various noise conditions, and to the waveforms containing the signals of other Sinkiang region events. In the third subsection the DRF signal separation capability is tested on a combination of synthetic signals and tried on the reference signal.

Since the Wiener filter performance is greatly affected by the power SNR, we will describe the test conditions in terms of the RMS SNR, rather than the peak-signal-to-RMS-noise ratio frequently used in seismic analysis:

$$\text{RMS SNR} = 20 \log_{10} \frac{\text{RMS sig amp}}{\text{RMS noi amp}} = 10 \log_{10} \frac{\text{mean sig power}}{\text{mean noi power}} . \qquad \text{(IV-1)}$$

For seismic signals, roughly, the RMS SNR is about 10 dB lower than the peak-to-RMS SNR and approximately equals the peak-to-peak SNR. For uniform envelope single chirp signals in seismic noise, the RMS SNR is 3 dB lower than the peak-to-RMS SNR and about 7 dB higher than the peak-to-peak SNR.

B. FILTER PERFORMANCE ON LINEAR CHIRP WAVEFORMS

Figure IV-1 shows the results of applying the basic DRF ($H(\omega, t) = 1$, followed by cosine tapering, within each NBF passband) to waveforms created by adding seismic noise to a synthetic linear chirp waveform for various SNR situations. In Figure IV-2 the DRF outputs from the low SNR input waveforms are plotted on a larger scale to show more detail. Down to 14 dB RMS SNR the DRF rather faithfully reproduces the original signal with the main distortions as mentioned in Section III: waveform tapering, followed by a 15% overshoot at the beginning, and the same phenomena in reverse sequence at the end of the waveform; some ripple along the rest of the waveform; a relatively larger error signal due to phase errors. The ripple increases with decreasing SNR due to a growing interference of signal and noise. From 6 dB SNR down the distortion increases considerably, in ripple as well as in amplitude error. The DRF output, however, always is a much better approximation of the original signal than is the unfiltered trace. Notice that the DRF produces parts of a chirp waveform from pure noise; if there is no information regarding the anticipated signal amplitude, this DRF output might be mistaken for a signal.

The TVWF performance (using the transfer function given by Equation III-5, followed by cosine tapering, within each NBF passband) on the same input waveform is displayed in Figures IV-3 and IV-4. In each SNR case, the true RMS SNR was input as the ESNR in the TVWF algorithm (see Section III). In the noise-only case a 0 dB ESNR was used to test the filter output. As anticipated, there is little difference in performance between the DRF and the TVWF for waveforms of 14 dB or higher SNR. For the lower SNR waveforms, the Wiener filter provides a better signal estimate than does the DRF; over the entire signal duration the amplitude error is smaller. Also the TVWF apparently can generate signal-like waveforms from pure noise.

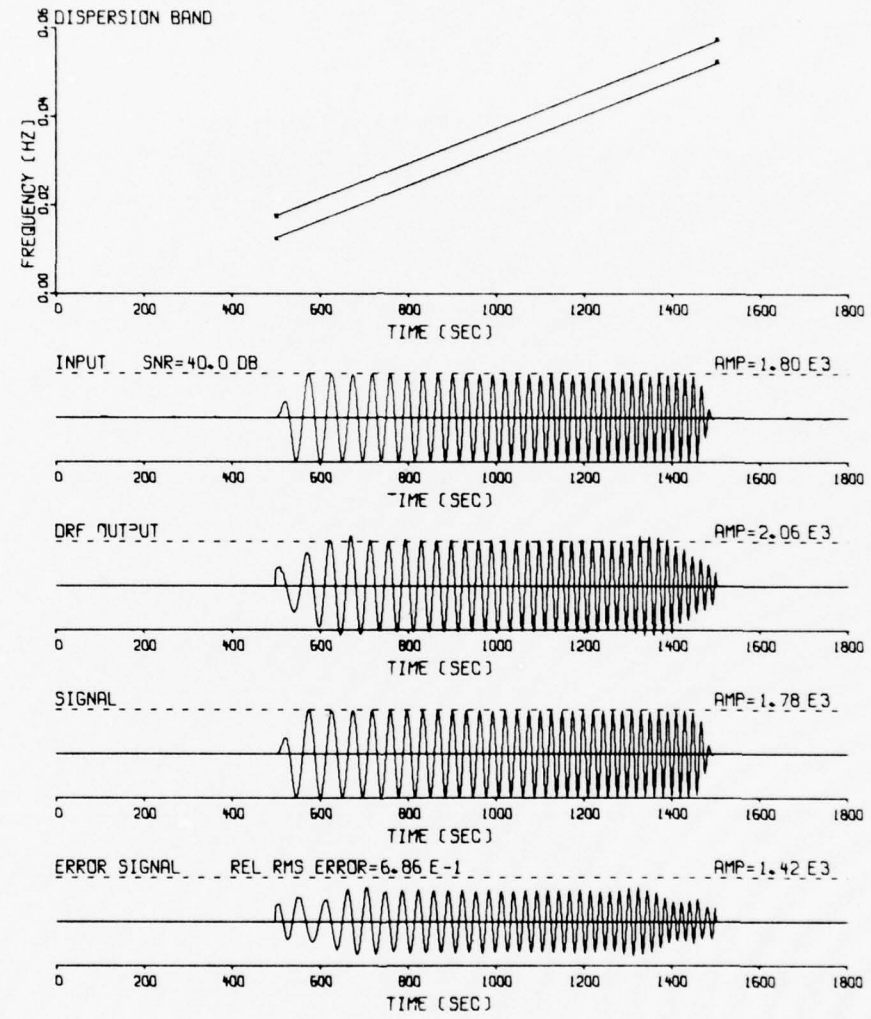

FIGURE IV-1

DRF PERFORMANCE ON LINEAR CHIRP SIGNAL
(PAGE 1 OF 4)

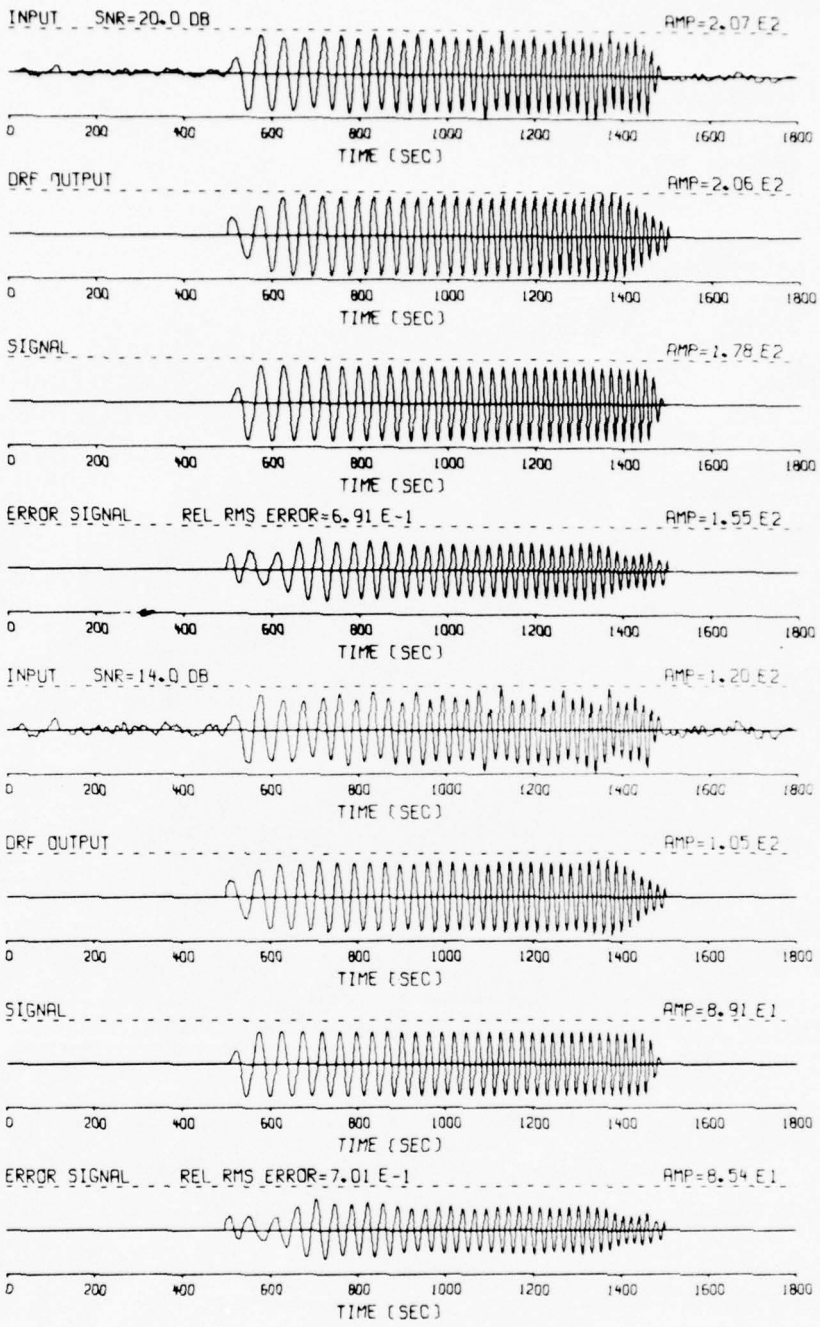

FIGURE IV-1

DRF PERFORMANCE ON LINEAR CHIRP SIGNAL
(PAGE 2 OF 4)

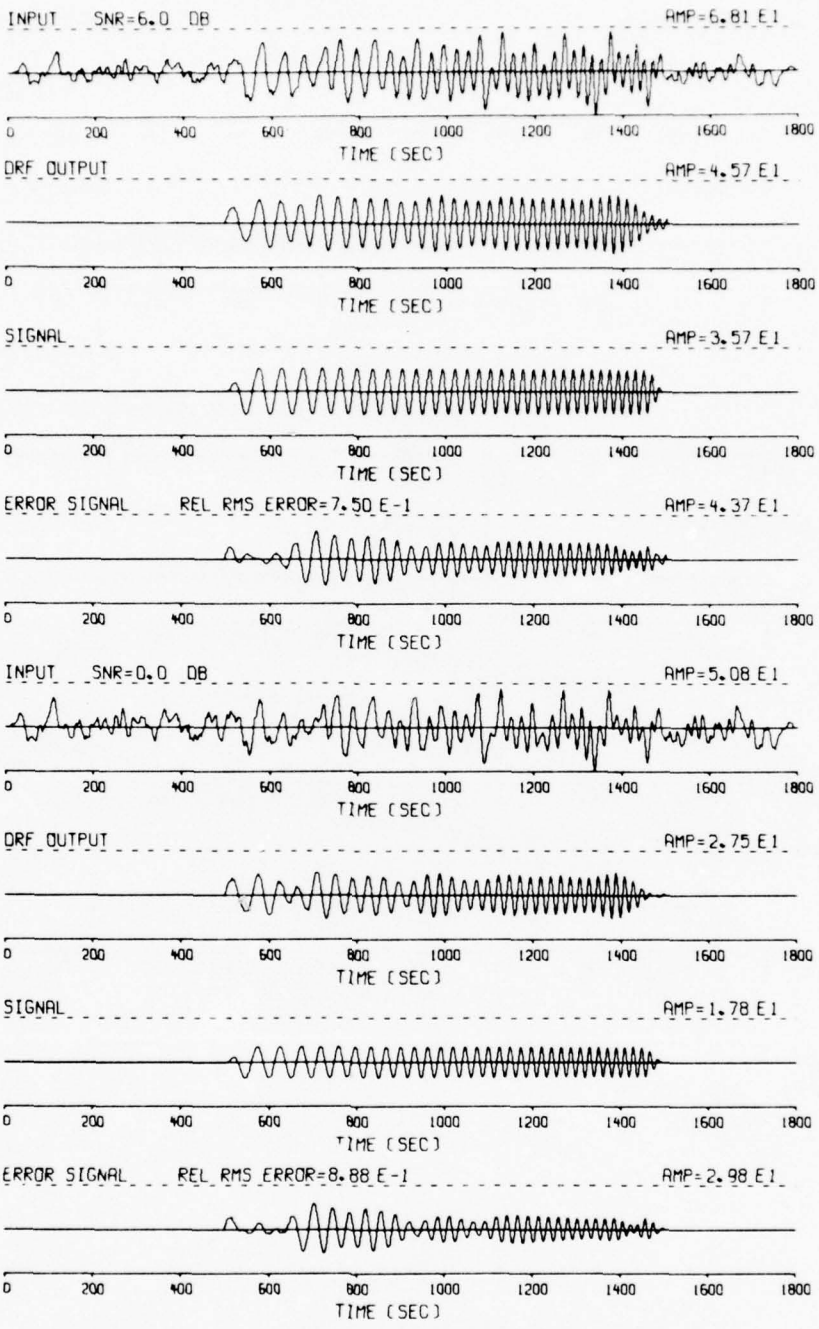

FIGURE IV-1

DRF PERFORMANCE ON LINEAR CHIRP SIGNAL
(PAGE 3 OF 4)

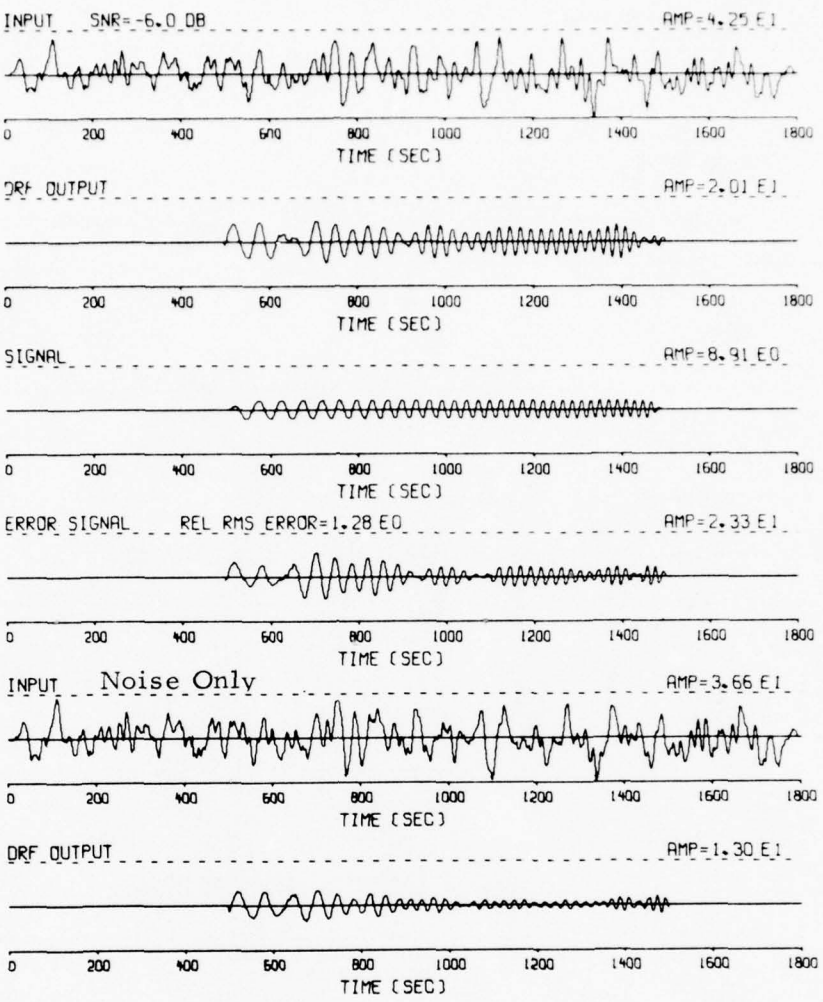

FIGURE IV-1

DRF PERFORMANCE ON LINEAR CHIRP SIGNAL
(PAGE 4 OF 4)

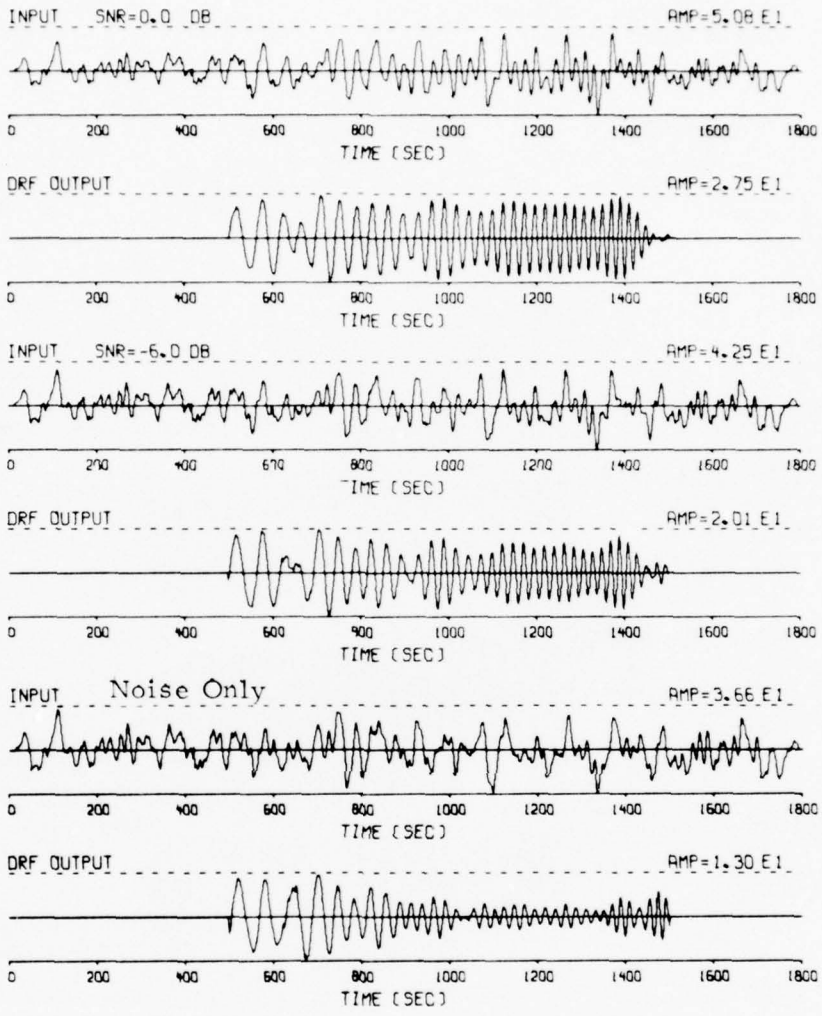

FIGURE IV-2

DRF PERFORMANCE ON LOW SNR CHIRP WAVEFORMS

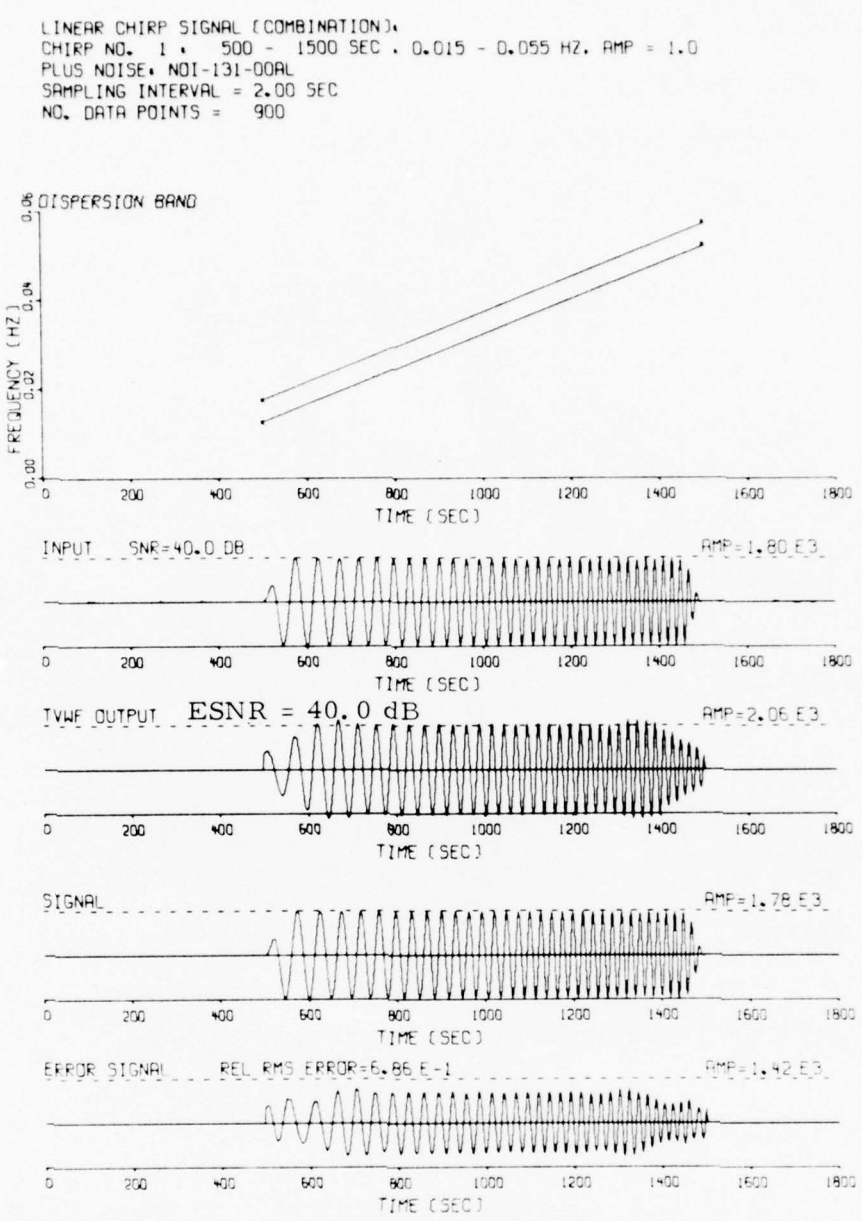

FIGURE IV-3

TVWF PERFORMANCE ON LINEAR CHIRP SIGNAL
(PAGE 1 OF 4)

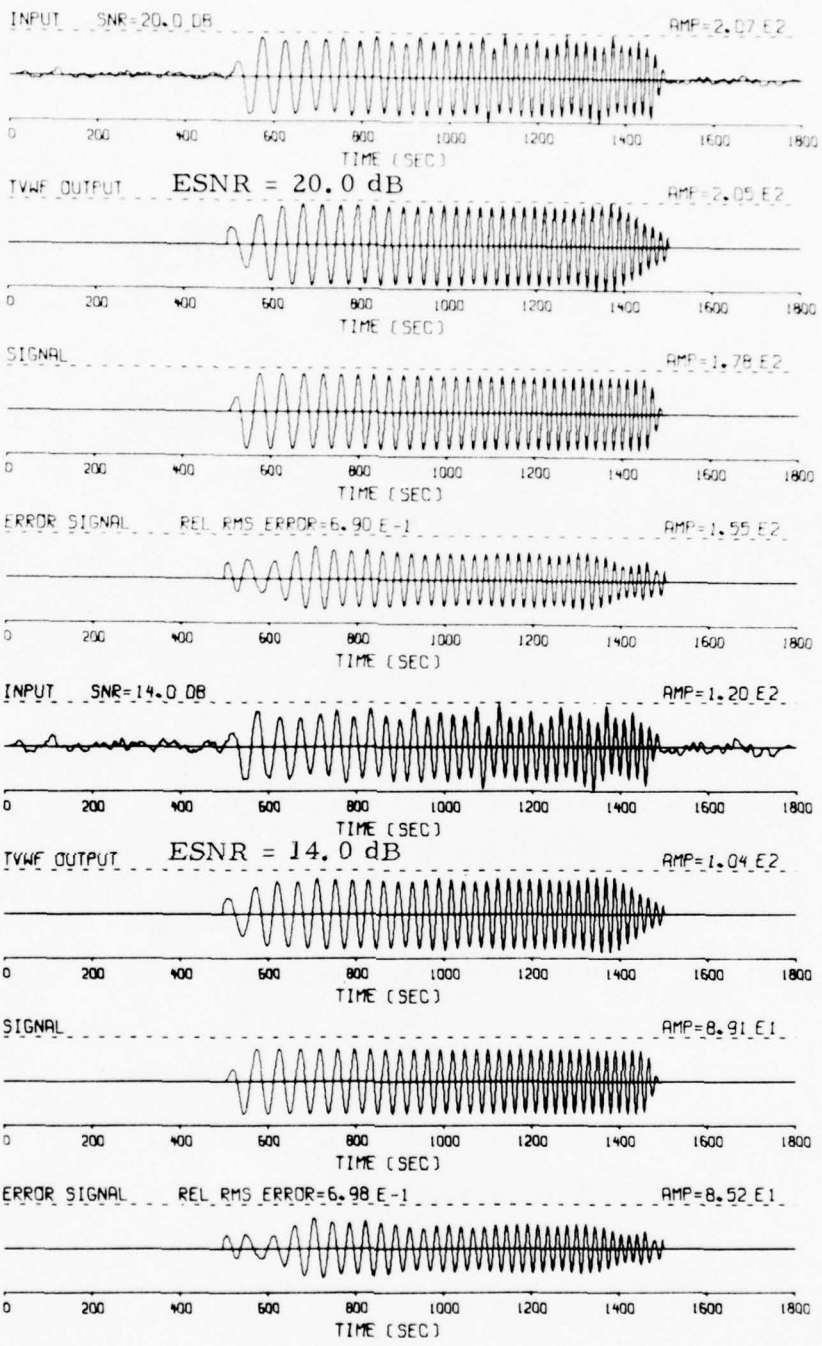

FIGURE IV-3

TVWF PERFORMANCE ON LINEAR CHIRP SIGNAL
(PAGE 2 OF 4)

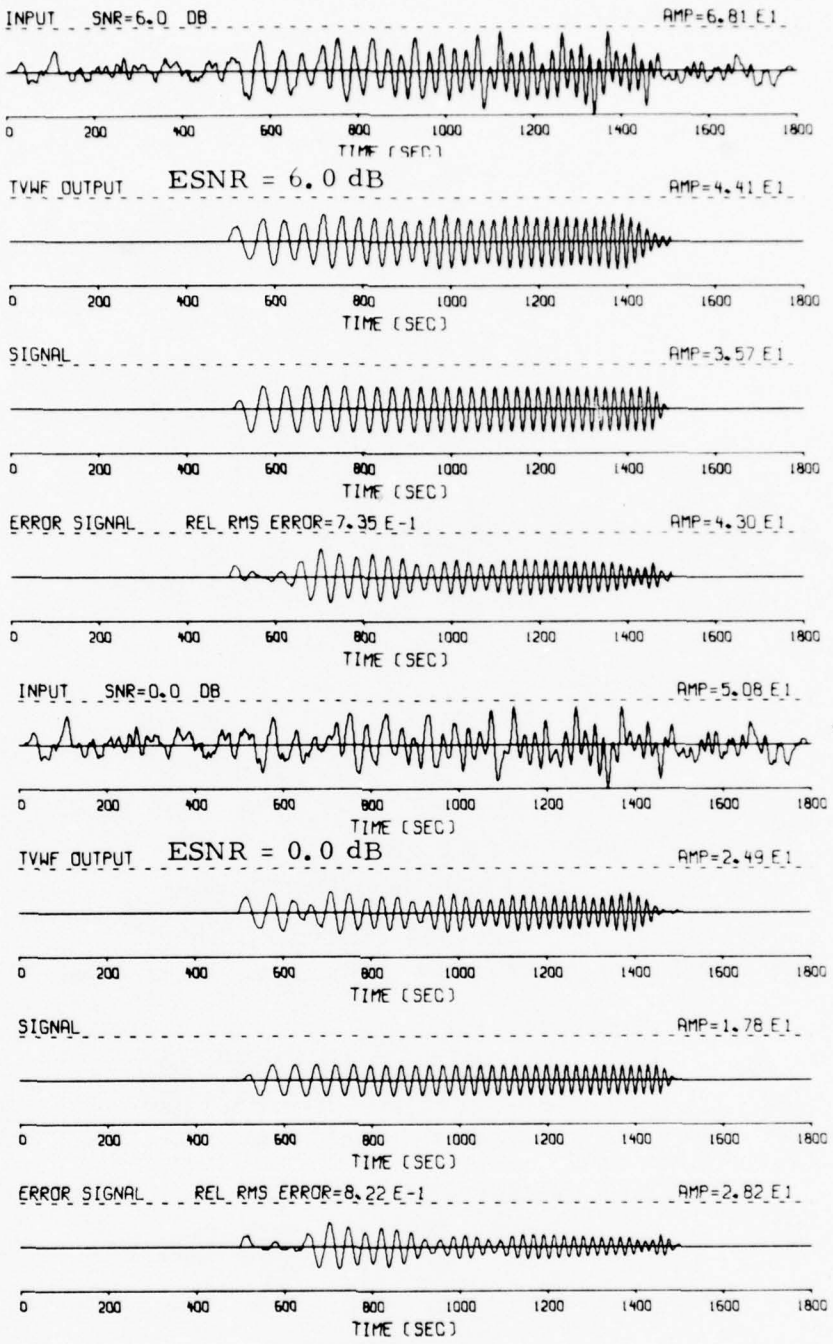

FIGURE IV-3

TVWF PERFORMANCE ON LINEAR CHIRP SIGNAL
(PAGE 3 OF 4)

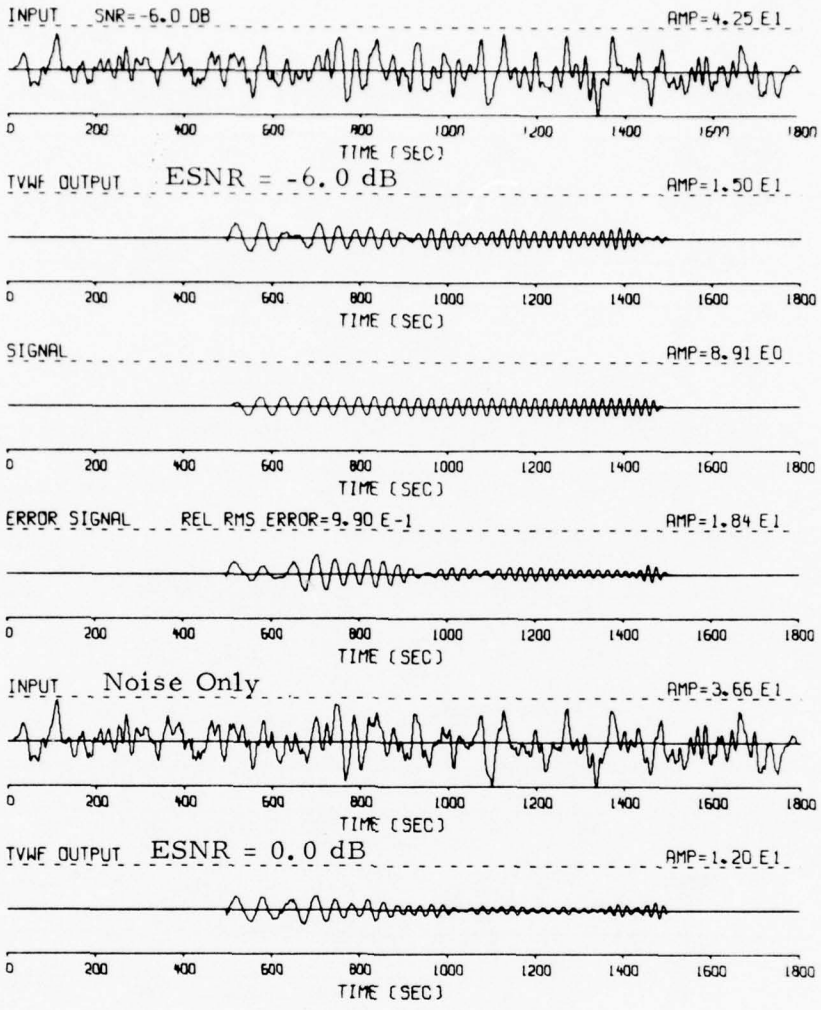

FIGURE IV-3

TVWF PERFORMANCE ON LINEAR CHIRP SIGNAL
(PAGE 4 OF 4)

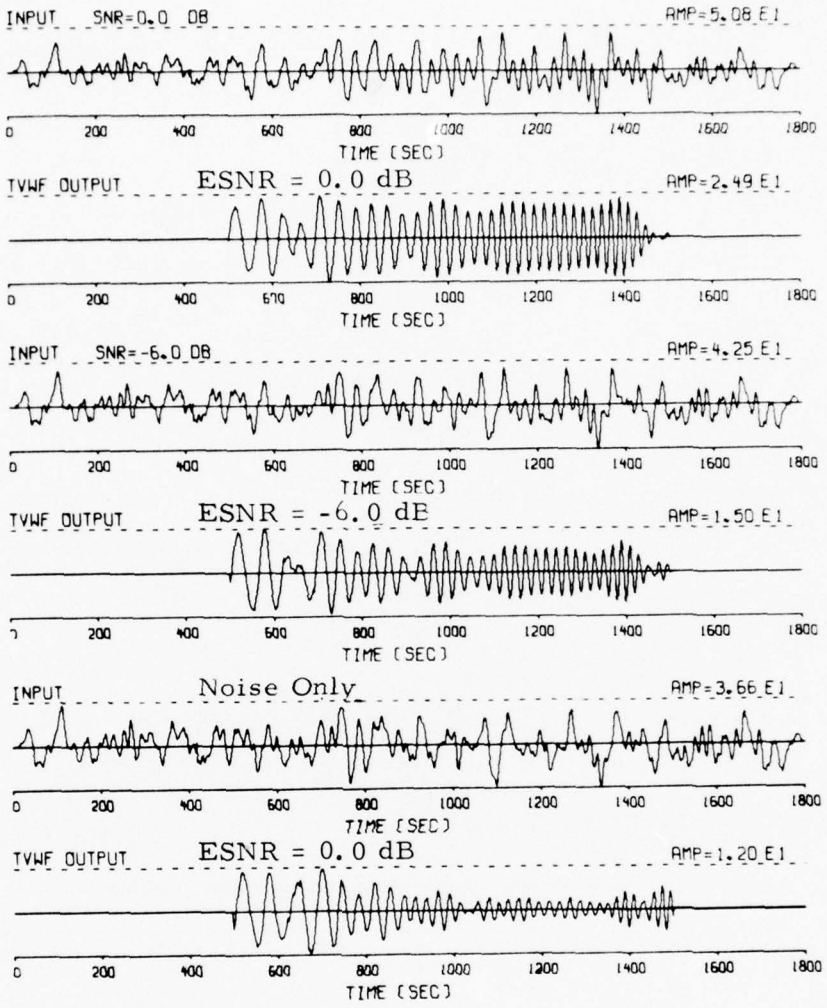

FIGURE IV-4

TVWF PERFORMANCE ON LOW SNR CHIRP WAVEFORMS

For a quantitative evaluation of filter performance, Figure IV-5 displays the errors in maximum amplitude, excluding the overshoot at the beginning and end of the signal, for the unfiltered trace, the 0.010-0.060 Hz bandpass filtered (BPF) trace, the DRF output, and the TVWF output, respectively, as a function of RMS SNR. We observe that the TVWF amplitude errors are in good agreement with the errors anticipated based on the curves of Figure III-2 and on the amount of noise spectral variation shown in Figure II-13. This amount of spectral variation establishes the limits of the TVWF performance.

The graphs, furthermore, indicate that the DRF and TVWF outputs permit accurate magnitude measurement at a significantly lower SNR than is possible with either the BPF or the unfiltered trace. For instance, measurement of the peak amplitude's logarithm (log A) within ± 0.1 is feasible for the unfiltered trace only for input waveforms with an RMS SNR of at least 16 dB: with TVWF the same accuracy of measurement can be obtained from waveforms with an RMS SNR as low as 5 dB. A number of magnitude measurability versus SNR relationships are listed in Table IV-1. This table indicates the increase in magnitude standard deviation caused by log A measurement errors, assuming a distance factor uncertainty (σ_Δ) of 0.3. We notice that a log A error of 0.1 does not significantly increase the overall magnitude error. Magnitude measurability improvement enhances the classification of seismic events, and in particular should improve m_b-M_s discrimination for events with an approximately known dispersion curve.

Comparing the merits of the TVWF with alternative methods, we remark that possibly similar results can be obtained with matched filtering (MF), since the amount of noise rejection is on the same order as that of TVWF. However, the large variance in MF gains prevents accurate calibration of the MF output (Strauss, 1973), and the MF log A measurement accuracy, therefore, is not known. The MF gain probably should be calibrated by

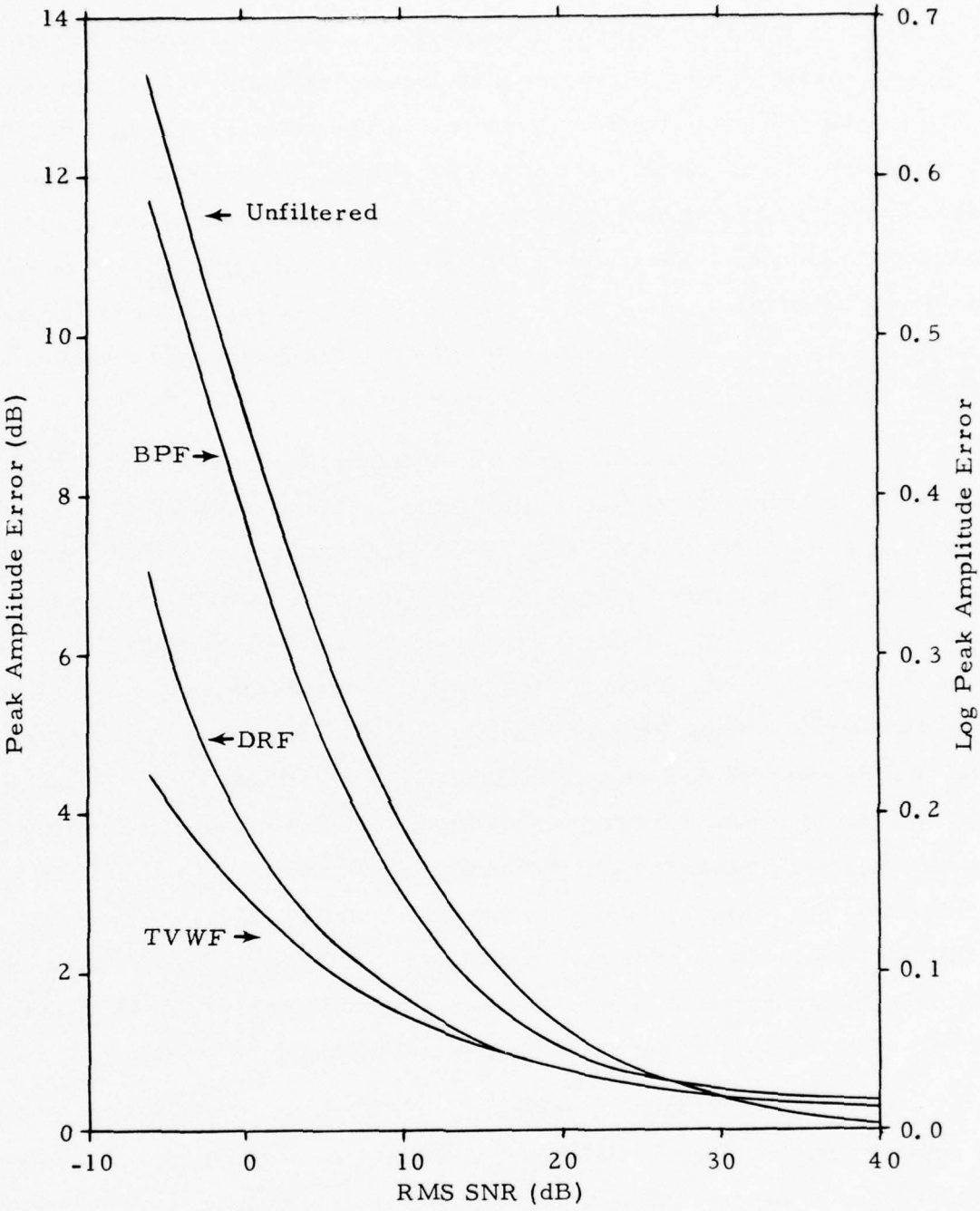

FIGURE IV-5

PEAK AMPLITUDE ERRORS FOR LINEAR CHIRP WAVEFORM

TABLE IV-1

SNR REQUIRED FOR DESIRED MACNITUDE MEASUREMENT ACCURACY *)

M_s Accuracy (assuming $\sigma_\Delta = 0.30$)	Log A Accuracy	Minimum RMS SNR Required (dB)	
		Unfiltered	TVWF**)
0.30	0.05	23	16
0.32	0.10	16	5
0.34	0.15	13	0
0.36	0.20	10	-4
0.39	0.25	7	-7***)

*) For linear chirp waveform in noise.
**) SNR presumed known exactly.
***) Extrapolated value.

measuring the gain when a reference waveform is matched to itself, rather than the present procedure of calibration with regionally average MF gains.

The above error analysis is based on the combination of one simulated chirp waveform and only one, presumably typical, sample of seismic noise. The curves in Figure IV-5, therefore, can give only an indication of the expected filter performance; true performance characteristics can be obtained only from analyzing a number of noise sample and signal combinations, or, perhaps equivalently, by time-shifting the noise waveform with respect to the signal. However, based on a quick visual inspection of other moving-window noise spectra, we expect the noise spectral power density fluctuations about an average noise spectrum not to deviate significantly from those displayed in Figure II-13. Since the peak amplitude errors are mainly determined by the WF misestimation of power density SNRs, it is anticipated that the curves in Figure IV-5 will not be much different from an average TVWF performance curve established from an ensemble of signal and noise sample combinations.

Also, this TVWF performance is based on an exact, a priori knowledge of the ESNR, which, especially for low SNR waveforms, is a sensitive WF design parameter. In normal filtering situations, additional errors are incurred since the ESNR must be estimated by visual inspection of the input trace, or by deduction from the bodywave magnitude, as discussed in Section III. Figures IV-3 and IV-6 indicate that the SNR of a 6 dB true SNR waveform can probably be estimated well within 3 dB accuracy. Thus, according to Figure III-2, the WF gain error due to SNR misestimation will be small (less than 2 dB) for waveforms of 6 dB or higher true RMS SNR, but they may become significant for lower SNR waveforms.

Besides improving the surface wave magnitude measurability, time-variant Wiener filtering may enhance source parameter estimation, Love wave versus Rayleigh wave energy ratio measurement, and possibly other signal analysis and classification techniques.

C. TVWF PERFORMANCE ON SEISMIC WAVEFORMS

Figure IV-6 shows the TVWF performance on waveforms composed of the Love wave beam signal of the Sinkiang region reference event (Event No. 3, Table II-1, Figure II-6) and added seismic noise for various SNR situations. Notice the shape of the dispersion band applied, made to contour the regional dispersion variation given in Figure II-9. The true RMS SNR value was input as the ESNR in each case.

We observe that the TVWF reproduces also the seismic signals fairly faithfully. There is some signal distortion, mainly due to the elimination of signal energy present outside the filter band (see Figure II-8). This again shows that the process of defining the signal spectrum, and selecting the corresponding dispersion band to be used by the filter, is somewhat ambiguous; it depends on the analyst's objective. The relatively low amplitude, and for the most part non-sinusoidal, error signal indicates that the TVWF output of a natural seismic waveform contains little phase error. For the 6 dB and lower SNR waveforms, signal overestimation occurs around 2000 sec travel time. Along this interval, as shown by the corresponding moving-window noise spectrum at 2800 sec in Figure II-13, the part of the noise spectrum coinciding with that of the signal spectrum (the frequencies around 0.024 Hz) is of relatively high power, and is about 6 dB underestimated by the expected noise spectrum. According to Figure III-2, this results in signal overestimation of 0.5, 2, and 6 dB, respectively, for the 6, 0, and -6 dB SNR waveforms, in good agreement with the amounts that can be measured from the TVWF output waveforms.

The errors incurred by the original signal peak amplitude, i.e., the amplitude at 2300 sec travel time, are plotted in Figure IV-7. It appears that the TVWF performs better on seismic waveforms than on the linear chirp waveforms. This is in part due to a low noise level relative to other parts in the waveform and a rather good agreement between expected

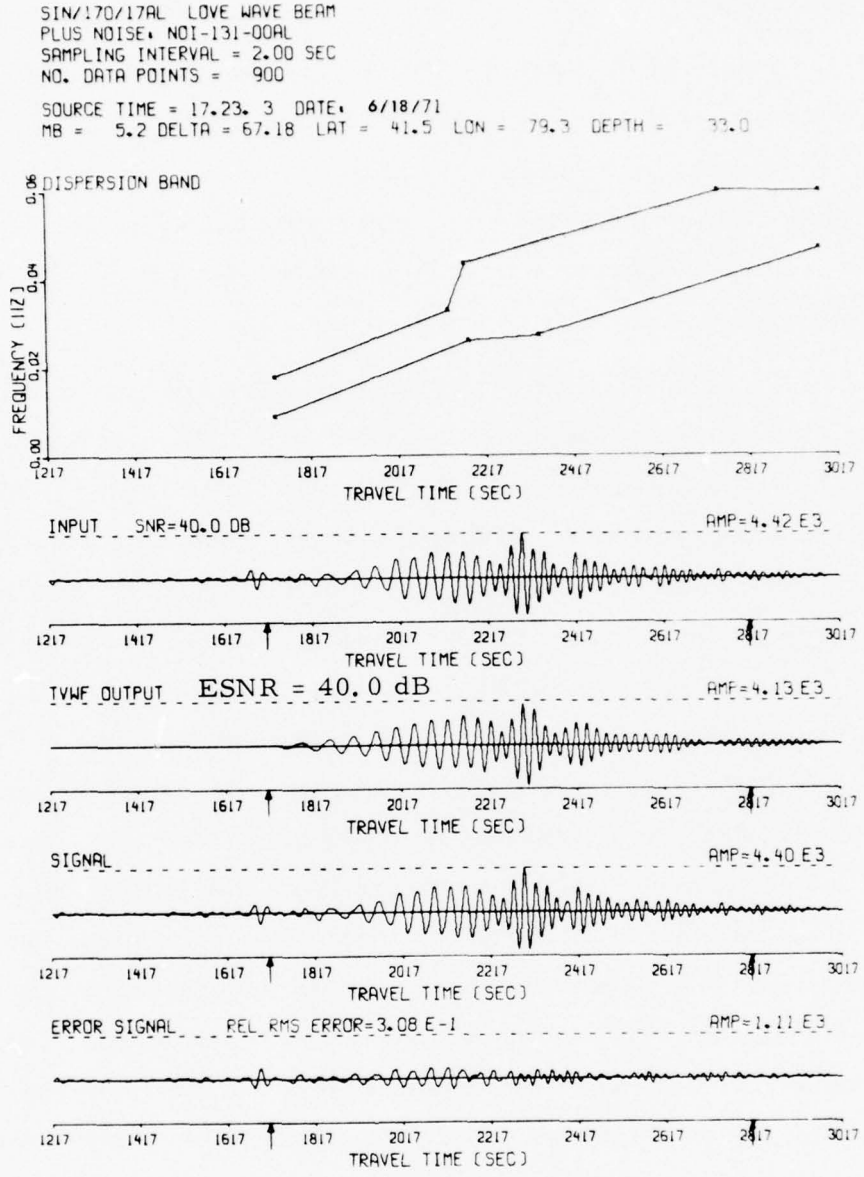

FIGURE IV-6

TVWF PERFORMANCE ON SEISMIC SIGNAL
(PAGE 1 OF 4)

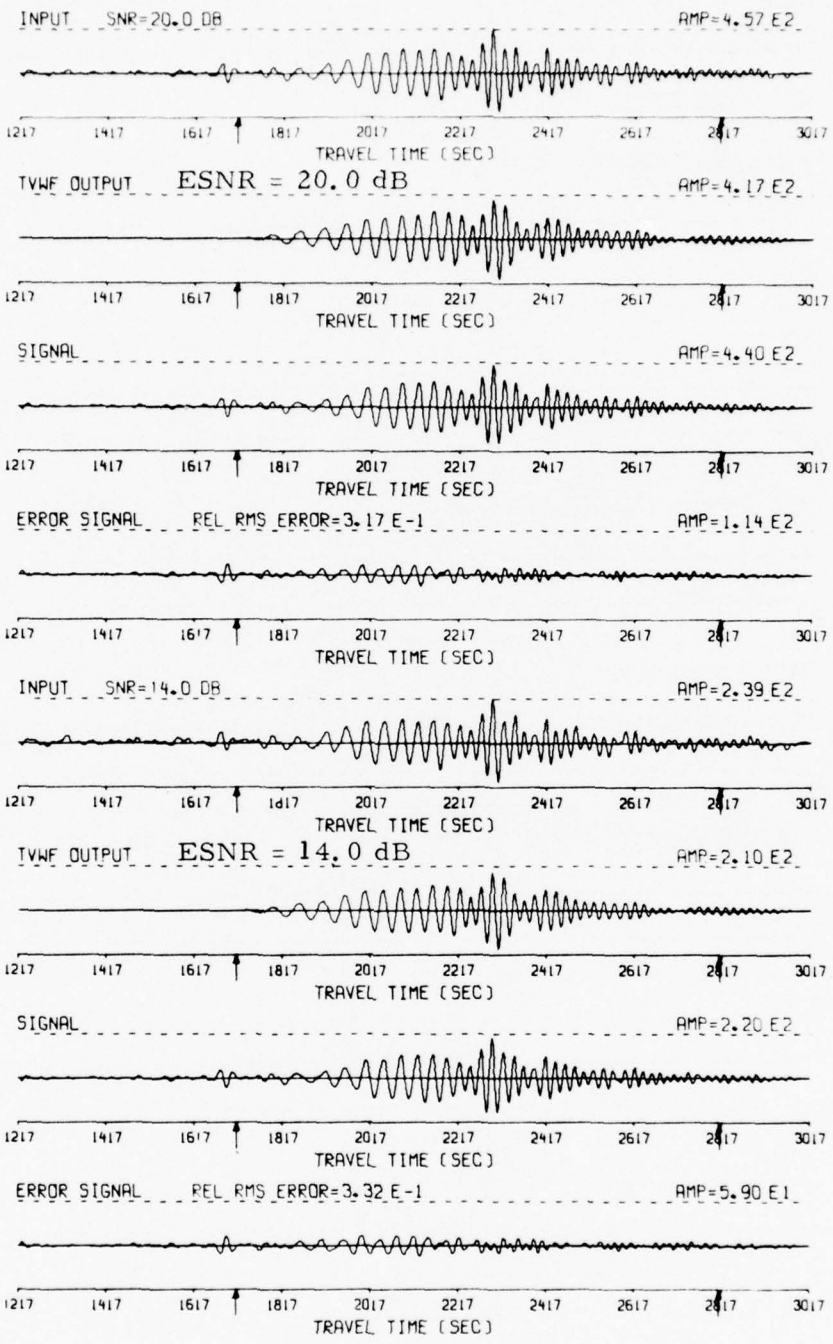

FIGURE IV-6

TVWF PERFORMANCE ON SEISMIC SIGNAL
(PAGE 2 OF 4)

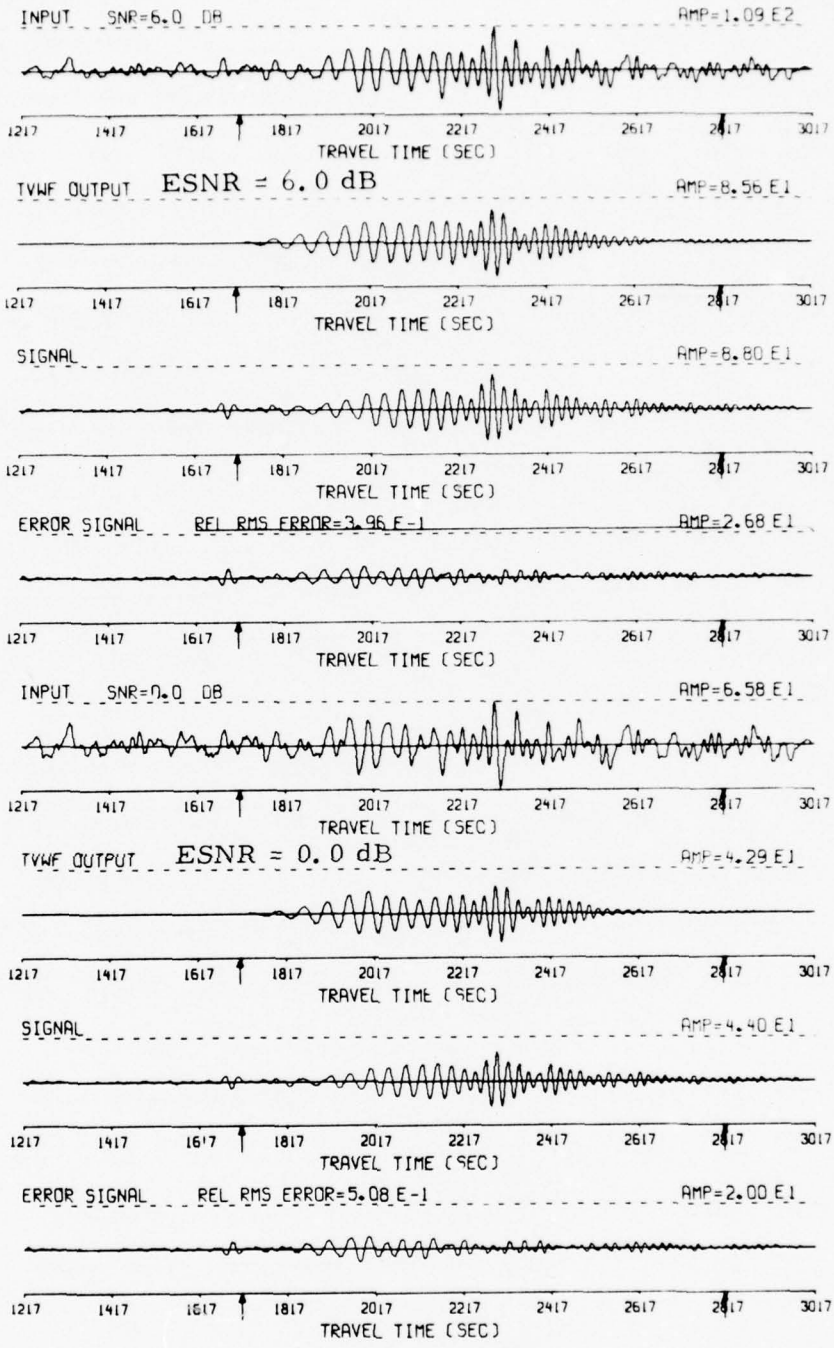

FIGURE IV-6

TVWF PERFORMANCE ON SEISMIC SIGNAL
(PAGE 3 OF 4)

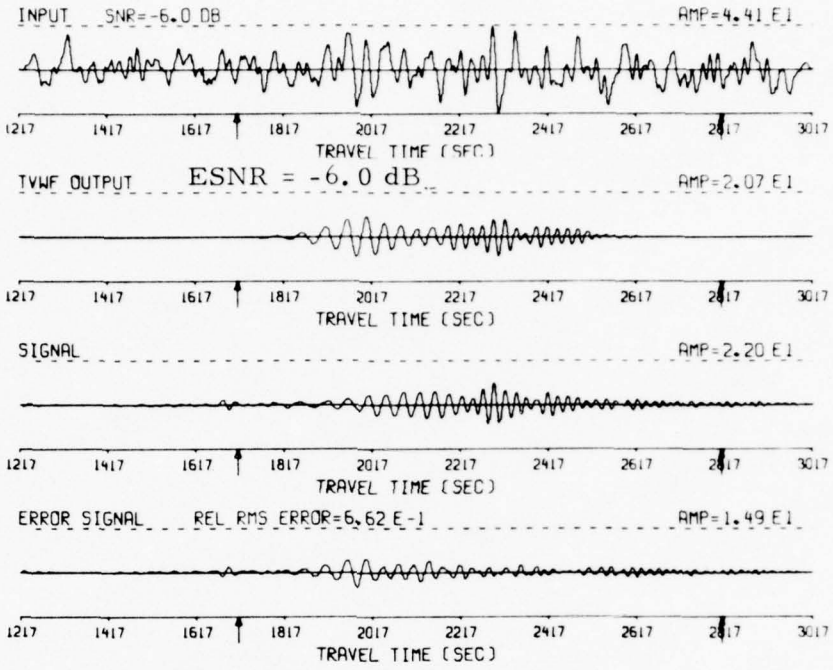

FIGURE IV-6

TVWF PERFORMANCE ON SEISMIC SIGNAL
(PAGE 4 OF 4)

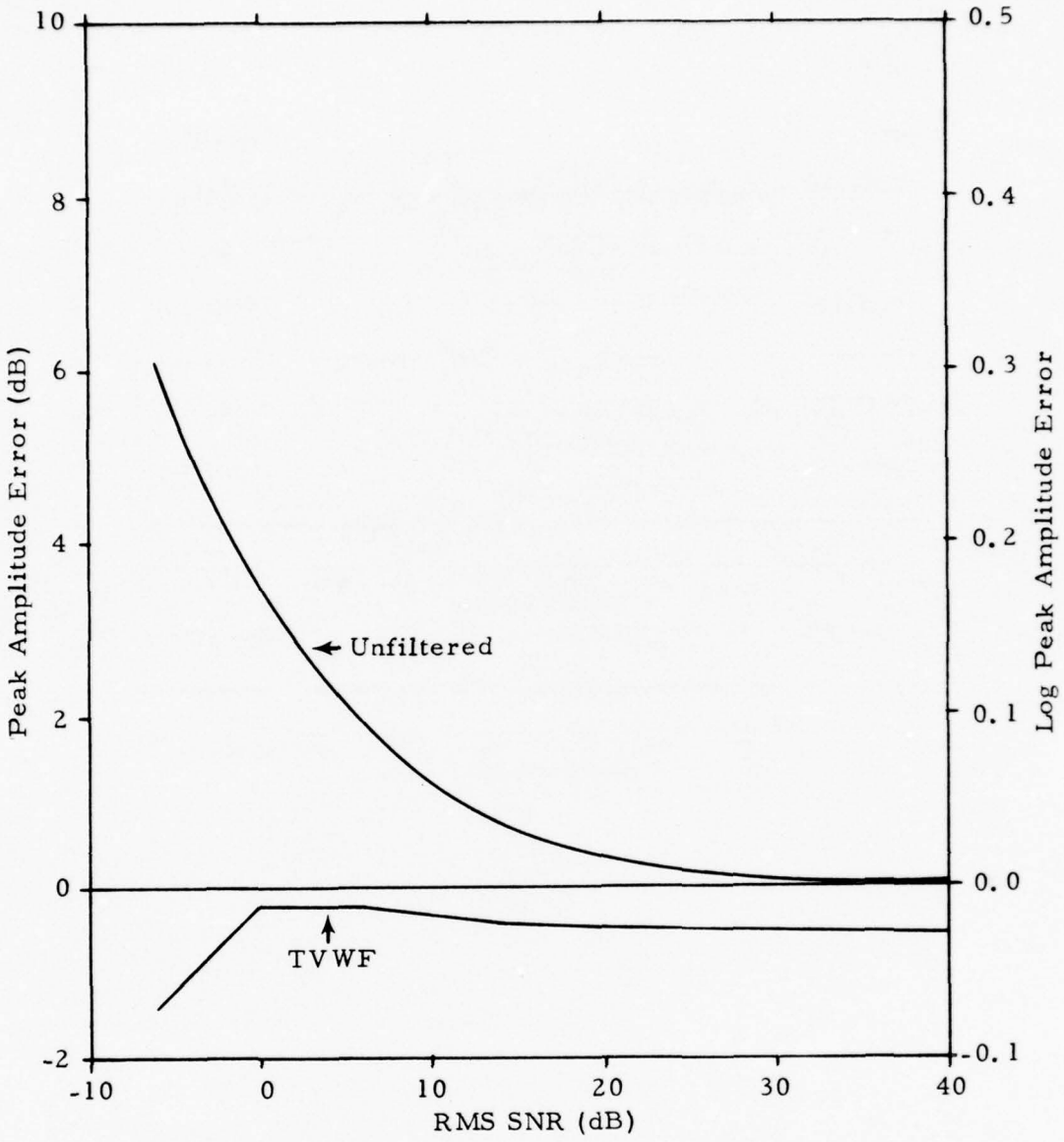

FIGURE IV-7

FILTER PEAK AMPLITUDE ERRORS FOR SEISMIC EVENT SIGNAL (SIN/170/17AL)

and actual noise spectrum for the signal peak amplitude time and frequency (3090 sec; 0.038 Hz, Figure II-13). A different time alignment between the signal and the noise sample, or combinations with different noise samples, therefore, could result in somewhat less favorable performance curves. Nevertheless, accurate M_s measurement (log amplitude measurement within $\pm$ 0.1) seems possible down to at least 0 dB RMS SNR, corresponding approximately to surface wave magnitudes reflecting the 50% detection capability of an array or station.

Using the same regional dispersion band, only shifted in time to align with the various signal start times, the TVWF was applied to the waveforms containing the signals of the other events listed in Table II-1. The results are given in Figures IV-8 and IV-9. For each event the expected noise spectrum and its average power level were measured from a 1440-sec gate just prior to the first P-wave arrival. The expected normalized signal spectrum is determined by the regional dispersion band, by the power densities measured and interpolated along the reference signal dispersion curve, and by the reference signal RMS value, as described in Section III. The ESNRs were determined by visual inspection of the waveforms and comparison with the simulated SNR conditions of Figure IV-6. The signal start times were estimated with the techniques described in Appendix B.

Since we do not know the actual shape of the signals, but anticipate them to be similar to the reference signal (Figure IV-6), we can merely observe that the results seem very plausible. Certainly, the filtered waveforms give the impression of being more accessible to further signal analysis than do the unfiltered traces. However, we do not know if and how much signal energy from frequencies outside the dispersion band has been eliminated in the filtering process. We notice that the TVWF outputs for the Events No. 1, 2, and 5, which are within 20-25 km from the reference event (Event No. 3, Figure II-6 and Table II-1) are indeed very similar to that of the reference event. The events at 100-300 km distance from the reference event display

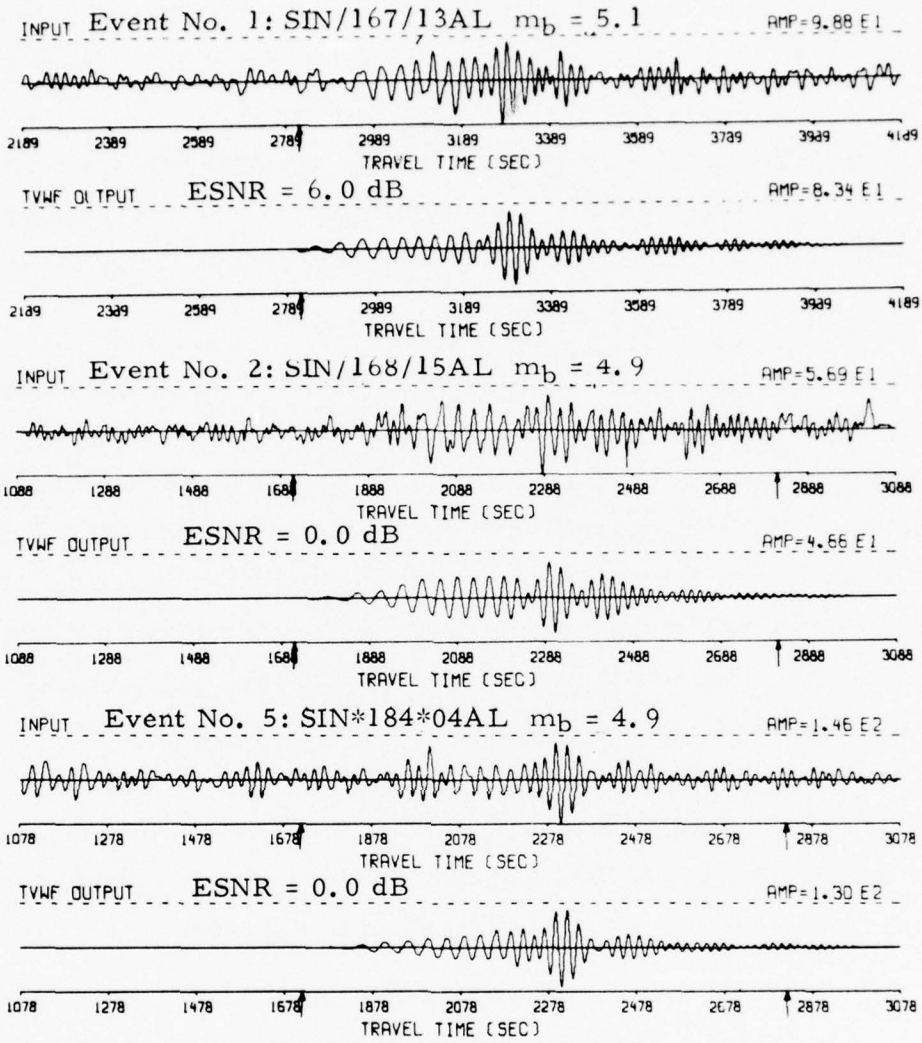

FIGURE IV-8

TVWF OF SINKIANG EVENT WAVEFORMS;
DISTANCE TO REFERENCE EVENT 20-25 KM

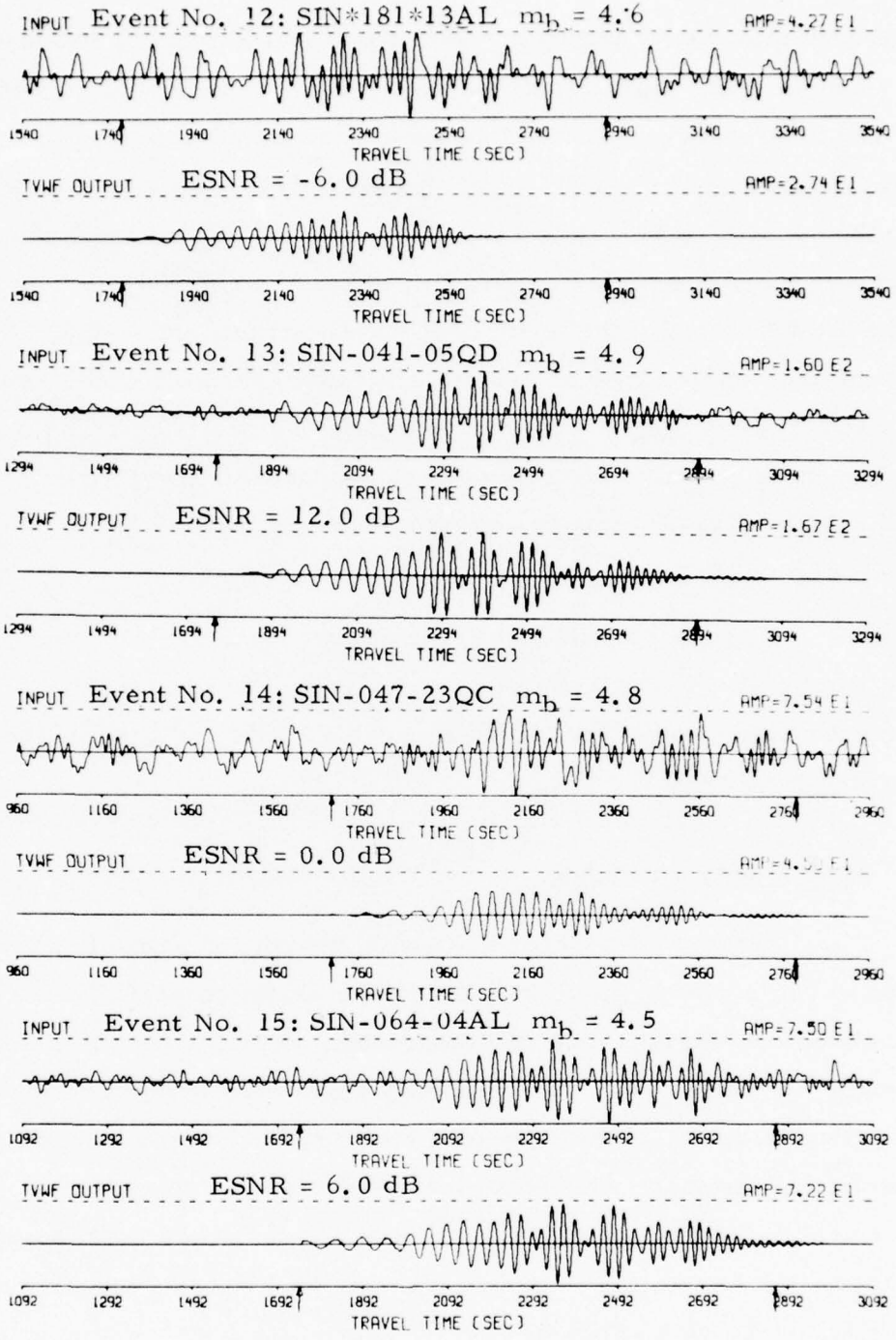

FIGURE IV-9

TVWF ON SINKIANG EVENT WAVEFORMS;
DISTANCE TO REFERENCE EVENT 100-300 KM

slightly different signal patterns. Note the signal similarity between Events No. 13 and 15. The signal of Event No. 12 may be somewhat uncertain due to the low SNR; however, in shifting the TVWF dispersion band in time through the trace, significant signal structure in the TVWF output was found only within the expected signal time gate indicated with arrows, with the given output yielding the highest peak amplitude. Also, the signal level compares well with the TVWF output of the -6 dB SNR waveform in Figure IV-6. The filtered peak amplitude of Event No. 13 is actually larger than the unfiltered one, probably due to the removal of interfering signal energy. The TVWF output of Event No. 14 is probably distorted due to unseparable low frequency noise around 2100 sec travel time, similar to the situation for the low SNR waveforms in Figure IV-6.

The magnitude changes resulting from the TVWF are summarized in Figure IV-10. No conclusions with regard to magnitude scatter improvement can be drawn from this figure; this would require a larger statistical population of events.

D. SIGNAL SEPARATION

Figure IV-11 shows the DRF separation capability for a combination of two signals: the first one a linear chirp waveform, the second one a monochromatic signal. The DRF adequately resolves the two signals by separately applying the two corresponding dispersion bands indicated in the figure. The chirp signal picks up part of the monochromatic signal at the intersection of the dispersion curves; the NBF for the monochromatic waveform, however, distributes the chirp signal energy of the corresponding frequency over the entire time interval of the monochromatic signal, causing a slight increase in its amplitude.

Another example of signal separation is given in Figure IV-12. Here, the input consists of three signals with parallel linear dispersion curves,

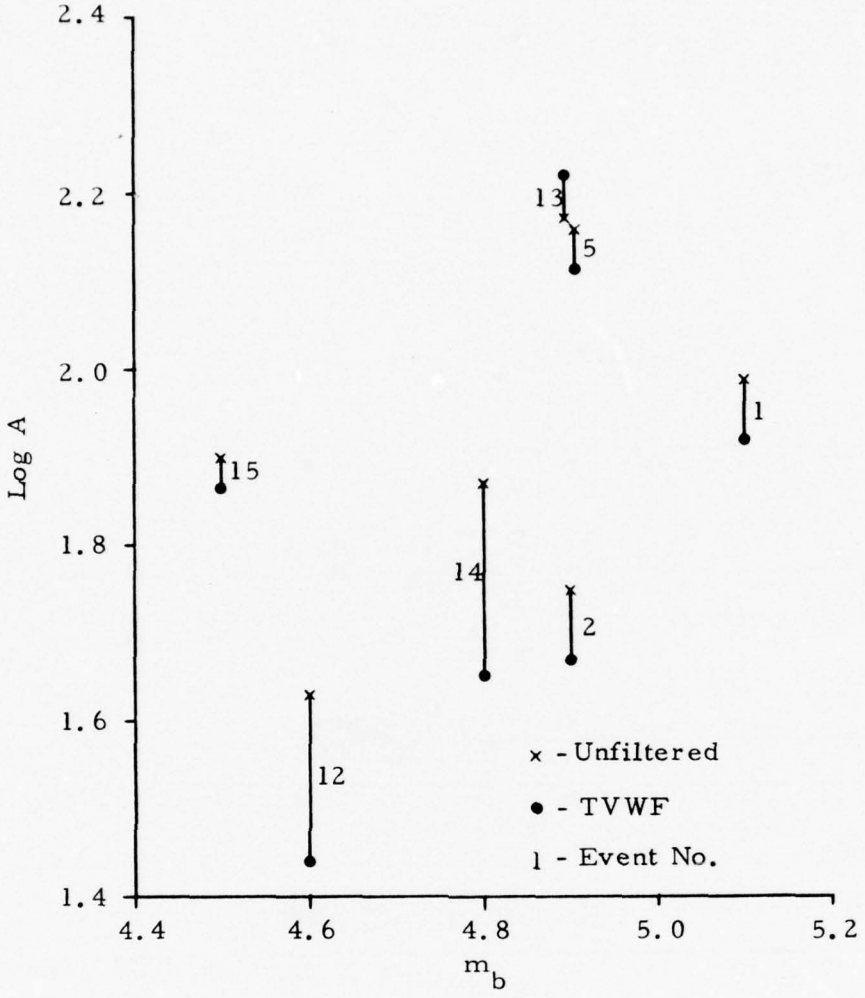

FIGURE IV-10

SURFACE WAVE MAGNITUDE CHANGES DUE TO TVWF FOR SINKIANG EVENTS

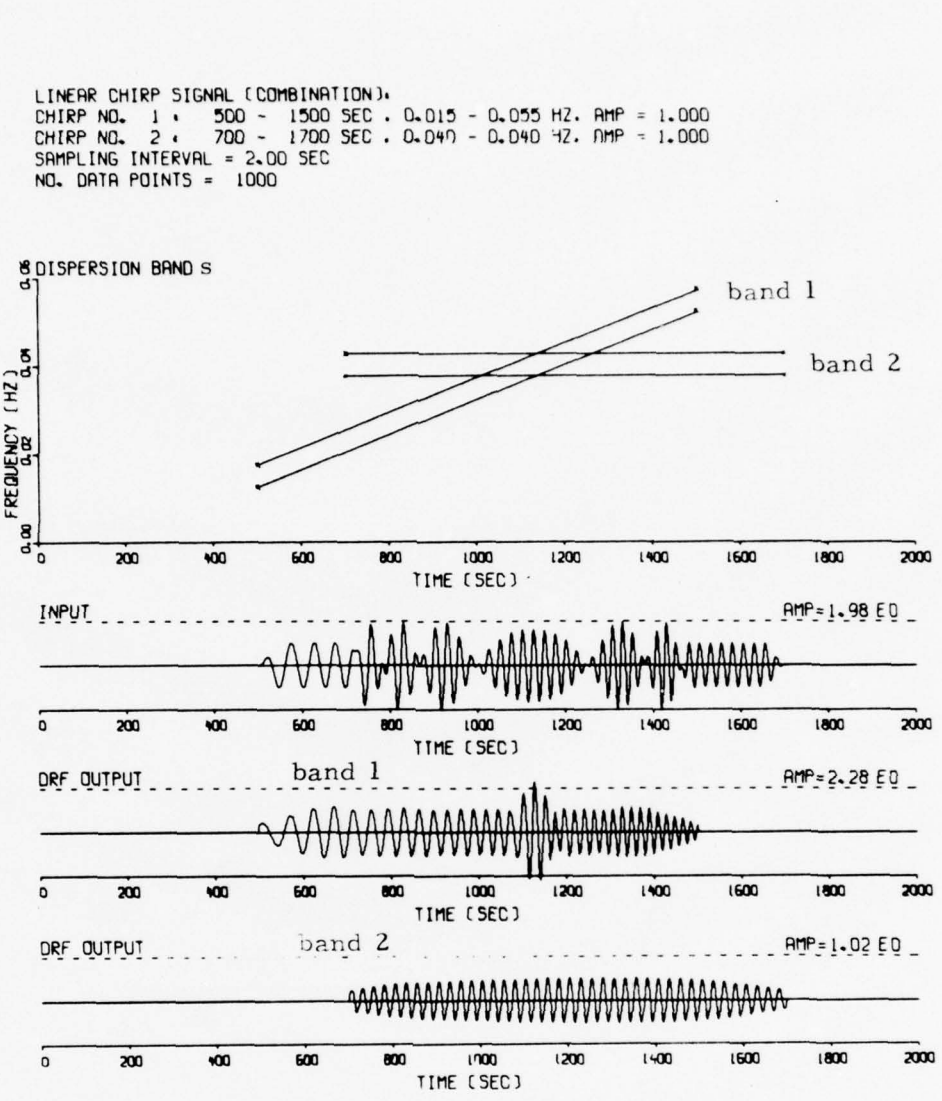

FIGURE IV-11

DRF SIGNAL SEPARATION, SYNTHETIC WAVEFORMS

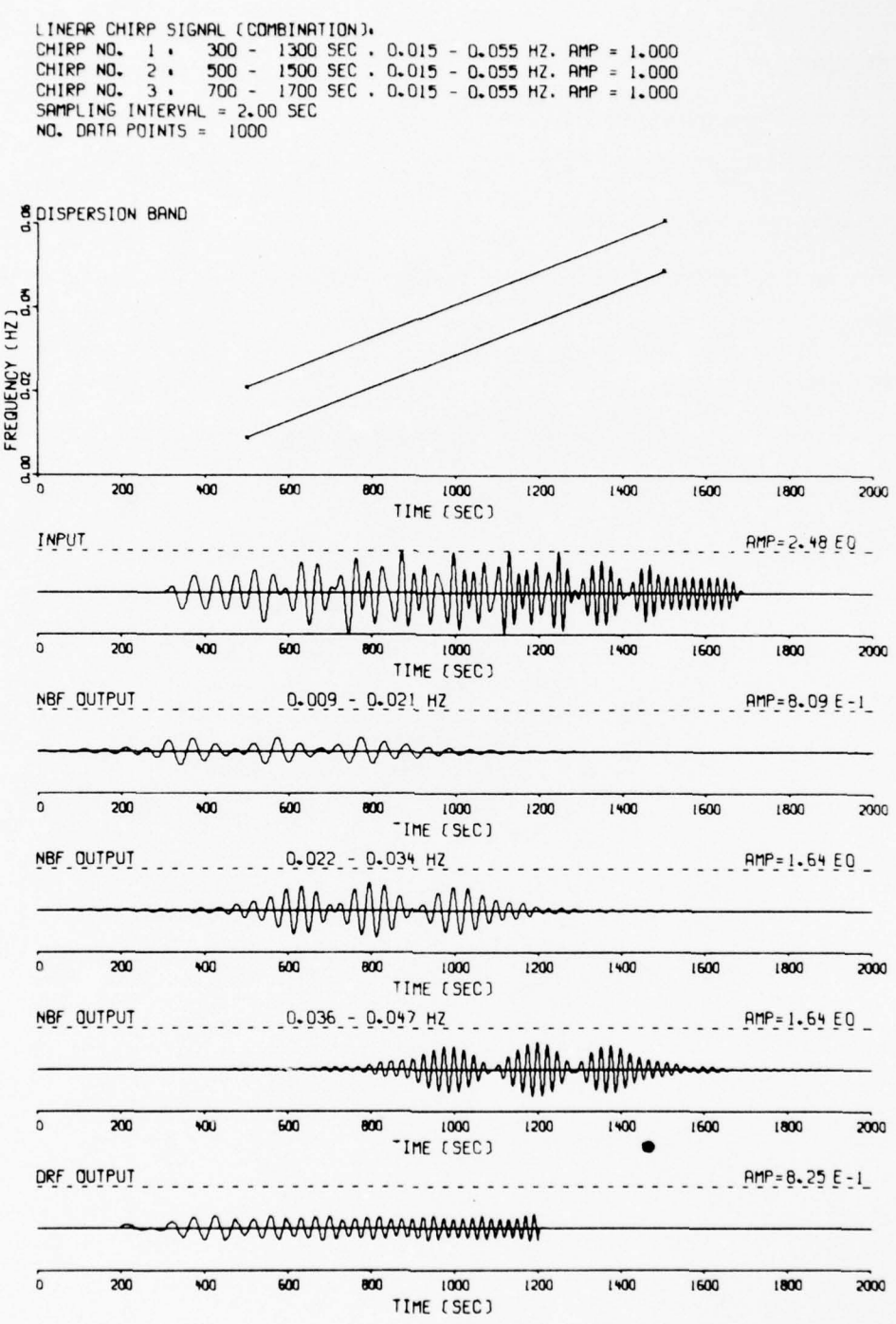

FIGURE IV-12

DRF SIGNAL SEPARATION, SYNTHETIC WAVEFORMS
(PAGE 1 OF 2)

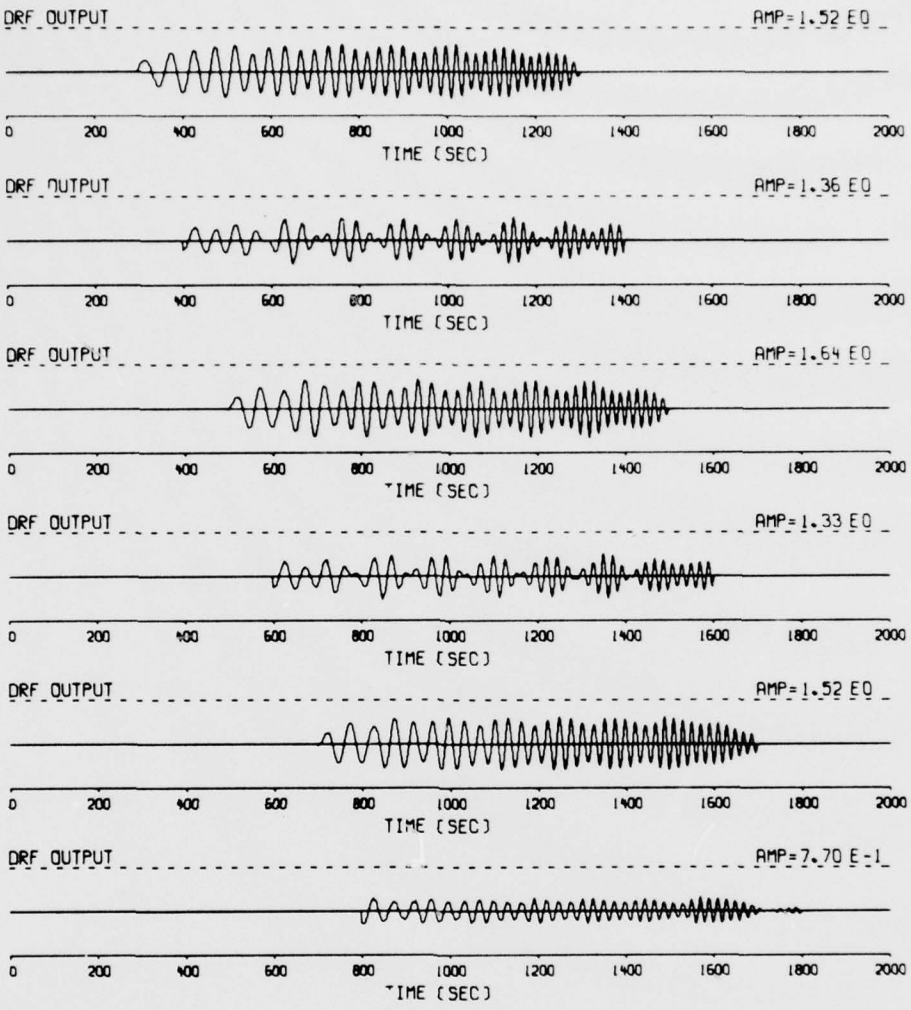

FIGURE IV-12

DRF SIGNAL SEPARATION, SYNTHETIC WAVEFORMS
(PAGE 2 OF 2)

simulating multiple signal arrivals. By sliding the DRF dispersion band for a single signal through the input waveform, each of the three signals is recovered whenever the DRF dispersion band lines up with a signal's dispersion curve, i.e., at 300, 500, and 700 sec, respectively. However, there is a high amount of distortion. In this case, the separation capability is severely limited by the width and side lobes of the NBF response envelope curve, determined by the DRF bandwidth. On the one hand, we want to make the width of this lobe small to reduce the interference caused by the adjacent main lobes of other signals, by increasing the DRF bandwidth. On the other hand, this would incur both stronger side lobes which, in turn, lead to interference, and the pick-up, within the wider DRF band, of adjacent signals with parallel dispersion curves. Disregarding the effect of the stronger side lobes, we can arrive at an optimum separation bandwidth $W_{s_{opt}}$, yielding a minimum separation interval $T_{s_{min}}$, as follows. The separation interval T_s is greater than the lobe width, determined by the DRF bandwidth W:

$$T_s \geq 2 W^{-1} . \qquad \text{(IV-2)}$$

But also, T_s must be greater than an interval determined by W and the dispersion rate D, as indicated in the figure:

$$T_s \geq 0.5 W D^{-1} , \qquad \text{(IV-3)}$$

so that

$$T_{s_{min}} = D^{-1/2} \qquad \text{(IV-4)}$$

for

$$W_{s_{opt}} = 2 D^{1/2} . \qquad \text{(IV-5)}$$

The above is only true if the DRF band is sufficiently narrow to preserve the lobe character of its NBF outputs. According to Appendix A, this condition seems to be satisfied for:

$$W \leq D^{1/2} . \qquad \text{(IV-6)}$$

Thus, the optimum bandwidth cannot satisfy this third constraint, leading to a compromise between losing to some extent the single lobe character on the one hand, and the lobe being too wide on the other. In Figure IV-12, where $D = 4.10^{-5}$ Hz/sec, the signals, which are 200 sec apart, were separated with an effective bandwidth of 0.008 Hz, taking into account the 0.002 Hz cosine taper. According to Equation (IV-2), this results in a potential separation interval of 250 sec, which still satisfies Equation (IV-3): $T_s \geq 200$ sec. The distortion in the DRF output, therefore, is probably caused mainly by the interference of the NBF response main lobe and side lobes.

Next, Figure IV-13 shows an attempt to delineate the reference waveform into separate signals, more or less similar to the method used in Figure IV-11. Moreover, dispersion band 1 is applied with various start times, in search of multiple signals with parallel dispersion curves. The chirp signal in this band does not seem to extend beyond 0.035 Hz; it merely picks up signal energy from band 2 at the intersection of the two dispersion curves, and some other scattered, small amounts of signal energy. Multiple signals with parallel dispersion curves do not seem to be present, consistent with the spectral analysis. The approximately monochromatic waveform with a frequency of about 0.040 Hz, recovered by band 2, is also consistent with the spectral analysis. Although these two signals seem to be dominant and together probably would synthesize most of the input waveform, other combinations of DRF dispersion bands could be made to separate or recover other signals as parts of the composite waveform.

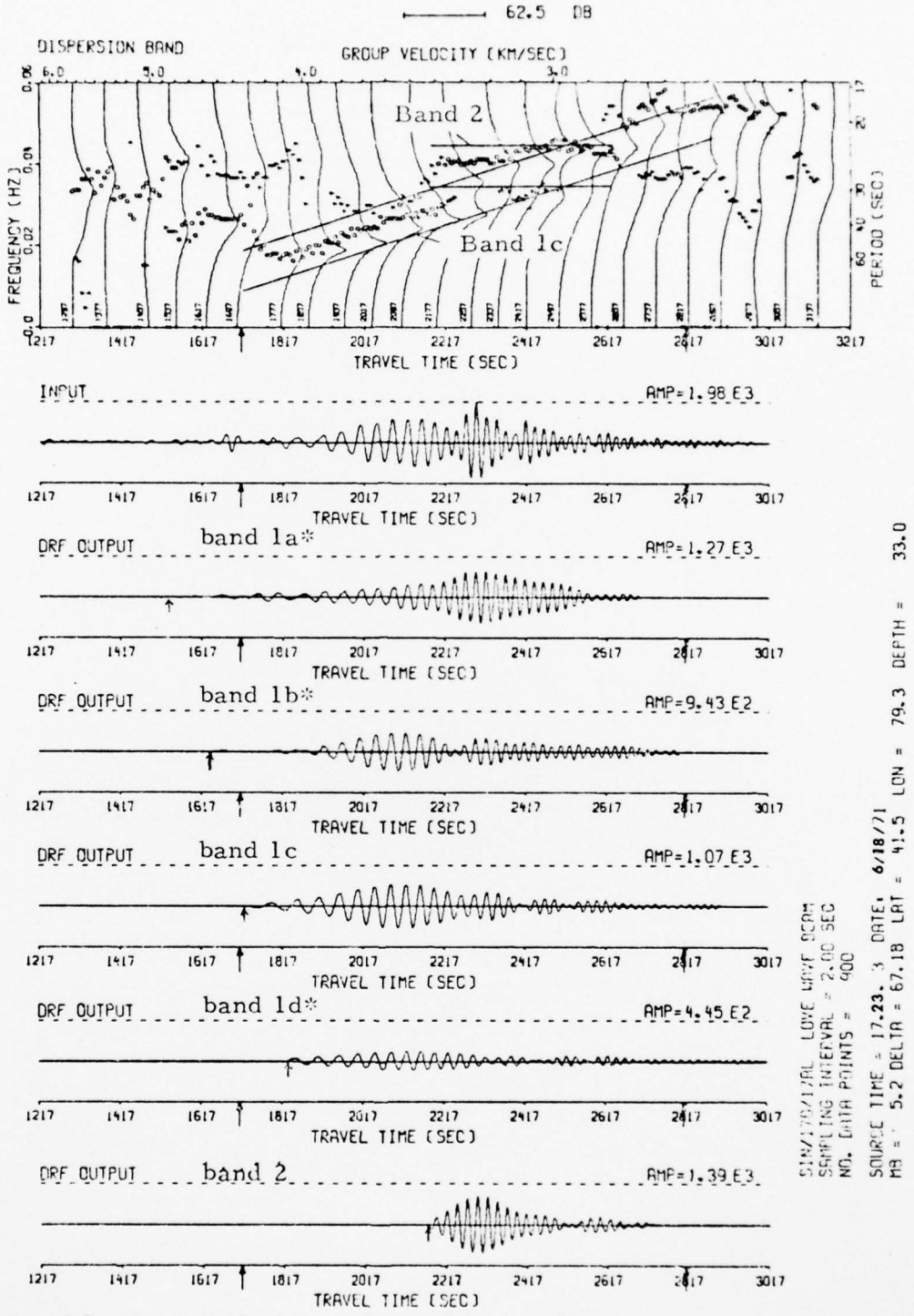

* band 1c time-shifted as indicated by small arrow.

FIGURE IV-13

DRF SIGNAL SEPARATION, SEISMIC SIGNAL

SECTION V
SUMMARY

A time-variant, dispersion-related Wiener filter (TVWF) was developed and tested on synthetic linear chirp waveforms and on signals from Sinkiang Region seismic events. The maximum entropy spectrum (MES) technique (Burg, 1968) was used to determine the Sinkiang Region dispersion curves.

These experiments led to the following conclusions and indications:

- The MES results are somewhat ambiguous and depend strongly on the MES algorithm parameters used (sample rate, waveform gate length, number of prediction error filter coefficients).
- The definition of regional dispersion curves is subject to an analyst's spectral interpretation.
- Despite some ambiguity, the MES technique provides high-resolution group velocity curves.
- The TVWF is effective as a signal estimator rather than as a detector.
- The TVWF enhances the estimation of signals at least down to 0 dB RMS SNR. In particular, it considerably improves the measurability of surface wave magnitudes.
- Below 0 dB RMS SNR, the estimates may become unreliable due to noise spectral variation with time, and the difficulty of

estimating the waveform's SNR, which is a sensitive parameter in the Wiener filter design.

- The TVWF noise rejection over stationary bandpass filtering ranges from 3 to 9 dB depending on the inherent bandwidth of a signal along its dispersion curve.

- Dispersion-related filtering is based on narrowband filtering about a known dispersion curve; narrowband filtering of time-variant waveforms produces amplitude and phase errors. The amplitude errors, which mainly depend on the filter bandwidth and the dispersion rate, can in general be corrected to within 1 dB; in unfavorable cases the remaining error may be as much as 2.5 dB. The phase error could not be corrected, but appears to be small for natural seismic signals.

- The filter's separation power is limited by the widths of the filter response main lobe and the presence of side lobes, determined by the filter bandwidth. For signals with parallel dispersion curves, the minimum separation interval and the corresponding bandwidth are determined by the dispersion rate. For a $4 \cdot 10^{-5}$ Hz/sec dispersion rate, signals separated by 200 sec can be resolved with a bandwidth of 0.008 Hz; however, the output contains about 50% amplitude distortion due to filter response lobe interference. Signals with non-parallel dispersion curves appear to be better separable.

- The TVWF requires that the signal start time be known; this may be found with any, or a combination, of the following methods:

  - deduction from given source location and time,
  - sliding the TVWF dispersion band through the waveform and searching for the maximum RMS output value,

- MES analysis,
- instantaneous signal phase detection.

The second and third methods appear to be most accurate, but are more computer time and core consuming.

- In the present design the filtering is performed in the frequency domain; this requires in principle one inverse Fourier transform for every dispersion point of non-overlapping bandwidths. For a signal with a 1000-sec dispersion, sampled at 2-sec intervals, with $5 \cdot 10^{-4}$ Hz frequency increments and a 0.04 Hz bandwidth, this amounts to more than 80 inverse transforms. Alternatively, one may conceive the filter design as a time-domain recursive convolution, using a digital resonant filter technique; this method should be considerably faster.

- The TVWF signal enhancement should prove useful in magnitude measurement, M_s-m_b discrimination, Love wave versus Rayleigh wave energy measurement, source parameter studies, propagation and geological structure studies, and possibly other signal analysis and classification techniques.

- A statistical filter performance evaluation using an ensemble of combinations of noise samples and known signals is required to establish the full range of filter performance characteristics.

SECTION VI
REFERENCES

Barnard, T. E., 1975, The Maximum Entropy Spectrum and the Burg Technique, Technical Report No. 1, Texas Instruments Report No. ALEX (03)-TR-75-01, NISC Contract Number N00014-75-C-0101, Texas Instruments Incorporated, Dallas, Texas.

Burg, J. P., 1967, Maximum Entropy Spectral Analysis, paper presented at the 37th Meeting of the Society of Exploration Geophysicists, 31 October, Oklahoma City, Oklahoma.

Burg, J. P., 1968, A New Analysis Technique for Time Series Data, paper presented at the NATO Advanced Study Institute on Signal Processing with Emphasis on Underwater Acoustics, Enschede, the Netherlands.

Capon, J., R. J. Greenfield, and R. T. Lacoss, 1969, Long-Period Signal Processing Results for the Large Aperture Seismic Array, Geophysics, 34, 305-329.

Oliver, J., 1962, A Summary of Observed Seismic Surface Wave Dispersion, Bull. Seismol. Soc. Am., 52, 81-86.

Papoulis, A., 1965, Probability, Random Variables, and Stochastic Processes, McGraw Hill, Inc., New York.

Strauss, A. C., 1973, Final Evaluation of the Detection and Discrimination Capability of the Alaskan Long Period Array, Special Report No. 8, AFTAC Contract Number F33657-72-C-0725, Texas Instruments Incorporated, Dallas, Texas.

Unger, R., 1973, Selection of Reference Waveforms for Matched Filter Processing of Long Period Signals from Seismic Events, Special Report No. 5, AFTAC Contract Number F33657-72-C-0725, Texas Instruments Incorporated, Dallas, Texas.

APPENDIX A

NARROWBAND FILTERING OF DISPERSED WAVEFORMS

A. INTRODUCTION

In the development of the time-variant, dispersion-related filter it was observed that narrowband filtering could lead to significant amplitude and phase errors. In this appendix we will discuss some of the possible causes and give a correction formula for the amplitude error stemming from one of these causes.

B. NARROWBAND FILTER AMPLITUDE ERRORS

Figure A-1 shows the effects of narrowband filtering with various bandwidths along the dispersion curve of a linear chirp waveform. The narrowband filter (NBF) transfer function and its response characteristics were described in Section III. The shape of the transfer function is basically rectangular, with 0.002-Hz cosine tapers near the cut-off frequencies. For sufficiently narrow filter bands (specified later in the text) the NBF response to a chirp signal input has a lobe character with reduced side lobes; the node intervals approximately equal the inverse of the effective filter bandwidth (see also Figure III-1).

Figure A-1a describes the variation in filter bandwidth applied along the dispersion curve. The solid lines indicate the cut-off frequencies, the effective filter bandwidth is approximately 0.002 Hz smaller due to the cosine taper. Figure A-1b is the input signal; Figures A-1c through A-1h are the outputs of the NBFs applied at the corresponding points along the dispersion curve. Figure A-1i is the dispersion-related filter (DRF) output

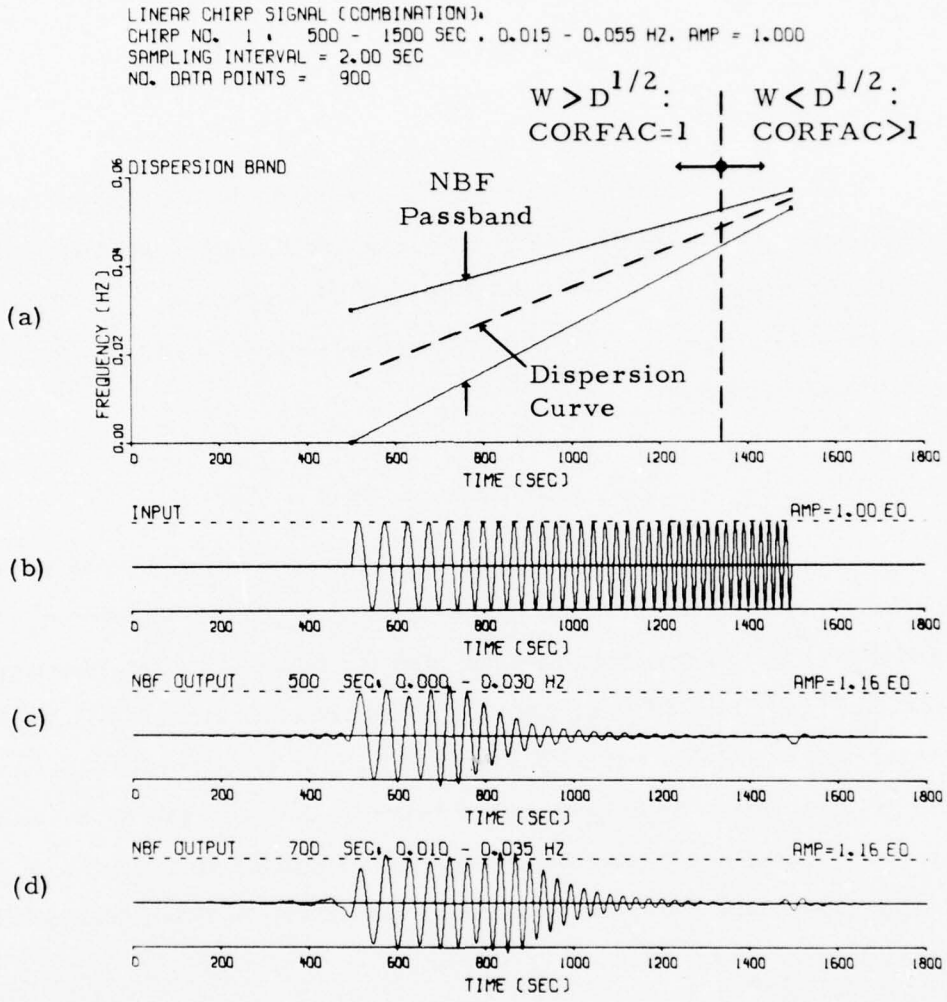

FIGURE A-1

NBF EFFECTS ON A LINEAR CHIRP WAVEFORM
(PAGE 1 OF 2)

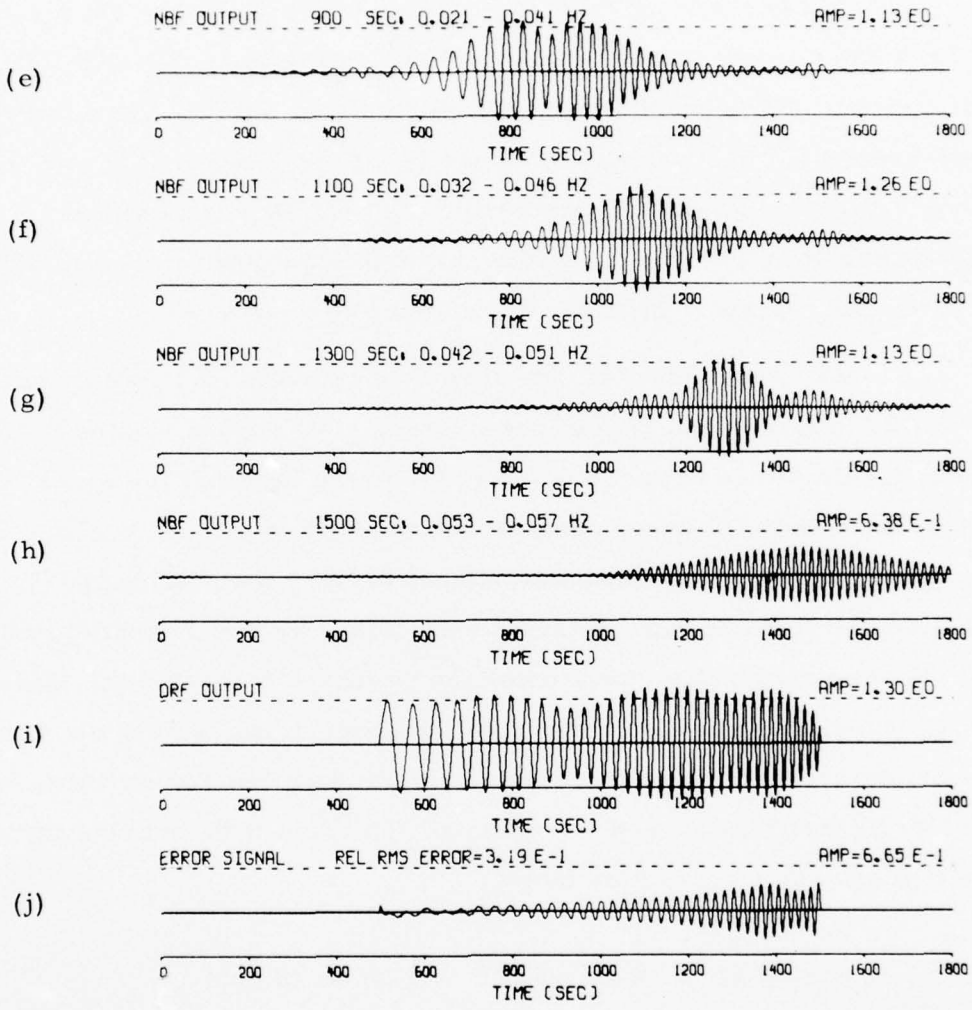

FIGURE A-1

NBF EFFECTS ON A LINEAR CHIRP WAVEFORM
(PAGE 2 OF 2)

synthesized from samples of the various NBF outputs. Figure A-1j is the error signal obtained by subtracting the input signal from the DRF output. All traces are plotted on the same scale.

We observe that the wider filter bands (0.030-0.020 Hz, applied from 500 to 850 seconds in the time trace) reproduce the corresponding signal peak fairly well. The convolution of the chirp signal with the NBF impulse response creates a small amount of ripple in the NBF outputs. From 0.020 through 0.010 Hz bandwidths (applied from 850 to 1300 seconds) there appears to be considerable interference, leading to amplitude errors of up to 30%, as shown in the DRF output. This error could not be corrected.

For bandwidths of less than 0.009 Hz with the given dispersion rate, the NBF outputs assume the lobe character as seen in Figure III-1. At this point, an amplitude error is created due to the fact that the signal energy carried by the frequency components within the NBF passband is distributed over an effective output time interval, determined by the NBF response curve, which is greater than the input interval established by the time-frequency relationship (the dispersion curve) over the passband frequencies. Based on empirical observations and on theoretical considerations, a formula was found which satisfactorily corrects this type of amplitude error for monotonely (not necessarily linearly) dispersed waveforms. To correct the output amplitude, it is multiplied with a correction factor:

$$\begin{aligned} \text{COR FAC} &= W^{-1} D^{1/2} \quad , \quad W < D^{1/2} \\ &= 1 \quad , \quad W \geq D^{1/2} \end{aligned} \tag{A-1}$$

where

D is the dispersion rate (Hz/sec) over the NBF passband frequency components,

W is the effective NBF bandwidth (Hz).

This formula was used in all NBF outputs generated in this study. The above conditions are indicated in Figure A-1a.

For lobed NBF outputs, this correction reduces amplitude errors to less than 5%, not counting the overshoot at the end of a waveform as reported in Section III and also presented in Figure A-1i. The formula was tested with linear chirp waveforms of different duration, with different dispersion rates, and with a cosine-modulated linear chirp waveform.

To show the significance of this correction, we calculate the CORFAC value for the case of Figure III-1, where $D = 4 \cdot 10^{-5}$ Hz/sec and the specified bandwidth of 0.005 Hz leads to an effective bandwidth of 0.003 Hz. The result is a correction factor of 2.1. Thus, without the correction, we would have underestimated the signal by more than 50%. The CORFAC values are plotted as a function of effective filter bandwidth, for several dispersion rates, in Figure A-2.

The condition $W < D^{1/2}$ has a two-fold significance. First, from Figure A-1 it is observed that this seems to be the condition under which the NBF output has the lobed character; for the given dispersion rate ($4 \cdot 10^{-5}$ Hz/sec) the lobes start occurring for specified bandwidths of less than 0.009 Hz, corresponding to an effective NBF bandwidth of 0.007 Hz, which is only slightly higher than $D^{1/2} = 0.0064$ Hz. For wider bands the lobed character does not seem to be present; the correction factor then is set equal to one since we cannot correct for the amplitude errors occurring in that case.

The second significance of the condition $W < D^{1/2}$ is that under this condition, as will be shown shortly, the effective output duration is greater than the length of the part of the input signal comprised by the NBF passband frequency components, causing the output amplitude to be too low with respect to the input amplitude. This condition requires amplitude correction.

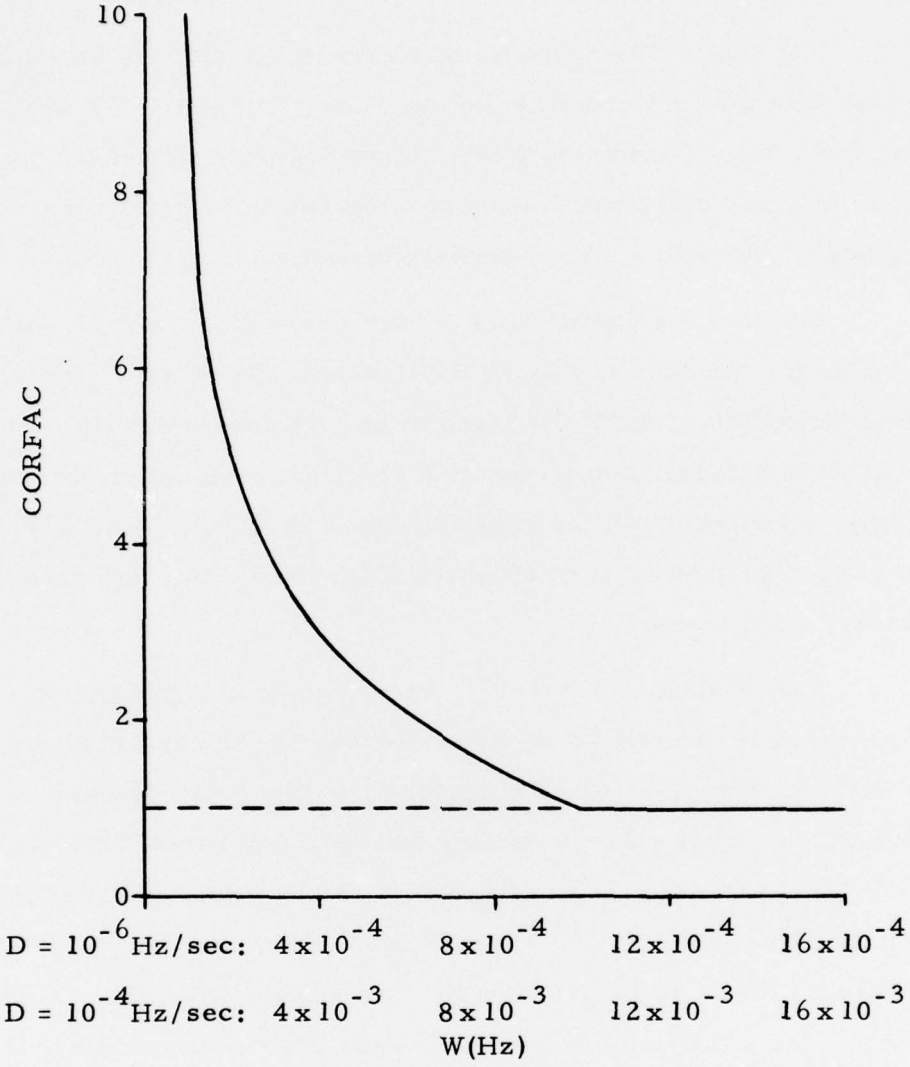

FIGURE A-2

CORFAC AS A FUNCTION OF BANDWIDTH
FOR DIFFERENT DISPERSION RATES

We will now present the reasoning which led to Equation (A-1). The effective input duration is determined by the NBF bandwidth and the dispersion rate over this band:

$$T_i = W D^{-1} . \qquad \text{(A-2)}$$

We define the effective output duration, T_o, as in Figure A-3. It is the interval over which a constant amplitude waveform has the same energy as the lobed NBF output waveform; the constant amplitude equals the maximum lobe value.

From visual inspection of the lobed waveforms encountered, it was found that the effective duration approximately equals one-half of the width of the main lobe, which is $2 W^{-1}$. Therefore,

$$T_o \approx W^{-1} \qquad \text{(A-3)}$$

was adopted as a practical value for the effective output duration. It is of interest to note that for the impulse response envelope of a rectangular filterband (a sin x/x function, with $x = \pi W t$) the relation is exact: $T_o = W^{-1}$. For any other lobed curve, T_o can be calculated from numerical integration. However, using the above approximate value returned satisfactory corrections, so that the numerical integration was not performed in the correction process. It now follows that:

$$T_o > T_i \quad \text{for} \quad W < D^{1/2} . \qquad \text{(A-4)}$$

The correction factor then follows from the fact that the input signal energy present over the interval T_i must be distributed over the larger interval T_o, causing the output amplitude to be smaller than the input amplitude by a factor $(T_i T_o^{-1})^{1/2}$. To obtain equal input and output amplitudes, the output must be multiplied by:

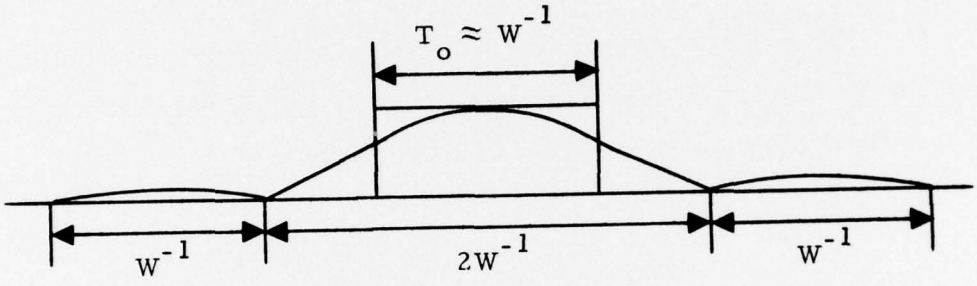

FIGURE A-3

TYPICAL NBF OUTPUT ENVELOPE FOR $W < D^{1/2}$

$$\text{COR FAC} = (T_o\, T_i^{-1})^{1/2} = W^{-1} D^{1/2}, \quad W < D^{1/2}. \qquad \text{(A-5)}$$

For $T_o \leq T_i$ (i.e., $W \geq D^{1/2}$) no lobed outputs are expected, in which case we cannot perform a correction in the above fashion, and the correction factor is set equal to one.

In the present stage of the DRF algorithm Equation (A-1) was implemented assuming a linear dispersion curve over the entire signal interval. The dispersion rate is automatically determined from the high and the low frequencies and the time interval of the dispersion band specified and input by the user. This method can easily be extended for the case of nonlinear dispersions by calculating the expected instantaneous dispersion rate from the dispersion band center frequencies. All data presented in this report were processed in the above fashion; for the measured condition $W \geq D^{1/2}$ the correction factor is automatically set equal to one.

Thus, the correction formula was effectively applied in generating the DRF and time-variant Wiener filter (TVWF) outputs of a synthetic linear chirp waveform (Figures III-1, IV-1, and IV-3). For the Sinkiang Region seismic waveforms, the dispersion curve variance required a bandwidth greater than the square root of the average dispersion rate, so that no correction was applied (COR FAC = 1) in that case (Figures IV-6 and IV-8).

C. NARROWBAND FILTER PHASE ERRORS

In Section III, Figure III-1g showed a large error signal despite good amplitude agreement throughout the waveforms. This large error of rather constant amplitude must be caused by a near-constant phase error, as shown below.

Consider a linearly dispersed waveform, and subtract this from the same waveform, only shifted in phase; then the difference signal is:

$$e(t) = \sin(\pi D f t^2 + \phi) - \sin 2\pi f t$$

$$= 2 \sin \frac{\phi}{2} \cos\left(\pi D f t^2 + \frac{\phi}{2}\right) . \qquad \text{(A-6)}$$

Thus, a DRF output phase shift ϕ results in an error signal of constant amplitude,

$$A_e = 2 \sin \frac{\phi}{2} , \qquad \text{(A-7)}$$

and phase-shifted an amount $\frac{\pi}{2} + \frac{\phi}{2}$ with respect to the DRF input.

In Figure III-1g the error signal amplitude, aside from end-effect overshoot, is approximately 0.7, indicating a phase error of about 42°. An overlay of the DRF output trace and the original signal trace confirmed a phase error of this order of magnitude.

The phase difference is caused by the convolution of the chirp waveform with the NBF impulse response. This convolution is rather complicated; the phase difference cannot be anticipated and, therefore, cannot be corrected in closed form. Notice in Figure A-1i that the phase error seems to be small for the relatively wide bands; it becomes more significant for bandwidths of less than 0.020 Hz (around 900 sec on the time axis).

Probably partly due to the wider filter bands applied, the phase error has not been noticed in the filter outputs of actual seismic waveforms. Because of this fact, and due to time limitations, the phase error cause and correction were not pursued further in this study.

APPENDIX B

DETERMINING THE START TIME OF DISPERSED SIGNALS IN NOISE

A. INTRODUCTION

Operation of the dispersion-related filter requires prior knowledge of the start of a signal's dispersion curve. Under marginal signal-to-noise ratio (SNR) conditions this may be difficult to establish. Below, four methods of determining the start time of a signal's dispersion curve under noisy conditions are discussed.

B. DETERMINING THE START TIME FROM TRAVEL TIME TABLES

This method has been incorporated in the EDIT routine of the long-period (LP) signal processing package. The resulting signal start times and signal duration intervals are carried in the LP record headers. Signal start and stop times are routinely indicated by arrows on the travel time axis. The start time accuracy is on the order of 100 sec and is independent of the SNR.

C. DETERMINING THE START TIME WITH THE TVWF

The start time of a signal's a priori known or assumed dispersion curve can be found by sliding the TVWF dispersion band through the waveform. Correct alignment of the TVWF dispersion band with the actual signal dispersion curve should yield the maximum TVWF output. This principle is correct for signals with narrowly defined dispersion curves. In the case of actual seismic signals a relatively wide inherent signal bandwidth and the presence of unresolved multiple signals may cause some start time uncertainty.

This method was performed on both a linear chirp waveform and a Sinkiang region seismic event signal, without noise and with a 0 dB RMS SNR. Figures B-1 and B-2 show the TVWF RMS output as a function of presumed signal dispersion start time. The method seems to work well even for the seismic signal in a 0 dB SNR waveform; the start time for the chirp waveform dispersion is estimated correctly; the start time estimate for the seismic signal is both plausible and consistent. The plots also indicate that a 50-second timing error results in less than 1 dB amplitude error, i.e., less than 0.05 surface wave magnitude error (E_{M_S}).

However, the process is either time or core consuming because of the large number of inverse Fourier transforms (one for each different NBF applied along the dispersion curve; see Section III) required by the filter. One has the choice between either storing the relevant intervals of all NBF outputs and shifting only the sampling time, or repeating the entire TVWF process for each presumed start time. The first method requires a high amount of computer memory; the second method requires considerable processing time. The choice depends on the available overall processing facilities and priorities.

If the filter were to be designed as a recursive digital resonance filter, the processing time could be reduced considerably, due to the possibility of fast time-domain convolution. In that case the procedure of repeating the TVWF process probably is preferable. Moreover, estimating the initial start time with travel time tables followed by a rough probing scheme with a subsequent fine search could be scheduled to avoid excessive processing.

The results in Figures B-1 and B-2 are only an indication of the start time accuracy obtainable with this method, since only one noise sample was used in conjunction with signals. For a statistical evaluation the method should be tested on an ensemble of noise samples. If this method shows consistently good results, also for lower SNR waveforms, this would enable the TVWF to be used also as a detector rather than only as a signal

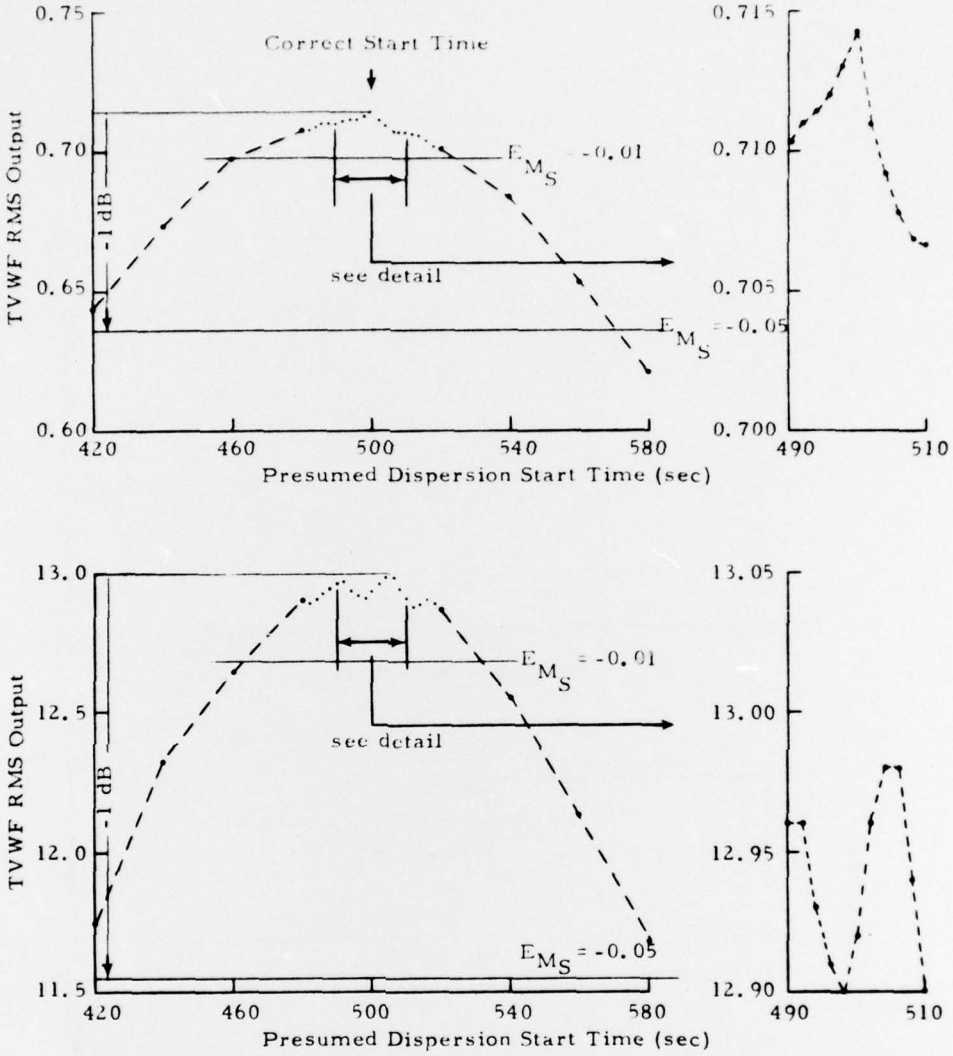

FIGURE B-1

DETERMINING THE DISPERSION START TIME WITH THE TVWF; LINEAR CHIRP SIGNAL. (a) SIGNAL ONLY; (b) 0 dB RMS SNR

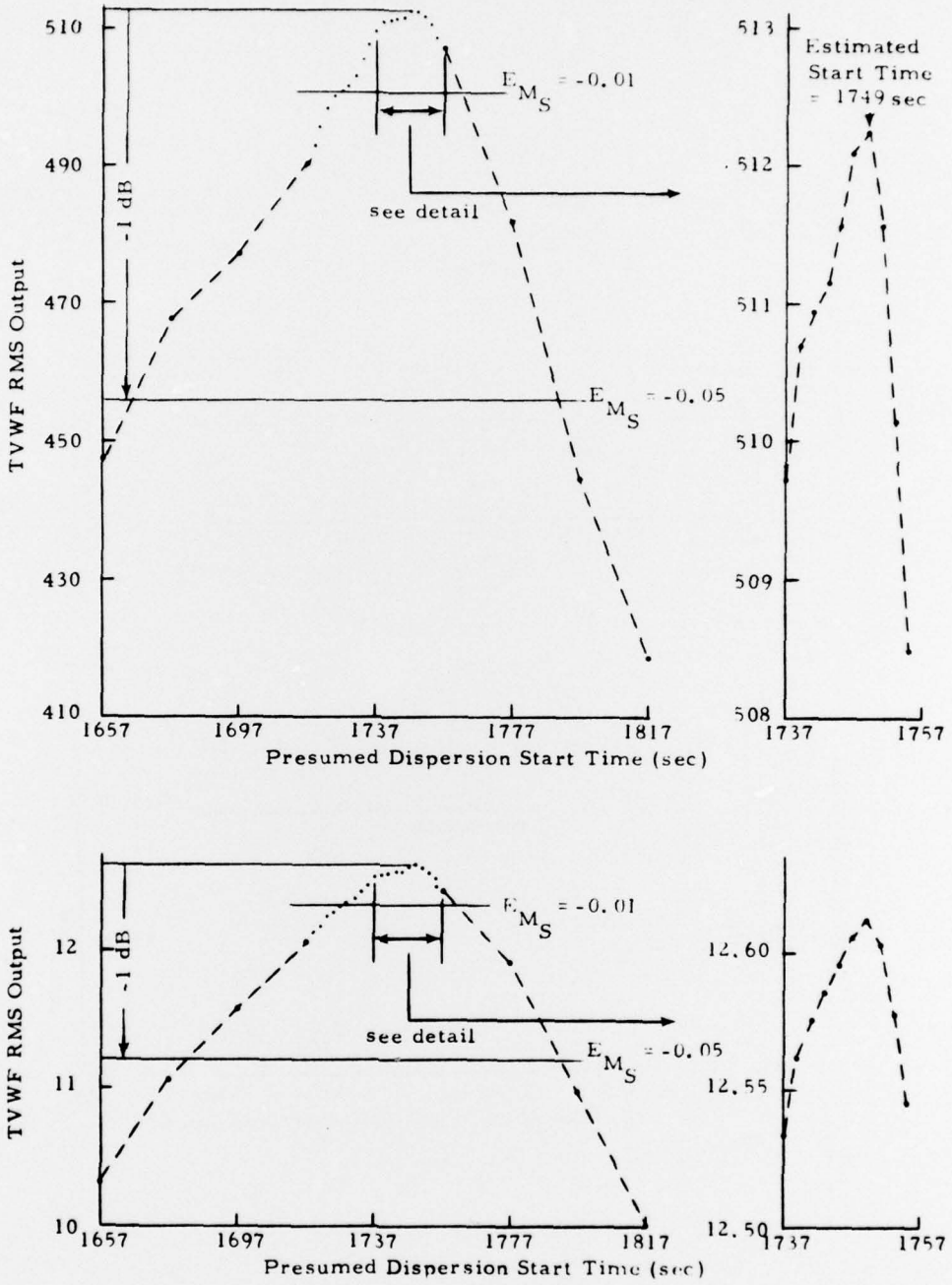

FIGURE B-2

DETERMINING THE DISPERSION START TIME WITH THE TVWF; SIN/170/17AL. (a) SIGNAL ONLY; (b) 0 dB RMS SNR

estimator. However, as it is possible to generate false signals from noise, it may also be possible to generate false start times. A statistical evaluation will have to indicate the potential false alarm rate.

D. DETERMINING THE START TIME WITH THE MAXIMUM ENTROPY SPECTRUM

The start time of the dispersion curve can also be determined from maximum entropy spectral analysis as performed in Section II. According to Figure B-3 the high resolution of this technique indicates the possibility of picking up the dispersion curves from waveforms of 0 dB RMS SNR, probably within 40 sec accuracy. Because the MES has to be performed on short overlapping time gates which slide through the waveform, also this method is rather time consuming. The method is furthermore sensitive to the choice of certain MES algorithm parameters; see Section II.

E. INSTANTANEOUS ENVELOPE, PHASE, AND FREQUENCY DETECTION

A waveform $r(t)$ can be expressed as:

$$r(t) = R(t) \cos \left[2\pi \int f(t)\ dt \right] \tag{B-1}$$

or, equivalently, as:

$$r(t) = R(t) \cos \left[2\pi f_o t + \phi(t) \right] \tag{B-2}$$

where, see Figure B-4,

$R(t)$ is the instantaneous envelope of $r(t)$,

$\phi(t)$ is the instantaneous phase of $r(t)$ with respect to a monochromatic waveform of frequency f_o,

$f(t)$ is the instantaneous frequency of $r(t)$,

f_o is an arbitrary reference frequency.

(a)

LINEAR CHIRP SIGNAL (COMBINATION):
CHIRP NO. 1 : 496 -1496 SEC . 0.015 - 0.055 HZ. AMP = 1.000
PLUS NOISE: NOI-131-00AL
SAMPLING INTERVAL = .00 SEC
NO. DATA POINTS = 225

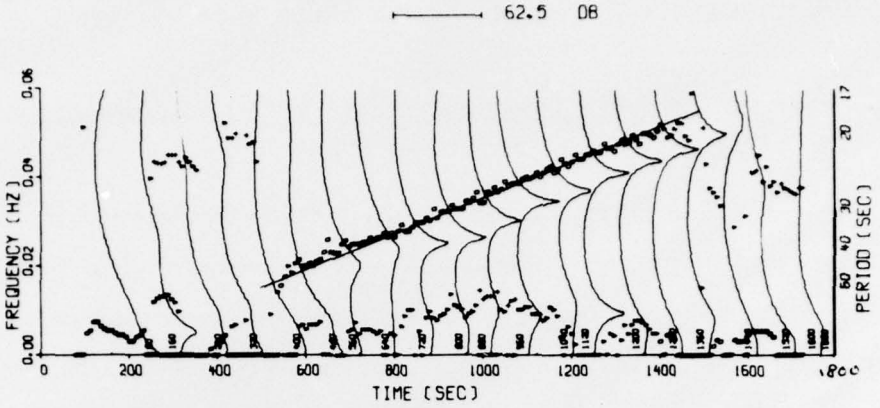

ORIGIN POWER LEVELS: -25 DB (1 C.C. REF.)
NO. LAGS = 6 POINTS = 48 SEC
GATE LENGTH = 20 POINTS = 160 SEC

(b)

SIN/170/17AL LOVE WAVE BEAM
PLUS NOISE: NOI-131-00AL
SAMPLING INTERVAL = 8.00 SEC
NO. DATA POINTS = 225

SOURCE TIME = 17.23. 3 DATE: 6/18/71
MB = 5.2 DELTA = 67.18 LAT = 41.5 LON = 79.3 DEPTH = 33.0

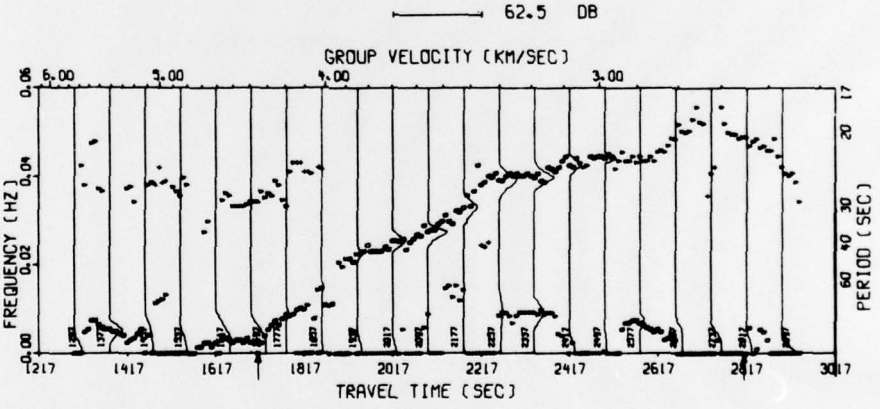

ORIGIN POWER LEVELS: 25 DB (1 C.C. REF.)
NO. LAGS = 6 POINTS = 48 SEC
GATE LENGTH = 20 POINTS = 160 SEC

FIGURE B-3

DISPERSION START TIME DETERMINATION WITH THE MES:
(a) LINEAR CHIRP WAVEFORM IN 0 dB RMS SNR;
(b) SEISMIC SIGNAL IN 0 dB RMS SNR

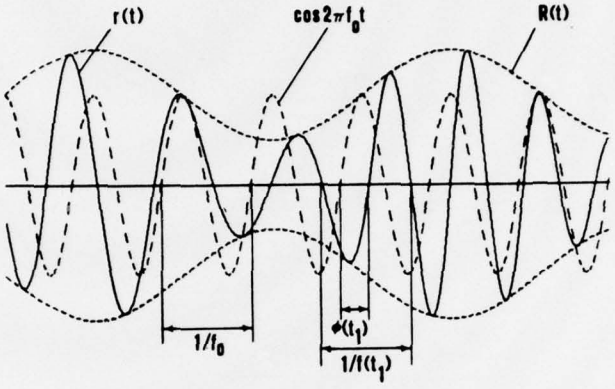

$$r(t) = R(t) \cos \left[2\pi \int f(t)\, dt \right]$$

Or:

$$r(t) = R(t) \cos \left[2\pi f_0 t + \phi(t) \right]$$

FIGURE B-4

WAVEFORM REPRESENTATION

The envelope and phase can be determined with the waveform's Hilbert transform $\overset{\vee}{r}(t)$, a 90^{o} phase-shift operator (e.g., Papoulis, 1965):

$$\overset{\vee}{r}(t) = R(t) \sin \left[2\pi f_o t + \phi(t) \right] , \tag{B-3}$$

by the relationships:

$$R(t) = \left[r^2(t) + \overset{\vee}{r}^2(t) \right]^{1/2} \tag{B-4}$$

and

$$\phi(t) = \arctan \frac{\overset{\vee}{r}(t)}{r(t)} - 2\pi f_o t . \tag{B-5}$$

The frequency is then found by differentiating the phase function after modulo 2π removal:

$$f(t) = f_o + \frac{1}{2\pi} \cdot \frac{d\phi(t)}{dt} . \tag{B-6}$$

For a linearly dispersed waveform the frequency is a linear function of time. Consequently, the phase function is parabolic. Since the phase cannot exceed an interval of 2π radians, random noise with its frequency band centered at f_o would have its phase fluctuations confined to this 2π radians interval. A systematic phase function such as that of a dispersed waveform, however, can be "unwrapped" by eliminating its 2π modulo, to expose its continuous function. This may result in a favorable SNR of the phase function, depending on the noise spectrum and the signal dispersion curve. The phase function, therefore, may be used as a detector, and could indicate the start and duration of LP signals.

In reality, however, there are several factors that may reduce the SNR of the phase function. First, the center frequencies of noise and signal bands may not coincide. One can choose f_o to coincide with the signal center frequency; in that case the offset of the noise center frequency causes

the noise phase function to have a linear bias. Inversely, one may choose f_o to be the noise center frequency; then the signal phase will have a linear bias. Experiments will have to indicate which choice of reference frequency is best.

Another problem is that the noise is in general non-white, due to one or more of the following causes:

- Propagated noise causing dispersion.
- Noise coherence due to instrument response and beamsteering; in particular, possible ringing of noise.
- Natural dominance of low-frequency noise.

This causes the noise phase function to have, over short intervals, a somewhat deterministic character. In "unwrapping" the phase the peak noise phase values then may become higher than 2π, thus reducing the phase SNR. Prewhitening will not give a solution since this would affect the signal spectrum.

Figures B-5 and B-6 show examples of envelope, phase, and frequency detection. After making the phase function continuous, some of the linear bias is eliminated by taking out the slope between the first and the last point of the function. The frequency is derived from the phase function before its rotation. Because of the differentiation, the frequency function is noisier than the phase function. In particular, it shows spikes where the phase function has discontinuities, for instance, due to multiple signals. For the high SNR waveforms, the parabolic character in the phase function can be clearly discerned, despite the remaining linear bias due to the choice of f_o (0.040 Hz); the frequency function is clearly linear. Envelope, phase, and frequency each show clearly the signal onset and duration. In the 0 dB SNR waveforms, still some structure can be recognized in each of these functions, but although this structure is probably sufficient to call a detection, it is no longer possible to determine the signal onset and duration. Experiments with other noise samples yielded somewhat more favorable results; the merits and limitations of this method will have to be determined in a separate study.

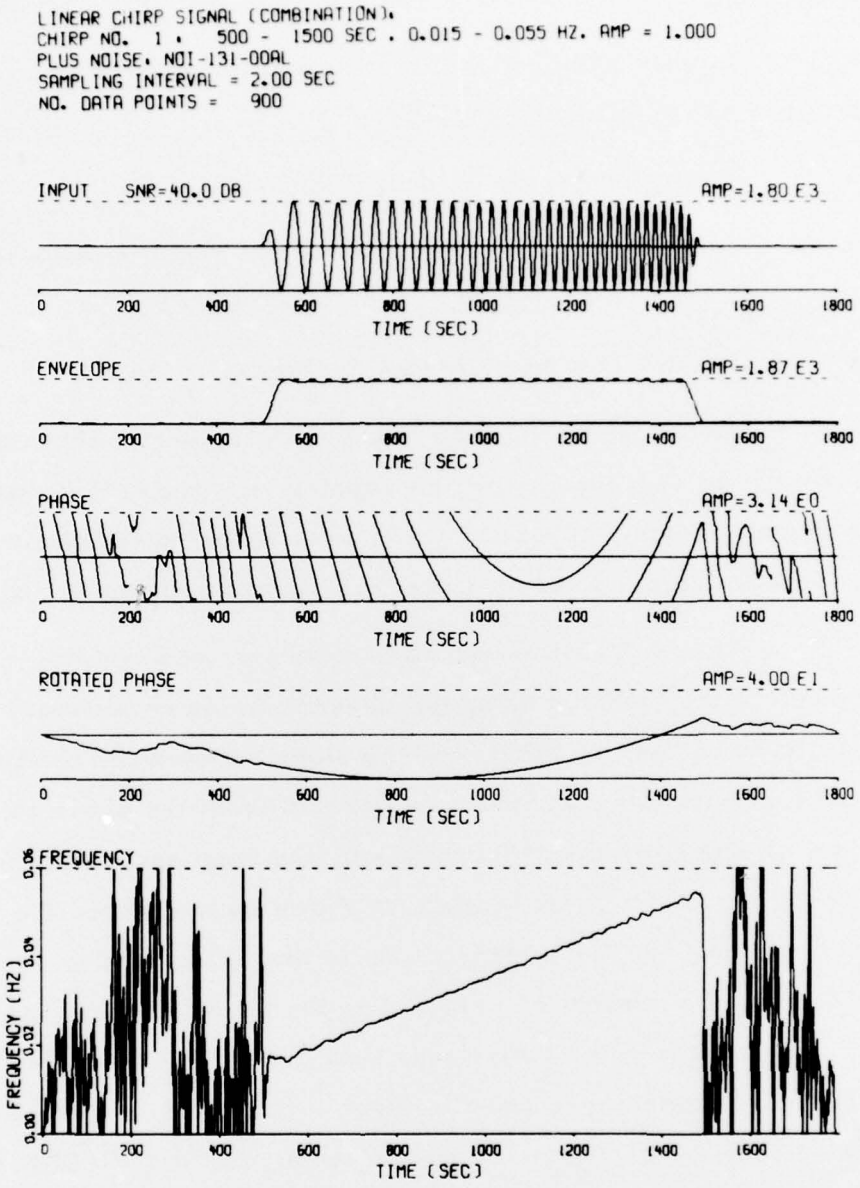

FIGURE B-5

ENVELOPE, PHASE AND FREQUENCY DETECTION OF LINEAR CHIRP WAVEFORM; f_o = 0.040 Hz
(PAGE 1 OF 2)

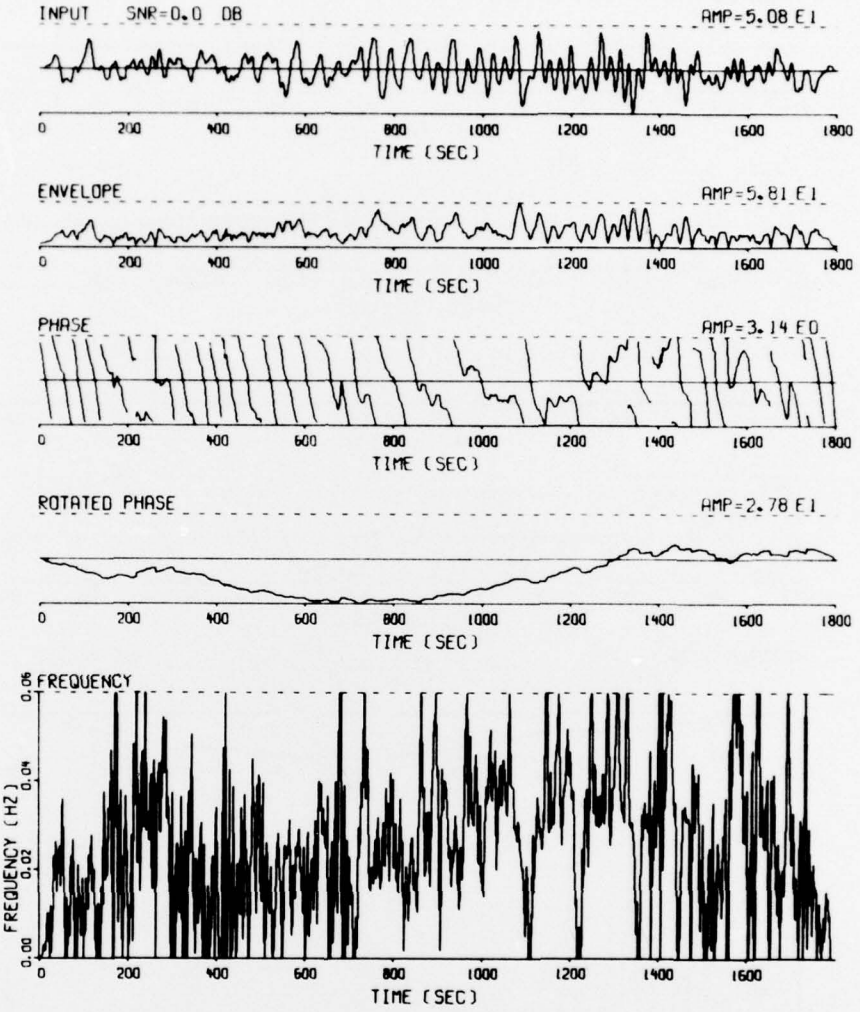

FIGURE B-5

ENVELOPE, PHASE AND FREQUENCY DETECTION OF LINEAR CHIRP WAVEFORM; f_o = 0.040 Hz
(PAGE 2 OF 2)

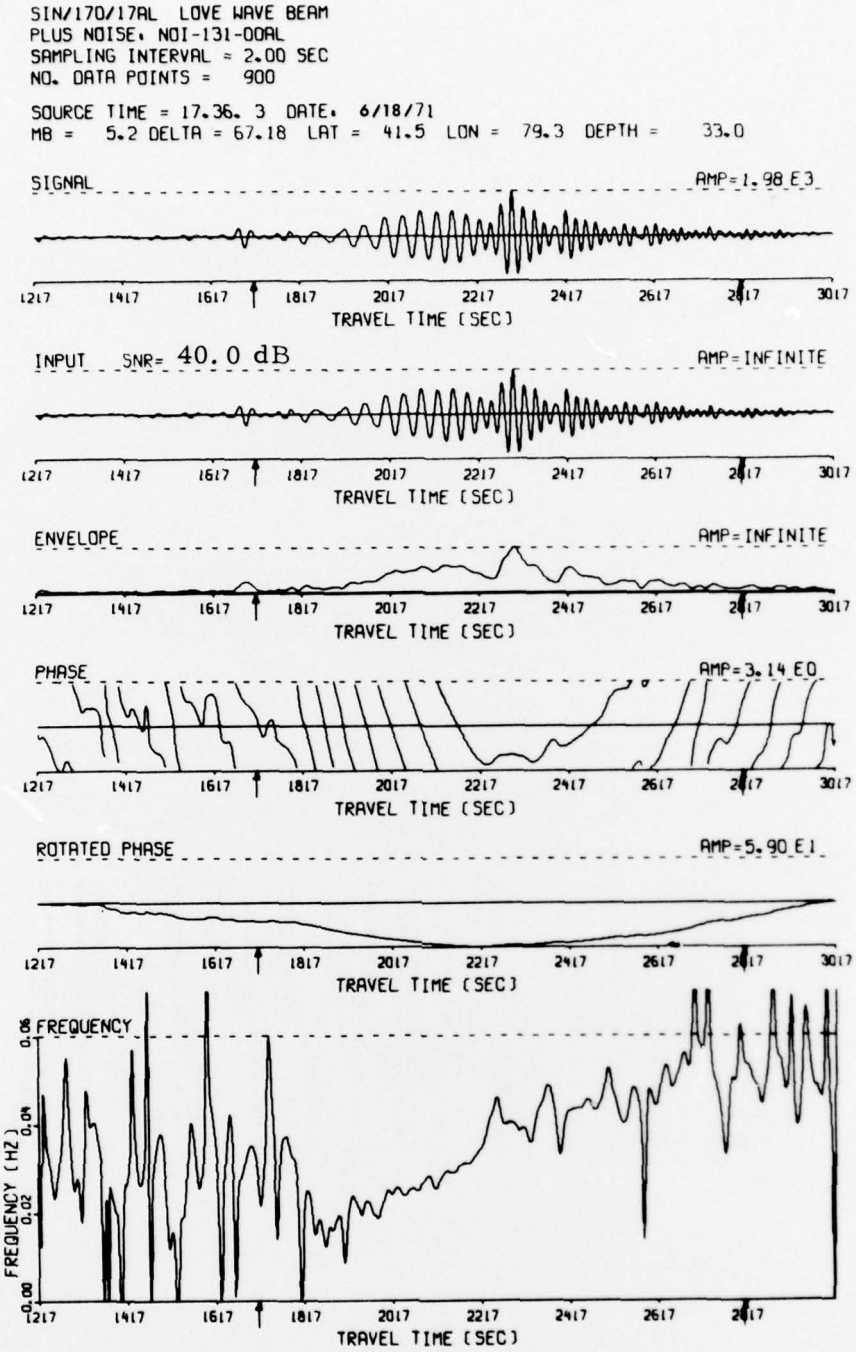

FIGURE B-6

ENVELOPE, PHASE AND FREQUENCY DETECTION OF SEISMIC SIGNAL; f_o = 0.040 Hz
(PAGE 1 OF 2)

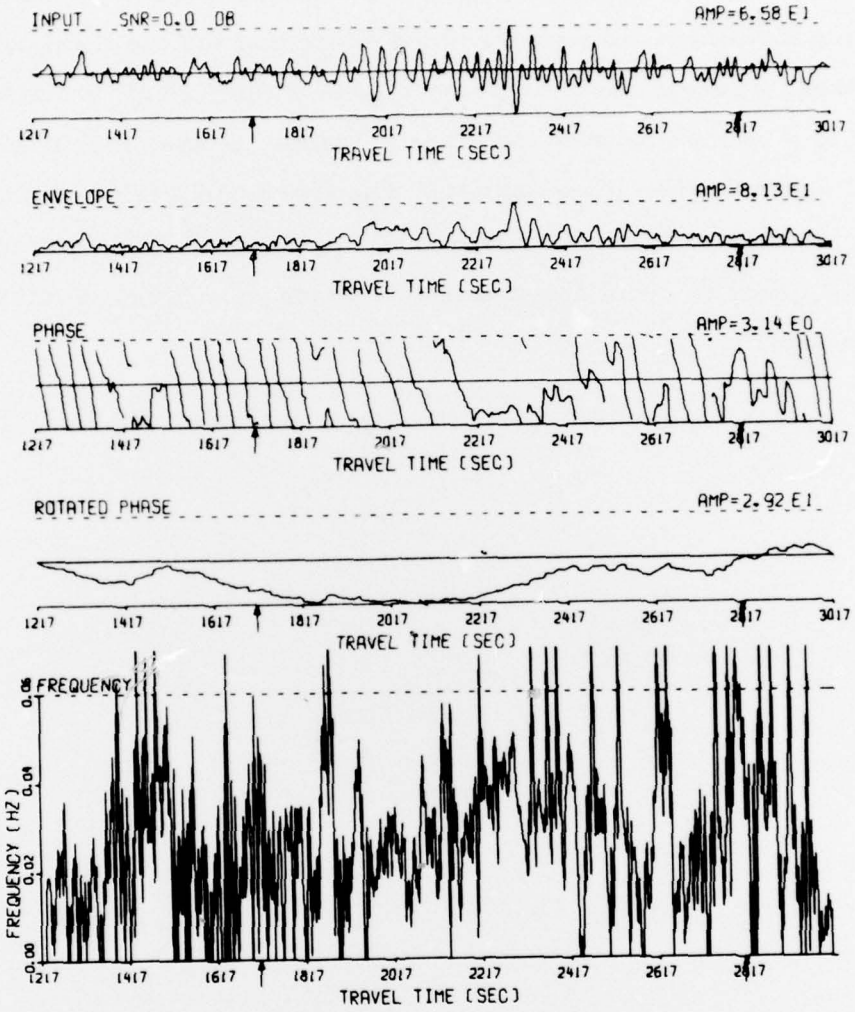

FIGURE B-6

ENVELOPE, PHASE AND FREQUENCY DETECTION OF SEISMIC SIGNAL; f_o = 0.040 Hz
(PAGE 2 OF 2)

F. SUMMARY

Considering the above analysis, it appears that determining the dispersion curve start time is probably most accurately done with the TVWF itself, by sliding it through the waveform and searching for the maximum output. This method, however, is time or core consuming. Next, the MES method seems to give the best results. The envelope, phase, frequency detection method needs further investigation. The travel time table method provides initial start time estimates. The signal start time must be determined within 50 sec accuracy to avoid significant magnitude errors due to dispersion curve misalignment.